# Assimilation and application of nearshore ocean wave models

Dissertation

zur Erlangung des Doktorgrades

der Mathematisch-Naturwissenschaftlichen Fakultät

der Christian-Albrechts-Universität zu Kiel

vorgelegt von

Qingyang Song

Kiel, 2018

| | |
|---|---|
| Erster Gutachter: | Prof. Dr. Roberto Mayerle |
| Zweite Gutachter: | Prof. Dr. Thomas Slawig |
| | |
| Tag der mündlichen Prüfung: | May 4th, 2018 |
| Zum Druck genehmigt: | May 4th, 2018 |

gez.

# Declaration

I declare that

- apart from the supervisor's guidance the content and design of the thesis is all my own work;
- the thesis has not been submitted either partially or wholly as part of a doctoral degree to any other examining body and it has not been published or submitted for publication;
- the thesis has been prepared subject to the Rules of Good Scientific Practice of the German Research Foundation.

Signed:

_____

Date:

_____

# Acknowledgements

First of all I would like to give my sincere gratitude to my supervisor Prof. Dr. Robert Mayerle. His encouragement not only in regard to my research but also to my life made me keep enhancing myself. Without his guidance and persistent help this dissertation would not have been possible.

In particular, my sincere thanks goes to Dr. Xiangyang Zheng. I was really fortunate to have you here, a friend and a colleague who is from the same country with me when I started my PhD program in a totally strange place. Also, the deep discussions with you were quite helpful for me to have a better understanding about assimilation researches and eventually complete my work.

I would like to thank my colleagues Dr. Katharina Niederndorfer, Dr. Jose Manuel Fernandez and Mr. Kadir Orhan, who kindly reviewed my dissertation. Your important experiences and valuable comments about my researches and writings further improved my dissertation.

In addition, I would like to thank Dr. Kalle Runte and Dr. Peter Weppen. When I had any problems or difficulties in my life or work, your doors were always open for me. Also I am grateful to my other colleagues Dr. Natacha Fery, Dr. Simon van der Wulp and Dr. Guilherme Dalledonne in CORELAB for their kindly help and company during these years.

I would also like to thank my parents for their wise counsel and persistent support. At last but not the least, I would like to leave a message to all the people who was concerned about me and who I was concerned about:

去国十年，少年心未老；艳阳犹在，青峰竹间照。

# Abstract

This thesis concentrates on wind-induced ocean waves in coastal areas including two main aspects: wave energy assessment with numerical models and development of a 4D variational assimilation scheme (4DVAR) for nearshore wave simulations.

The method for assessing the wave energy potential was developed out in three steps: long-term wave power estimation, detailed wave condition analysis and suitable location selections for wave energy farms. The method was applied to the south coast of Java Island. A long-term analysis of a 10-year wave dataset obtained from the ERA-Interim database was able to suggest that the annual median power is expected to exceed 20 kW/m along the coast showing the potential for wave energy extraction. A coastal wave model with an unstructured grid was run over one year in the coastal area, revealing that swells from the southwest were the major source of wave energy and highest monthly median wave power reached about 33 kW/m. General criteria regarding wave conditions, water depth and distance from the coast were established and applied in the study area revealing two suitable zones for wave energy farms.

The 4D variational assimilation scheme including partition methods for nearshore wave models has been tailored to SWAN model for adjusting both, wave boundary conditions and wind fields. Nonstationary wave boundary conditions were assimilated by providing defined correlations of model inputs in time. Twin experiments covering both stationary and nonstationary wave conditions were carried out to assess the adequacy of the proposed scheme. The value of the cost function declined to less than 5% and root mean square errors (RMSE) of spectrum were reduced to less than 10% under stationary wave conditions. Under nonstationary wave conditions, the RMSE were reduced to less than 10% after 30 iterations in most assimilation windows. Also, the proposed scheme was modified for low spatial observation coverage by assuming a group of 'basic' inputs to contain all errors so as to be applied in the German Bight. The modified scheme using a single observing location performed comparable assimilation effect with the original scheme without the basic inputs assumption using 25 observing locations in twin experiments. For both schemes wave

spectrum RMSE were reduced by around 50% throughout the whole computation domain. The practical experiment revealed that the wave spectrum RMSE at the validation buoy declined by more than 60% by means of the modified assimilation scheme with observations from a single in-situ buoy. The results can suggest that the developed 4D variational scheme is capable of improving the model results effectively under wave conditions when nonlinear interactions are insignificant. The modified scheme with 'basic' inputs can be applied in coastal areas where observations are spatially limited provided sea states are strongly correlated in space.

# Zusammenfassung

Diese Arbeit befasst sich mit wind-induzierten Ozeanwellen in Küstengebieten und umschließt zwei Aspekte: eine Untersuchung zur Wellenenergie mittels numerischer Modelle und die Entwicklung eines 4D variationellen Datenassimilationsverfahrens (4DVAR) für küstennahe Wellensimulation. Die Methode zur Bestimmung der Wellenenergie wurde in drei Schritten entwickelt: Langzeit Abschätzung der Wellenenergie, detaillierte Analyse von Wellenbedingungen und Auswahl geeigneter Gebiete für Wellenkraftanlagen. Die Methode wurde an der Südküste Javas angewendet. Die Langzeitanalyse eines Datensatzes der ERA-Interim Datenbank über 10 Jahre deutete darauf hin, dass die mittlere jährliche Leistung entlang der Küste 20 kW/m übersteigt, was auf ein Potenzial zur Gewinnung von Wellenenergie hindeutet. Ein Wellenmodell für die Küste mit unstrukturiertem Gitter, welches für ein Jahr simuliert wurde, zeigt, dass Wellengang aus Südwest die Hauptquelle für Wellenenergie war und das Gebiet eine mediane maximale monatliche Leistung von etwa 33 kW/m erreichte. Allgemeine Kriterien zur Beschreibung von Wellenbedingungen, Wassertiefe und Entfernung zur Küste wurden eingeführt und im Untersuchungsgebiet angewendet, wodurch zwei geeignete Zonen für Wellenkraftanlagen identifiziert werden konnten. Das 4D variationelle Datenassimilationsverfahren, das die Partitionsmethode für küstennahe Wellenmodelle beinhaltet, wurde für SWAN Modelle zugeschnitten, um sowohl die Wellenrandbedingungen als auch Windfelder anzupassen. Nichtstationäre Modellrandbedingungen für den Seegang wurden assimiliert indem definierte Korrelationen von Modelleingabewerten über die Zeit eingebracht wurden. Parallel-Experimente welche stationäre und nichtstationäre Wellenbedingungen berücksichtigen wurden durchgeführt, um die Eignung des vorgeschlagenen Verfahrens zu untersuchen. Unter stationären Bedingungen verringerte sich der Wert der cost-function auf weniger als 5% und die Fehler des quadratischen Mittelwertes (root mean square error, RMSE) des Spektrums wurden auf weniger als 10% reduziert. Unter nichtstationären Bedingungen wurden die RMSE nach 30 Iterationen in den meisten Assimilationsfenstern auf weniger als 10% reduziert. Zudem wurde das vorgeschlagene Verfahren an eine geringe

räumliche Datendichte angepasst und so in der Deutschen Bucht angewendet, indem eine Gruppe von "Basiseingaben" angenommen wurde, die alle Fehler beinhaltet. Das angepasste Verfahren, welches einen einzelnen Beobachtungort verwendet, leistete einen vergleichbaren Assimilationseffekt wie das Originalschema ohne die Basisvorgabe-Annahme unter Verwendung von 25 Beobachtungsstellen in den Parallel-Experimenten. Für beide Verfahren wurden die RMSE des Wellenspektrums im gesamten Modellgebiet um ca. 50% reduziert. Das angewandte Experiment zeigte, dass die RMSE des Wellenspektrums an der Validierungs-Boje um mehr als 60% abnahm, wenn das angepasste Assimilationsverfahren mit Beobachtungen einer einzelnen in situ Boje verwendet wurde. Die Ergebnisse weisen darauf hin, dass das entwickelte 4D variationelle Datenassimilationsverfahren die Modellergebnisse unter Wellenbedingungen, bei denen nichtlineare Interaktionen nicht signifikant sind, effektiv verbessern kann. Das modifizierte Verfahren mit "Basisannahmen" kann in Küstengebieten in denen die räumliche Messdichte begrenzt ist, angewendet werden, vorausgesetzt der Seegang im Gebiet weist eine starke räumliche Korrelation auf.

# Contents

# List of Figures

# List of Tables

# Chapter 1

# Introduction

## 1.1 Overview

Ocean surface waves, as a most common and visible ocean phenomenon, have risen the research attention of human kind for thousands of years. Nowadays, studies on ocean waves from planetary-scale Rossby waves to diurnal-scale tidal waves or even second-scale wind induced waves, constitute the foundation of oceanography (Massel, 1996). Especially, when it comes to human activities such as marine transportation, fishery, coastal engineering or other offshore exploitation, the importance of the small-scale wind induced waves can not be overestimated. Also, wind waves play a crucial role in other coastal processes. They are a important force for sediment transport and the energy exchange between waves and currents leads to complicated nearshore flow patterns. Furthermore, in present world, where the shortage of fossil fuel energy is becoming a significant problem, ocean waves are considered as one kind of promising renewable energy which can be harvested in the coastal areas in a relatively convenient way (Antonio, 2010; Gunn and Stock-Williams, 2012). All those researches on the ocean waves require solid and sufficient nearshore wave informations. Thus, this study focuses on simulation and assimilation problems of nearshore wave models.

No doubt, in-situ measurements of sea state, expected to be relatively credible (Portilla, 2009; Young, 1998), make great contributions to revealing wind wave properties. However, the measurements are limited by topography, hydrology or other factors are normally sparse in space, making it difficult to determine wave conditions over whole research ares such as for wave energy farm selections. Nowadays, numerical simulation is becoming a widely-used tool in studies on waves and other oceanic phenomena. A straightforward way to simulate waves is directly solving the momentum equations to obtain sea level fluctuations or water particle motions

with either Euler or Lagrange view. Numerical models based on those equations are called the phase-resolved model which can provide temporary positions and velocities of water particles (Blumberg and Mellor, 1987). However, phase-resolved models require huge amounts of computation resource when simulating small scale processes such as wind waves, making their applications difficult in relatively large areas. On the other hand, uncertainties such as turbulence or other randomized processes make the small scale waves almost impossible to be predicted correctly. Therefore, a statistic view focusing on the evolution of wave energy, by assuming wind waves are combinations of countless sine waves with randomized phases, is widely accepted in wind wave studies (Whitham, 2011). Based on those theories of stochastic waves by Pierson (1952) and Longuet-Higgins (1957), several numerical wave models solving power density or action density balance equations, have been developed and applied in researches and engineering problems. Theoretically, those models can provide relatively credible information of wave conditions with high spatial and temporal coverage giving a good opportunity to evaluate wave energy over whole research area. Recently, some assessment of wave energy potential using the wave informations simulated with the above wave models have been reported (Gallagher et al., 2016; Henfridsson et al., 2007; Iglesias et al., 2009; Iglesias and Carballo, 2010; Nobre et al., 2009; Rusu and Soares, 2009; Stopa et al., 2011). Nevertheless, some of the studies utilized only global wave data for their analysis in coastal areas (Henfridsson et al., 2007; Iglesias et al., 2009; Nobre et al., 2009) and others only paid attention to wave power itself, neglecting other technical, financial and evironmental factors affecting the selection of suitable wave energy farm sites (Iglesias and Carballo, 2010; Rusu and Soares, 2009; Stopa et al., 2011). When it comes to coastal areas, the accuracy of wave models become an inevitable problem.

Compared with large scale global wave models, the accuracy of wave simulations in coastal areas characterized by shallow water depth, small wind fetches and short time periods is more sensitive to wave boundaries, initial conditions, bathymetry and other model inputs. Therefore, to guarantee the credibility of coastal wave models, assimilation techniques combining the model results and observations are widely applied. The basic conception of all assimilation approaches is to find a proper combination of two groups of data making the results have the minimum variance from true values. Based on the Bayesian formulation and the assumption of Gaussian distributions, the problem can be solved by finding the extreme value of a cost function consisting of variances of observations and first guess modeled values (Evensen, 2009). Hence, according to the different approaches used to obtain the extremum, assimilation methods are roughly classified into two categories:

sequential assimilation methods and variational assimilation methods (Fig. 1.1). In the sequential case, the observations are "fed-back" into the model at each time they are available producing a best estimate. In the variational case a feasible state trajectory is found that best fits the observed data over a time window (Lahoz et al., 2010). Various assimilation schemes based on Optimum interpolations (OI), Kalman filter (KF) and 4D variational assimilations (4DVAR) belonging to either of the two categories are developed for wave models (Emmanouil et al., 2010, 2012; Greenslade, 2001; Hasselmann et al., 1997; Hersbach, 1998; Lionello et al., 1992; Sannasiraj et al., 2006; Siddons et al., 2009; Voorrips et al., 1997, 1999). It is difficult to conclude which scheme is the most suitable one for nearshore wave simulations since each one has its own deficiencies and strengths. Among them, the schemes by means of 4D variational assimilation method usually perform better than relatively simple schemes with OI and requires fewer computation resources than schemes with Kalman filter. Besides, 4D variational assimilation method is more convenient to be applied to correct other model inputs apart from sea state itself. Nevertheless, the variational method is normally expensive to develop since in most cases, complex models such as tangent linear equations or adjoint models need to be coded, making assimilation schemes with that method intimately tied to a particular model difficult to be attached to a different one (Talagrand, 2012).

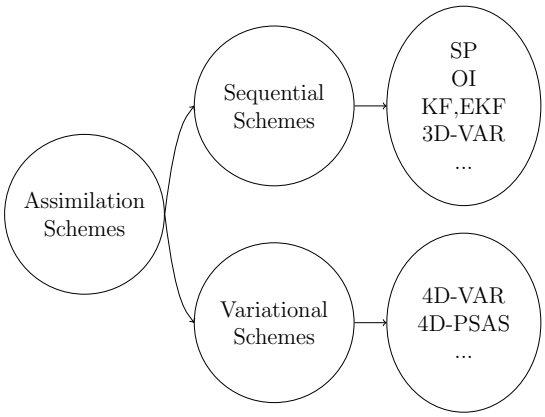


Figure 1.1: Applied data assimilation schemes. SP (Successive Correction); OI (Optimal Interpolation); KF (Kalman Filter); EKF (Extended Kalman Filter); 3D-VAR (3D Variational); 4D-VAR (4D Variational); 4D-PSAS (4D Physical-space Statistical Analysis System);

This work intends to provide a feasible method for wave farm selection in coastal areas with wave information from numerical wave models. At the same time, a 4D variational assimilation scheme suitable for nearshore wave simulation is developed so as to confirm the model accuracy. In order to identify wave energy and error sources, two important contributions of wave systems in coastal areas, swells and

windsea, are discussed separately in the assembled three papers. Wave processes are regarded as the superposition of the two contributions in the assimilation scheme. New approaches are proposed to improve the effect of the developed assimilation scheme in practical applications with limited observations in space. Two coastal areas, the south coast of the Java Island and the German Bight are introduced in this study. Detailed information and related questions regarding those areas will be presented in the next chapters, outlining the motivation for the papers assembled in this work.

## 1.2 Wave energy along the coast of the Java Island

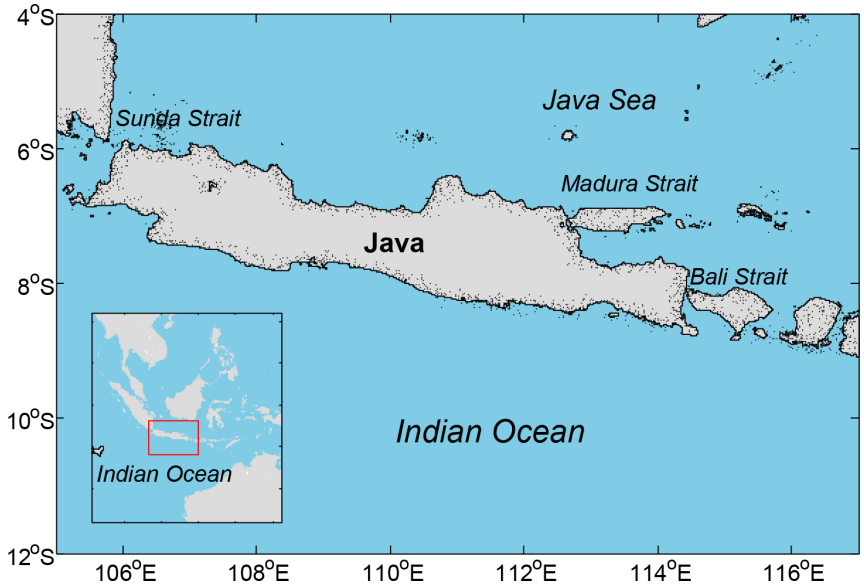


Figure 1.2: The south coast of the Java Island

The wave energy level is usually expressed as power per unit length (along the wave crest or along the shoreline direction) named power density. The regions with annual average power above 20 kW/m are regarded as having 'good' wave conditions (Antonio, 2010; Arinaga and Cheung, 2012). Obviously, the energy of wind induced waves mainly come from wind inputs and grows through oceans. As the waves propagate and grow with the wind, coasts in the downwind direction are expected to have suitable wave conditions for energy extraction. As it is known, the westerlies in the mid-latitude region have the broadest fetch with the persistent wind direction from west to east on the earth making the suitable areas for wave farms mostly occurring along the east coast of oceans (Arinaga and Cheung, 2012). The

westerlies are relatively strong in the southern hemisphere where less area is covered by land. Furthermore, seasonal variations are in general considerably larger in the northern than in the southern hemisphere, which makes the west coasts of South America, Africa and Australia particularly attractive for wave energy exploitation (Antonio, 2010).

Java Island is surrounded by the Java Sea to the north, Sunda Strait to the west, the Indian Ocean to the south and Bali Strait and Madura Strait in the east (Fig. 1.2). In the Indian Ocean, the west and south coast of Australia, as the boundary of the fetch of the westerlies, have an average annual wave power of 60 kW/m during the winter months (Arinaga and Cheung, 2012; Hughes and Heap, 2010). Some instruments for wave energy extraction called wave energy converters have already been deployed there (Antonio, 2010). Since the main direction of these swells are northeast, it is expected that they approach the south coast of Java Island with considerable wave energy. Apart from those swells from median latitude area, Java island is dominated by the Indo-Australian monsoon system. The seasonal varying monsoon induced waves are supposed to have a great influence on the wave climate in this area. Therefore, to reveal the wave climate and address the wave problems in this area, wave information over the whole coast covering at least two seasons is required.

However, wave climate is not the only limitation for deployment of wave energy farms. There are various types of wave energy converters such as: oscillating water column, oscillating body systems and overtopping systems. Different types of converters have different ranges of mooring depth (from dozens meters to thousands meters) and require different hydrologic conditions (Antonio, 2010). The extraction efficiency is also different making it difficult to estimate the exploitable wave energy. For example, the efficiency of the converter Pelamis in the Spanish nearshore area is around 20% and that of the converter Wave Dragons in the same area is around 40% (Rusu, 2014). Transportation cost of the extracted power, maintaining cost of the instruments and other financial issues determine whether the wave farms are valuable. Additionally, since the extraction of wave energy will change the wave conditions nearby, some environmental issues such as sediment deposition after the deployment should be considered as well. Nevertheless, it is still possible to find a set of general criteria to roughly assess suitable locations for wave energy farms.

The main objectives and questions regarding the wave energy along the coast of the Java Island in this study are:

- Are the wave conditions in this area adequate for wave energy extraction?
- How do swells and local wind contribute to the wave energy in this region?

- How to select wave energy farms considering the wave climate and other environmental aspects?

To address those questions, the aim of the work in Ch. 2 is to:

- Analyze the long-term variations of wave conditions in this area.
- Setup a credible coastal wave model to provide sufficient wave information and estimate the potential wave power in nearshore area.
- Set general criteria based on different conditions. Select suitable locations for wave farms.

## 1.3 Nearshore wave assimilation system

For the wave models concentrating on nearshore wave processes, such as the coastal wave model applied here for wave energy assessments, not only local wind inputs but also wave boundary inputs are crucial. The input wave conditions and wind fields normally are provided by global models of which accuracy can not be guaranteed in coastal areas. In fact, results from different global models are inconsistent in some sea areas (Stopa and Cheung, 2014). Expanding the computational domain to open seas may ease the problem but computation cost will be extremely increased. On the other hand, some of the source and sink terms in the balance equation applied in the phase-average wave models are empirical or based on observations in specific sea areas, which makes the related coefficients inappropriate when the models are applied in other areas with entirely different wave climates. Therefore, observations ether in-situ or remote are always required to ensure the credibility of the wave models. Data assimilation is an efficient technique to combine observations and wave model results to improve the model performance.

Early attempts of data assimilation applications in wave simulations started from 1980s with the rise of remote sea surface observations. The most implemented assimilation method in wave models is optimum interpolations (Portilla, 2009). The OI method is a simple sequential assimilation method requiring relative low computation cost by replacing the evolving background error covariance matrix with a constant one (Lahoz et al., 2010). The assumption of constant covariance matrix makes the method easier and cheaper to be applied. But obviously the constant covariance matrix will become inaccurate with the extension of assimilation windows and consequently, decay the assimilation effect. Kalman filter is another widely

applied sequential assimilation method. The Kalman filter and the subsequent extended Kalman filter (EKF) (Kalman et al., 1960) are able to guarantee the accuracy of the background error covariance matrix to some extend by evolving the covariance matrix with forward models, but at the same time, the evolution requires a huge storage space and lowers the assimilation efficiency. Besides, the ideal of sequential assimilation method, that the forward model gets fed-back at the time when observations are available, is more suitable to directly adjust initial condition for a forecasting system. Involving observations only at one time point is obviously not sufficient to choose model inputs such as wave boundary conditions and winds as control variables. This is due to the fact that those model inputs force the forward model thereby affecting waves constantly during a period and normally cannot be instantly reflected by observed sea states. On the contrary, variational assimilation method can find sets of model inputs fitting the observations best over an assimilation window. In that sense, a 4D variational assimilation scheme is more suitable for nearshore wave simulations in this study.

### 1.3.1 4D variational scheme

For 4Dvar schemes, the adjoint technique is the most commonly used method to minimize the cost functions by revealing its advantage in reducing the computational load especially for control vectors with high dimensions. Generally, there are two ways to obtain the adjoint model for forward models. One is deriving the adjoints from the analytical form of governing equations and discretizing them later. The other is deriving the adjoint model directly from the discretized governing equations which is applied in the forward models. Both ways work and have been applied in some studies: De Las Heras et al. (1994) and Veeramony et al. (2010) obtained the analytical adjoints, and Hersbach (1998) and Orzech et al. (2013) directly derived the discretized adjoint model using a so called adjoint compiler. The main advantage of the adjoint compiler is that non-linear terms in governing equations can be easily preserved, while deriving the analytical adjoints for non-linear terms is far more complex. On the other hand, nonlinear wave-wave interactions redistribute the wave energy in frequencies and directions through wave evolutions. The most important part of the interaction is the energy transfer between swell and windsea contributions. Nevertheless, the assimilation task in this study is going to consider the errors from both local winds and swells simultaneously, making identification and classification for different wave energy contributions important. If the interactions between those two contributions are significant, the classification will become difficult thereby degrading the assimilation effect crucially. Therefore, for

this study, only wave conditions without strong wave-wave non-linear interactions are considered. In this case the analytical adjoints become more straightforward to apply.

As mentioned above, classification of wave energy contributions is crucial for the assimilation. Some simple classification criteria based on wave age such as the formula provided by Komen et al. (1984) require accurate wind informations. Some others based on Pierson-Moskowitz (PM) spectrum by Pierson and Moskowitz (1964) are far too simple to work properly under varying wave conditions. Another widely used effective algorithm to separate different wave systems is the so called partition method, which is able to split the 2D wave spectrum into windsea and swell components taking the topography of the spectrum into account (Waters et al., 2013). Partition method has been applied in wave simulations since the early 1990s (Gerling, 1992; Voorrips et al., 1997; Hasselmann et al., 1997). The partition methods are appropriate in studies in which the accuracy of wind fields is doubtful, since they separate wave energy contributions by utilizing watershed algorithms which are mainly based on wave spectra themselves.

Hence, the desired variational wave assimilation scheme is revealed:

- A 4D variational scheme with adjoint method.
- Suitable for nearshore wave model taking swell and windsea contributions into account.

To fulfill the demands, the aim of the present work in Ch. 3 is to:

- Derive the analytical adjoints and discretize them to establish the adjoint model.
- Select proper partition algorithm to perform assimilations separately.
- Validate the adjoint model.
- Design twin experiments to assess the developed assimilation scheme.

### 1.3.2 Application in the German Bight

Apart from the schemes themselves, there are several external factors affecting the performance of assimilation schemes in applications. For example, background and observation error covariance matrixes are usually unknown, whereas the accuracy of those matrixes is crucial for assimilations by constituting gain matrix in the

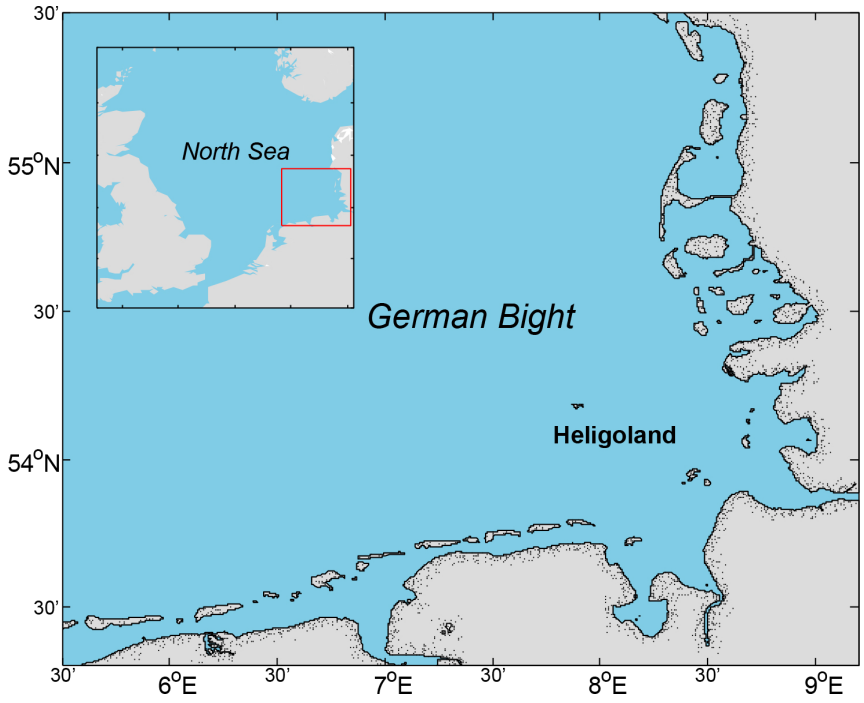


Figure 1.3: The German Bight

Kalman filters or serving as weights of cost functions in variational schemes. However, in most studies on ocean waves, the error covariance of sea states or winds are estimated by a priori exponential decay curves with respect to distance (Greenslade and Young, 2004). Obviously the accuracy cannot be guaranteed. Besides, usually only the error covariance of wave total energy are estimated but the covariance of spectra in different frequencies and directions are dismissed. Some studies have tried to improve the error covariance estimation by providing a more physical-based estimate curve (Portilla, 2009). Nevertheless, even once the accurate error covariance are obtained, the question is, does the assimilation scheme still work with a reduced number of observations in space and time?

Therefore, the study in Ch. 4 concentrates on the application problem of the developed 4D variational assimilation scheme. The German Bight, in the southeastern North Sea is selected as the research area (see Fig. 1.3). The motivation to choose the German bight includes two aspects. First of all, the North Sea is one of the sea areas which are most frequently observed and studied. Therefore, relatively accurate bathymetry data are available. Furthermore, many empirical formulas or coefficients applied in wave models are obtained based on the observations in North Sea (Hasselmann et al., 1973). So, it is expected that in this area, the errors of some experimental coefficients which are not considered in the assimilation scheme can be kept as small as possible. Secondly, the wave conditions are various in the German Bight. Sometimes the swells from the northwest or southwest dominate the bight

and sometimes pure windsea waves are caused by the easterly winds (Hasselmann et al., 1973), providing a good opportunity to assess the scheme under different wave conditions and to examine the applied partition method as well. But still the in-situ observations are limited. Although some high frequency radars have been deployed in the area, credible wave data from the radars are not available for now (Gurgel et al., 2011; Wahle et al., 2015). Hence, a solution guaranteeing the assimilation effect with limited observations is demanded.

There are several problems when applying the scheme into the German Bight:

- How does observation coverage affect the assimilation effect in the German Bight?
- How to modify the assimilation scheme to make it more effective when observations are limited?

To address those questions, the aim of the work in Ch. 4 is to:

- Find out the impact of the observation coverage on the scheme.
- Propose a modified scheme that can work with limited observations
- Assess the modified scheme in the German Bight.

# Bibliography

Antonio, F. d. O. (2010). Wave energy utilization: A review of the technologies. *Renewable and sustainable energy reviews*, 14(3):899–918.

Arinaga, R. A. and Cheung, K. F. (2012). Atlas of global wave energy from 10 years of reanalysis and hindcast data. *Renewable Energy*, 39(1):49–64.

Blumberg, A. F. and Mellor, G. L. (1987). A description of a three-dimensional coastal ocean circulation model. *Three-dimensional coastal ocean models*, pages 1–16.

De Las Heras, M. M., Burgers, G., and Janssen, P. a. E. M. (1994). Variational Wave Data Assimilation in a Third-Generation Wave Model. *Journal of Atmospheric and Oceanic Technology*, 11(5):1350–1369.

Emmanouil, G., Galanis, G., and Kallos, G. (2010). A new methodology for using buoy measurements in sea wave data assimilation. *Ocean dynamics*, 60(5):1205–1218.

Emmanouil, G., Galanis, G., and Kallos, G. (2012). Combination of statistical kalman filters and data assimilation for improving ocean waves analysis and forecasting. *Ocean Modelling*, 59:11–23.

Evensen, G. (2009). *Data Assimilation: The Ensemble Kalman Filter*.

Gallagher, S., Tiron, R., Whelan, E., Gleeson, E., Dias, F., and McGrath, R. (2016). The nearshore wind and wave energy potential of ireland: a high resolution assessment of availability and accessibility. *Renewable Energy*, 88:494–516.

Gerling, T. W. (1992). Partitioning sequences and arrays of directional ocean wave spectra into component wave systems. *Journal of atmospheric and Oceanic Technology*, 9(4):444–458.

Greenslade, D. (2001). The assimilation of ers-2 significant wave height data in the australian region. *Journal of Marine Systems*, 28(1):141–160.

Greenslade, D. J. and Young, I. R. (2004). Background errors in a global wave model determined from altimeter data. *Journal of Geophysical Research: Oceans*, 109(C9).

Gunn, K. and Stock-Williams, C. (2012). Quantifying the global wave power resource. *Renewable Energy*, 44:296–304.

Gurgel, K.-W., Schlick, T., Voulgaris, G., Seemann, J., and Ziemer, F. (2011). Hf radar observations in the german bight: Measurements and quality control. In *Current, Waves and Turbulence Measurements (CWTM), 2011 IEEE/OES 10th*, pages 51–56. IEEE.

Hasselmann, K., Barnett, T. P., Bouws, E., Carlson, H., Cartwright, D. E., Enke, K., Ewing, J. a., Gienapp, H., Hasselmann, D. E., Kruseman, P., Meerburg, a., Muller, P., Olbers, D. J., Richter, K., Sell, W., and Walden, H. (1973). Measurements of Wind-Wave Growth and Swell Decay during the Joint North Sea Wave Project (JONSWAP). *Ergnzungsheft zur Deutschen Hydrographischen Zeitschrift Reihe*, A(8)(8 0):p.95.

Hasselmann, S., Lionello, P., and Hasselmann, K. (1997). An optimal interpolation of spectral wave data. *Journal of Geophysical Research*, 102(C7):15,823–15,836.

Henfridsson, U., Neimane, V., Strand, K., Kapper, R., Bernhoff, H., Danielsson, O., Leijon, M., Sundberg, J., Thorburn, K., Ericsson, E., et al. (2007). Wave energy potential in the baltic sea and the danish part of the north sea, with reflections on the skagerrak. *Renewable Energy*, 32(12):2069–2084.

Hersbach, H. (1998). Application of the adjoint of the WAM model to inverse wave modeling. *J. Geophys. Res.*, 103:10469–10487.

Hughes, M. G. and Heap, A. D. (2010). National-scale wave energy resource assessment for australia. *Renewable Energy*, 35(8):1783–1791.

Iglesias, G. and Carballo, R. (2010). Wave energy resource in the estaca de bares area (spain). *Renewable Energy*, 35(7):1574–1584.

Iglesias, G., López, M., Carballo, R., Castro, A., Fraguela, J. A., and Frigaard, P. (2009). Wave energy potential in galicia (nw spain). *Renewable Energy*, 34(11):2323–2333.

Kalman, R. E. et al. (1960). A new approach to linear filtering and prediction problems. *Journal of basic Engineering*, 82(1):35–45.

Komen, G., Hasselmann, K., and Hasselmann, K. (1984). On the existence of a fully developed wind-sea spectrum. *Journal of physical oceanography*, 14(8):1271–1285.

Lahoz, W., Khattatov, B., and Menard, R. (2010). *Data assimilation: making sense of observations*. Springer Science & Business Media.

Lionello, P., Günther, H., and Janssen, P. A. (1992). Assimilation of altimeter data in a global third-generation wave model. *Journal of Geophysical Research: Oceans*, 97(C9):14453–14474.

Longuet-Higgins, M. S. (1957). The statistical analysis of a random, moving surface. *Philosophical Transactions of the Royal Society of London A: Mathematical, Physical and Engineering Sciences*, 249(966):321–387.

Massel, S. R. (1996). *Ocean surface waves: their physics and prediction*, volume 11. World scientific.

Nobre, A., Pacheco, M., Jorge, R., Lopes, M., and Gato, L. (2009). Geo-spatial multi-criteria analysis for wave energy conversion system deployment. *Renewable energy*, 34(1):97–111.

Orzech, M. D., Veeramony, J., and Ngodock, H. (2013). A variational assimilation system for nearshore wave modeling. *Journal of Atmospheric and Oceanic Technology*, 30(5):953–970.

Pierson, W. J. (1952). A unified mathematical theory for the analysis, propagation and refraction of storm-generated ocean surface waves, part 1 and 2. *NYU, Coll. of Eng., Res. Div.*, 461.

Pierson, W. J. and Moskowitz, L. (1964). A proposed spectral form for fully developed wind seas based on the similarity theory of sa kitaigorodskii. *Journal of geophysical research*, 69(24):5181–5190.

Portilla, J. (2009). *Buoy data assimilation in nearshore wave modeling*. PhD thesis, Ph D dissertation, KU Leuven, Belgium.

Rusu, E. (2014). Evaluation of the wave energy conversion efficiency in various coastal environments. *Energies*, 7(6):4002–4018.

Rusu, E. and Soares, C. G. (2009). Numerical modelling to estimate the spatial distribution of the wave energy in the portuguese nearshore. *Renewable Energy*, 34(6):1501–1516.

Sannasiraj, S., Babovic, V., and Chan, E. S. (2006). Wave data assimilation using ensemble error covariances for operational wave forecast. *Ocean Modelling*, 14(1):102–121.

Siddons, L. a., Wyatt, L. R., and Wolf, J. (2009). Assimilation of HF radar data into the SWAN wave model. *Journal of Marine Systems*, 77(3):312–324.

Stopa, J. E. and Cheung, K. F. (2014). Intercomparison of wind and wave data from the ecmwf reanalysis interim and the ncep climate forecast system reanalysis. *Ocean Modelling*, 75:65–83.

Stopa, J. E., Cheung, K. F., and Chen, Y.-L. (2011). Assessment of wave energy resources in hawaii. *Renewable Energy*, 36(2):554–567.

Talagrand, O. (2012). Four-Dimensional Variational Assimilation-I. *Les Houches Data Assimilation Summer School*.

Veeramony, J., Walker, D., and Hsu, L. (2010). A variational data assimilation system for nearshore applications of SWAN. *Ocean Modelling*, 35(3):206–214.

Voorrips, A., Heemink, A., and Komen, G. (1999). Wave data assimilation with the kalman filter. *Journal of Marine Systems*, 19(4):267–291.

Voorrips, a. C., Makin, V. K., and Hasselmann, S. (1997). Assimilation of wave spectra from pitch-and-roll buoys in a North Sea wave model. *Journal of Geophysical Research*, 102(C3):5829.

Wahle, K., Staneva, J., and Guenther, H. (2015). Data assimilation of ocean wind waves using Neural Networks: A case study for the German Bight. *Ocean Modelling*, 96:117–125.

Waters, J., Wyatt, L. R., Wolf, J., and Hines, A. (2013). Data assimilation of partitioned HF radar wave data into Wavewatch III. *Ocean Modelling*, 72:17–31.

Whitham, G. B. (2011). *Linear and nonlinear waves*, volume 42. John Wiley & Sons.

Young, I. (1998). An intercomparison of geosat, topex and ers1 measurements of wind speed and wave height. *Ocean Engineering*, 26(1):67–81.

# Chapter 2

# Wave energy potential

*Assessment of wave energy potential along the south coast of Java Island.* Song, Q. and R. Mayerle. IOP Conference Series: Earth and Environmental Science (EES). 2018.

# Assessment of wave energy potential along the south coast of Java Island

**Qingyang Song and Roberto Mayerle**

**Abstract:** *The south coast of Java Island has a great potential for wave energy. A long-term analysis of a 10-year wave dataset obtained from the ERA-Interim database is performed for preliminary wave energy assessment in this area, and it was seen that the annual median power is expected to exceed 20 kW/m along the coast. A coastal wave model with an unstructured grid was run to reveal the wave conditions and to assess the wave energy potential along the coast in detail. The effect of swells and local wind on the wave conditions is investigated. Annual median wave power, water depth and distance from the coast are selected as criteria for the identification of suitable locations for wave energy conversion. Two zones within the study area emerge to be suitable for wave energy extraction. Swells from the southwest turned out to be the major source of wave energy and highest monthly median wave power reached about 33 kW/m.*

**Keywords:** wave energy; swell; local wind; coastal wave model; Java; Indonesia

## 2.1 Introduction

Wave energy has recently become the interest of many researchers around the world. Several studies on global wave resource based on the data obtained from global wave models such as ECMWF (European Centre for Medium-Range Weather Forecasts) and NWW3 (National Oceanic and Atmospheric Administration WAVEWATCH III) reveal that higher wave heights are more likely to appear on the east coast of oceans in both hemispheres (Pontes et al., 2002; Antonio, 2010; Arinaga and Cheung, 2012). As Fig. 2.1 shows, the south of Java Island in Indonesia has a coast to the east of Indian Ocean. In the southern Indian Ocean, wave activities

are heightened due to strong westerlies in mid-latitude area and propagate north where they combine with trade wind waves as swells (Arinaga and Cheung, 2012). Based on the wave energy atlas from Arinaga and Cheung (2012), the highest power for primary swell appears off the western Australian coast, reaching an average of 60kW/m during the winter months of the southern hemisphere. Since the main direction of these swell are northeast, they reach the Java Island with considerable wave energy. Another advantage of exploiting the wave energy in this area is that the seasonal variation of wave conditions is much lower than in most areas of the Northern Hemisphere (Antonio, 2010). Thus, wave converters can give more stable output power throughout the year and the lower appearance of extreme conditions can reduce the costs of wave projects (Pontes et al., 2002).

Site selection for the installation of wave energy devices depends on available power, site characteristics, and possible environmental and socio-economic impacts of the projects. However, wave conditions are still decisive criteria (Nobre et al., 2009). Several studies have successfully applied wave models to assess the wave energy potential at different locations in Europe and North America utilizing the wave data covering around 10 years from WAM or WAVEWATCH III to analyze the long-term wave variability and to roughly estimate exploitable wave energy (Henfridsson et al., 2007; Iglesias et al., 2009; Iglesias and Carballo, 2010; Stopa et al., 2011). Coastal wave models with refined computational grids and more accurate bathymetric data were also put in progress to determine optimum locations for a wave farm in those studies.

In this study, results of an assessment of the wave conditions and the wave energy potential in the south coast of Java Island are presented.

## 2.2 Methodology

Ocean waves are the result of occurrence of a certain number of individual wave systems originating from different meteorological events. Within the investigated domain in this study, waves produced in the Indian Ocean spreading to the south coast of Java Island, and local winds, as a part of the monsoon system, are main sources of wave energy. Therefore, different wave systems due to swell and local wind can be expected, and separate parameters for the windsea waves and swells allow estimation of the power from the dominant wave components using respective peak periods. Thus, precise information can be provided for planning and design of wave farms (Arinaga and Cheung, 2012). Generally, the wave conditions and the associated wave energy in the area are assessed in different time scales. The year-

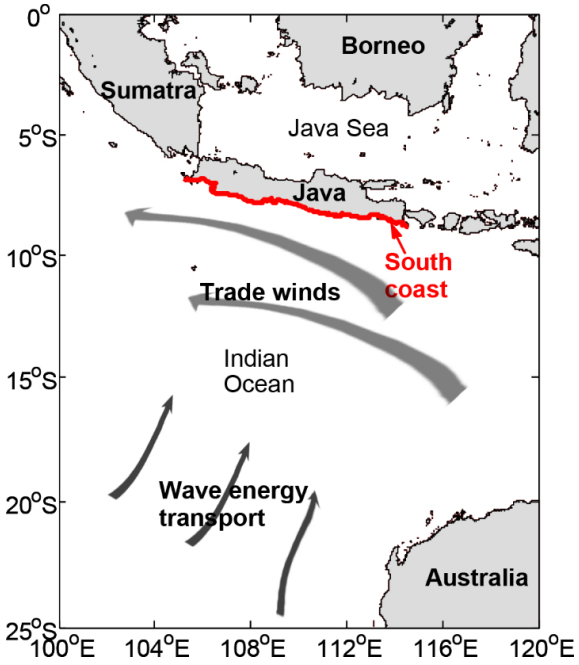


Figure 2.1: Overview of the wind and wave environment surrounding the south coast of Java Island.

to-year variability of the wave conditions is revealed by long-term analysis. After that, the detailed seasonal variations as well as the evolutions over swell events of the wave condition and the wave energy in coastal area are presented through wave simulations.

### 2.2.1 Wave data and numerical models

The ERA-Interim dataset from ECMWF is chosen for a long-term wave analysis. It provides 6-hourly values on significant wave height, mean wave period and wave direction (Dee et al., 2011). The data from ECMWF in deep water are more credible than in coastal areas due to topographical conditions (Stopa and Cheung, 2014). The wave conditions in deep water along the coast using wave data covering 10 years (2004-2014) are analyzed to evaluate the wave potential in down-wave directions, and to reveal year-to-year and longer-term variability (Pontes et al., 2002). For the analysis, 18 points along the 2000 m isobath line off the coast are selected (Fig. 2.2). The wave data from ERA-Interim are also utilized to drive the coastal wave model. Numerical wave simulations are performed with SWAN to reveal detailed wave conditions near the coast. An unstructured triangle grid is constructed and applied to keep the high resolution in the coastal area, and avoiding unnecessary computation resource cost in deep water (Fig. 2.3). The coarsest meshes are on the open boundary matching the grid of the ERA-Interim dataset with a resolution

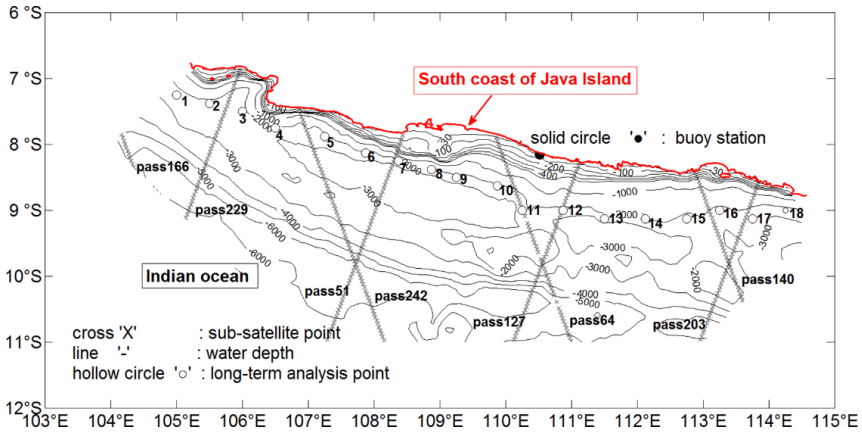


Figure 2.2: Study domain with bathymetry and locations of satellite tracks, wave buoy station and long-term analysis points

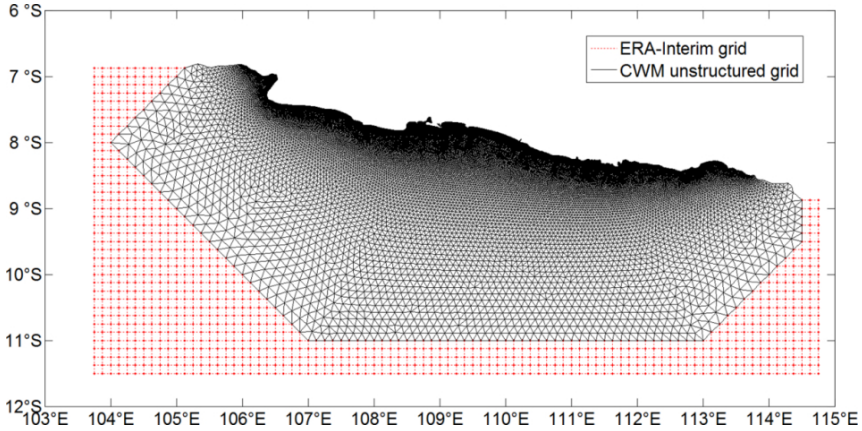


Figure 2.3: Established unstructured mesh grids in the study area

around 14 km, while the finest meshes are off the coast with an average resolution of about 500 m. The criteria based on a 2D spectrum, which have been used also in WAM, are implemented in SWAN for the wind-swell-wave identification (Komen et al., 1994). The criteria formulation is based on wave age $U_{10}/c_p$, shown in the inequation below:

$$\beta \frac{U_{10}}{c_p} \cos(\theta - \phi) > 1 \tag{2.1}$$

where $\theta$ is wave direction, $\phi$ is wind direction, $c_p$ is phase speed and $U_{10}$ is wind speed in 10 m height above sea surface. $\beta$ is a calibration factor which is typically set to be smaller than 1.3 in the region of pure wind sea. (Hasselmann et al., 1996).

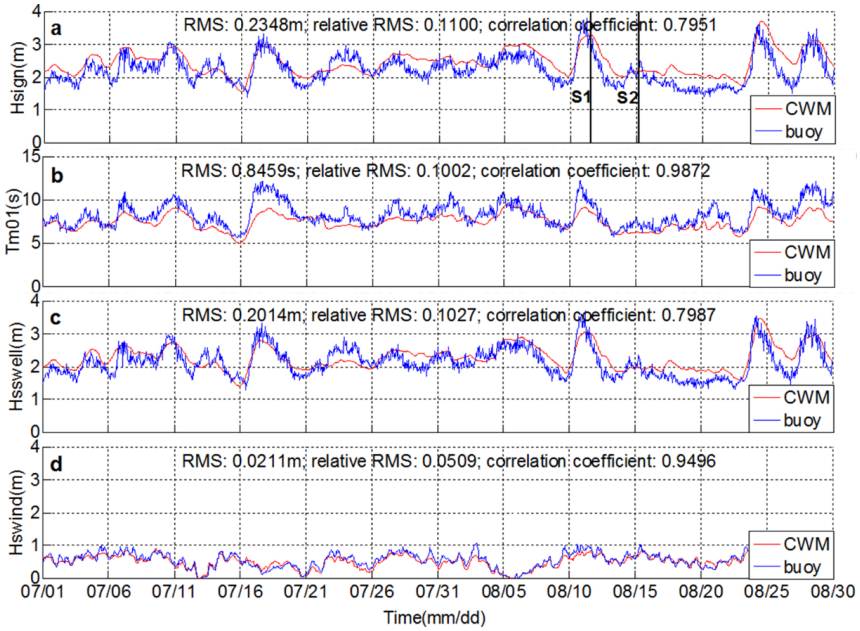


Figure 2.4: Comparison of time series between CWM and buoy: (a) significant wave height; (b) mean wave period; (c) significant wave height due to swells; (d) significant wave height due to local winds.

### 2.2.2 Wave model validation

Coastal wave model (CWM) is validated based on both wave buoy and satellite data. Location of the wave buoy, which generates raw north, west and vertical displacements at a rate of 1.28 Hz, is indicated in Fig. 2.2. Fig. 2.4a-b show the comparisons of significant wave height and mean wave period between CWM and buoy observations, and the comparison of significant wave height due to swell ($H_{sswell}$) and local wind ($H_{swind}$) can be seen in Fig. 2.4c-d. They also reveal that the main wave energy comes from swell at the location of the buoy. The satellite altimeter data from Jason-2, provided by AVISO (Achieving Validation and Interpolation of Satellite Oceanographic Data), is also employed to validate the model due to lack of in-situ wave measurements along the south coast of Java Island. The dataset contains significant wave height only. The measurement interval at one sub-satellite point is about 10 days. The locations of sub-satellite points on 8 passes in the model domain are showed in Fig. 2.2. Fig. 2.5a-b show significant wave height scatter plot of CWM versus altimetry data from Jason-2. The figures show that CWM has a better agreement with altimetry data in the dry season (2014/5 to 2014/10) than in the rainy season (2013/11 to 2014/04). It is seen that the difference of significant wave height between CWM and the altimetry data are usually smaller than 0.5 m. Fig. 2.6a-d reveals that swells dominate the wave field both in extreme wave condition (Fig. 2.6a-b) and the average wave condition (Fig. 2.6c-d). Primary

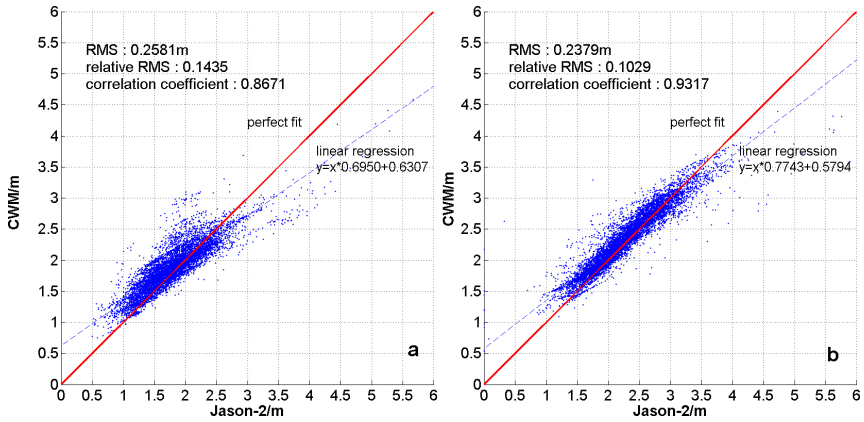


Figure 2.5: Significant wave height scatter plot of CWM versus altimetry data from Jason-2: (a) rainy season; (b) dry season.

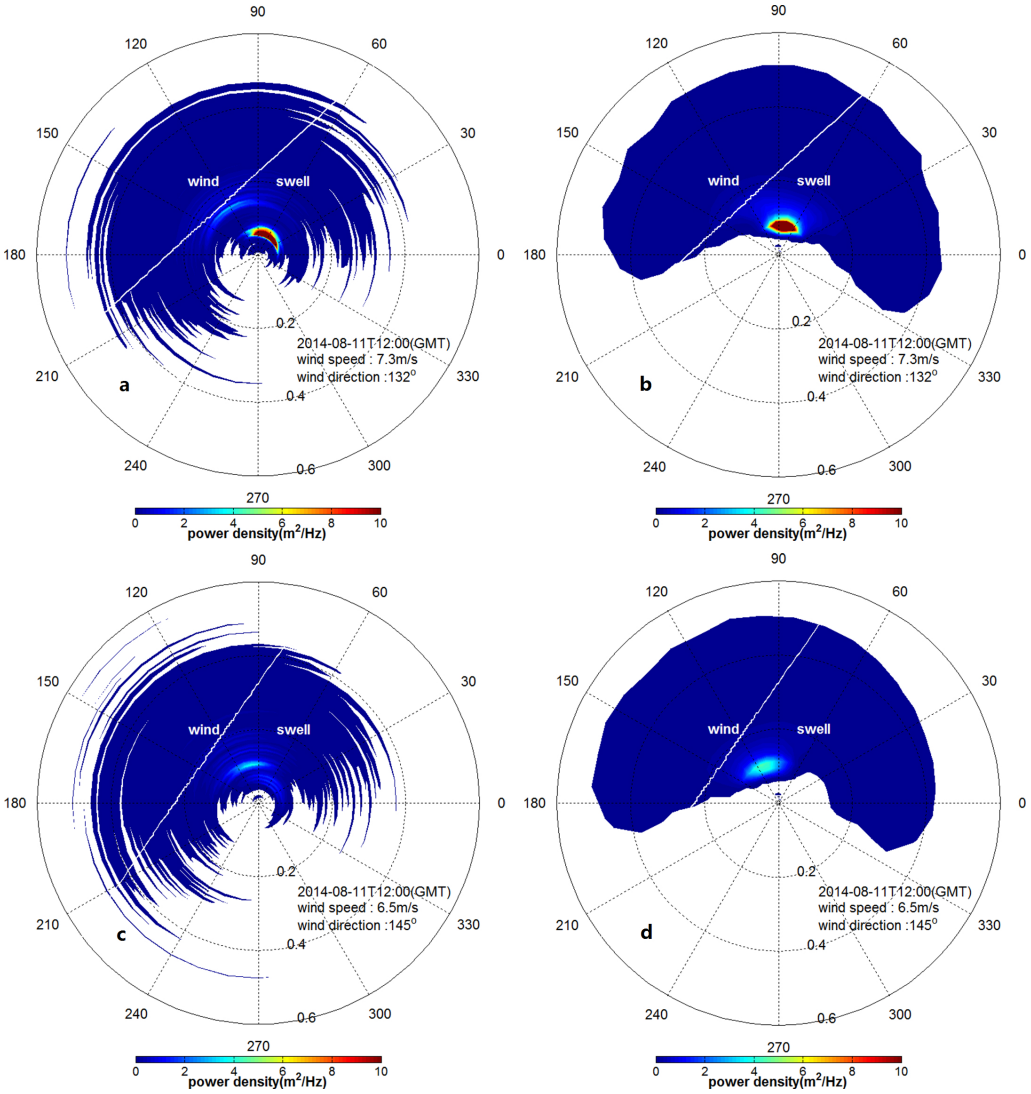


Figure 2.6: 2D spectrum comparison between CWM and buoy: (a, c) buoy; (b, d) CWM.

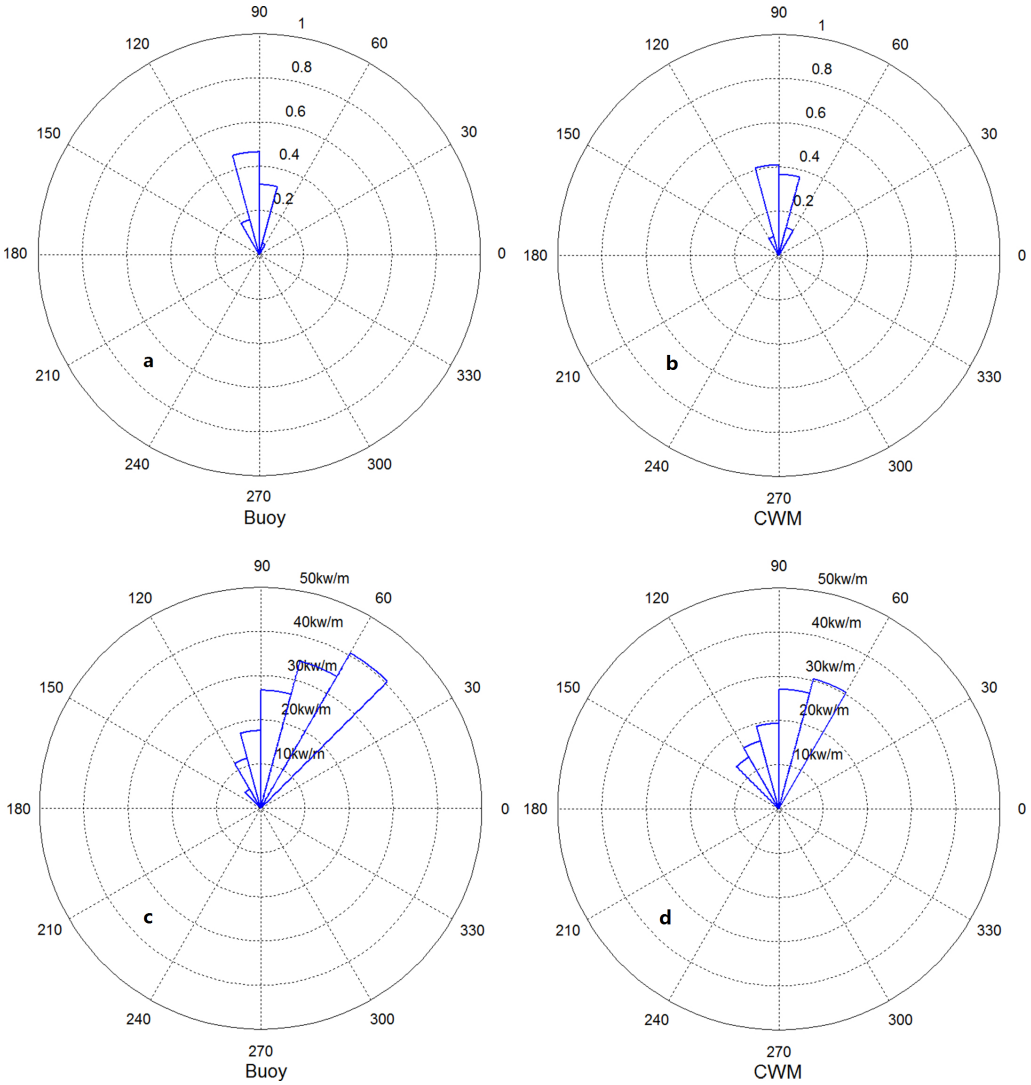


Figure 2.7: Wave rose (a,b) and average wave power (c,d) from 24/05/2014 to 16/09/2014.

swells in two time points (S1, S2 in Fig. 2.4a) are from different directions. In the southern hemisphere, the strong westerlies result in heightened wave activities in mid-latitude throughout the year and those waves combine with the trade wind waves when propagate to north (Arinaga and Cheung, 2012). This fact implies that the southwesterly primary swell in the extreme wave condition is due to the westerlies while the southeasterly primary swell in the average wave condition is due to the trade wind. Analysis showed that most waves in studied domain come from south direction. Peak wave direction is in a directional sector of 60 degree, and waves from southwest contain more energy (Fig. 2.7).

## 2.3 Characterization of wave energy potential in the study area

### 2.3.1 Long term analysis of wave data

The 10-year wave data from the 18 points along the 2000 m isobath line off the coast are analyzed in this section. Results are shown in table 1 and table 2. Mean significant wave height is about 2.04 m and the mean wave period is about 10.69 s. The inter-annual variation of these two wave parameters is small. In addition, significant wave height in dry seasons is higher than in rainy seasons with a mean difference of about 0.43 m. Furthermore, mean wave period in dry seasons is approximately 0.4 s higher than rainy seasons. Since the points for the analysis are located in deep waters, mean annual median wave power can be estimated with the wave statistic parameters as follows by Waters et al. (2009):

$$P = \frac{\rho g^2}{64\pi} H_s^2 T_{m01} \tag{2.2}$$

where $\rho$ is water density, $g$ is gravitational acceleration, $H_s$ is significant wave height, $T_{m01}$ is mean wave period. Estimated mean annual median wave power based on Eq. (2.2) is 22 kW/m, while required annual median wave power for most commercial wave energy converters is around 20 kW/m (Antonio, 2010). From Table 1, it can also be seen that the seasonal variation of wave power in this area is insignificant. Even in rainy seasons, the seasonal median wave power reaches 17 kW/m. Spatial variations of the two wave parameters along the coast can be found in Table 2. Generally, mean wave period in the west part of the coast is lower than in the east part, while the significant wave height does not show a similar pattern. Highest average significant wave height of about 2.14 m and highest average wave power of 23.89 kW/m appear at point 11. On the other hand, the lowest average significant wave height of about 1.91 m is observed at point 18 (figure 1), while the lowest average wave power is observed at point 2. Although the long-term analysis reveals the wave conditions and the wave energy distributions along the coast, more detailed evaluations of regional wave conditions with CWM are required for the wave energy assessment.

Table 2.1: Temporal variations of average wave statistic parameters from 2004 to 2014.

| year | Hs(m) | | | Tm01(s) | | | Power(kW/m) | | |
|---|---|---|---|---|---|---|---|---|---|
| | An. | Dry | Rainy | An. | Dry | Rainy | An. | Dry | Rainy |
| 04-05 | 2.08 | 2.29 | 1.87 | 11.04 | 11.20 | 10.88 | 23.52 | 28.93 | 18.73 |
| 05-06 | 2.13 | 2.33 | 1.93 | 10.93 | 11.09 | 10.78 | 24.50 | 29.70 | 19.85 |
| 06-07 | 2.08 | 2.33 | 1.83 | 10.82 | 11.08 | 10.55 | 22.97 | 29.55 | 17.34 |
| 07-08 | 2.10 | 2.28 | 1.91 | 10.61 | 10.79 | 10.43 | 22.94 | 27.70 | 18.69 |
| 08-09 | 2.05 | 2.25 | 1.85 | 10.69 | 10.96 | 10.42 | 22.07 | 27.31 | 17.49 |
| 09-10 | 1.89 | 2.14 | 1.64 | 10.56 | 10.78 | 10.33 | 18.55 | 24.93 | 17.38 |
| 10-11 | 1.98 | 2.13 | 1.84 | 10.28 | 10.57 | 9.99 | 19.94 | 23.61 | 16.65 |
| 11-12 | 2.02 | 2.19 | 1.85 | 10.43 | 10.56 | 10.30 | 20.96 | 24.93 | 17.38 |
| 12-13 | 2.07 | 2.28 | 1.85 | 10.77 | 10.91 | 10.63 | 22.66 | 27.98 | 17.95 |
| 13-14 | 2.04 | 2.34 | 1.74 | 10.81 | 10.93 | 10.69 | 22.19 | 29.43 | 16.03 |
| mean | 2.04 | 2.26 | 1.83 | 10.69 | 10.89 | 10.50 | 22.03 | 27.34 | 17.38 |

Table 2.2: Spatial variations of average wave statistic parameters at 18 selected points from 2004 to 2014.

| | Hs(m) | | | Tm01(s) | | | Power(kW/m) | | |
|---|---|---|---|---|---|---|---|---|---|
| | An. | Dry | Rainy | An. | Dry | Rainy | An. | Dry | Rainy |
| 1 | 2.03 | 2.26 | 1.81 | 10.33 | 10.54 | 10.13 | 21.08 | 26.58 | 16.31 |
| 2 | 1.97 | 2.19 | 1.75 | 10.33 | 10.53 | 10.13 | 19.78 | 24.84 | 15.38 |
| 3 | 2.13 | 2.39 | 1.87 | 10.23 | 10.31 | 10.15 | 22.90 | 29.05 | 17.53 |
| 4 | 2.13 | 2.39 | 1.87 | 10.23 | 10.31 | 10.15 | 22.90 | 29.05 | 17.53 |
| 5 | 2.06 | 2.28 | 1.85 | 10.58 | 10.78 | 10.38 | 22.22 | 27.66 | 17.47 |
| 6 | 2.02 | 2.22 | 1.82 | 10.65 | 10.89 | 10.42 | 21.44 | 26.55 | 16.97 |
| 7 | 2.01 | 2.21 | 1.81 | 10.68 | 10.92 | 10.45 | 21.19 | 26.21 | 16.80 |
| 8 | 2.00 | 2.21 | 1.80 | 10.69 | 10.90 | 10.49 | 21.19 | 26.25 | 16.76 |
| 9 | 2.02 | 2.23 | 1.81 | 10.68 | 10.87 | 10.50 | 21.43 | 26.58 | 16.92 |
| 10 | 2.01 | 2.22 | 1.80 | 10.69 | 10.86 | 10.52 | 21.37 | 26.47 | 16.90 |
| 11 | 2.14 | 2.37 | 1.91 | 10.58 | 10.70 | 10.46 | 23.89 | 29.72 | 18.77 |
| 12 | 2.12 | 2.34 | 1.89 | 10.68 | 10.81 | 10.54 | 23.62 | 29.28 | 18.63 |
| 13 | 2.10 | 2.32 | 1.89 | 10.76 | 10.91 | 10.60 | 23.46 | 28.98 | 18.60 |
| 14 | 2.08 | 2.28 | 1.87 | 10.84 | 11.03 | 10.65 | 23.07 | 28.39 | 18.39 |
| 15 | 2.04 | 2.24 | 1.85 | 10.94 | 11.17 | 10.71 | 22.57 | 27.66 | 18.09 |
| 16 | 2.00 | 2.19 | 1.82 | 11.07 | 11.35 | 10.80 | 21.96 | 26.80 | 17.70 |
| 17 | 1.97 | 2.15 | 1.79 | 11.06 | 11.33 | 10.79 | 21.29 | 25.97 | 17.17 |
| 18 | 1.91 | 2.08 | 1.74 | 11.14 | 11.42 | 10.86 | 20.15 | 24.52 | 16.30 |

### 2.3.2 Seasonal variation

Detailed information of wave conditions in the coastal area are based on the results from CWM. Wave power calculations are made using equation as follows:

$$P = \int_0^{\pi} \int_{f_{min}}^{f_{max}} \rho g c_g E(\theta, f) \mathrm{d}f \mathrm{d}\theta \tag{2.3}$$

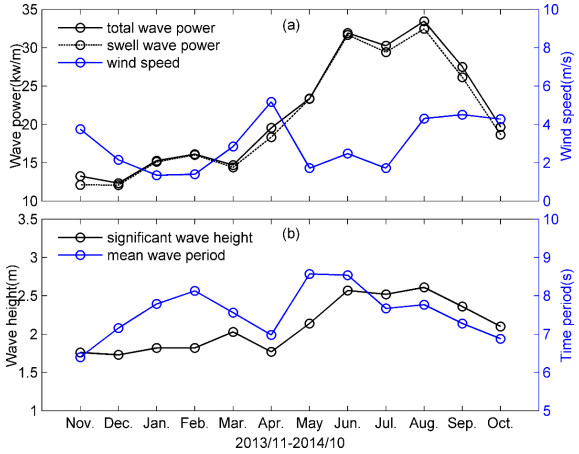


Figure 2.8: (a) Seasonal variations of monthly median wave power, wave power due to swells and wind from 2013/11 to 2014/10 over the area within 30 nautical miles off the coast. (b) Seasonal variations of monthly median significant wave height and mean wave period.

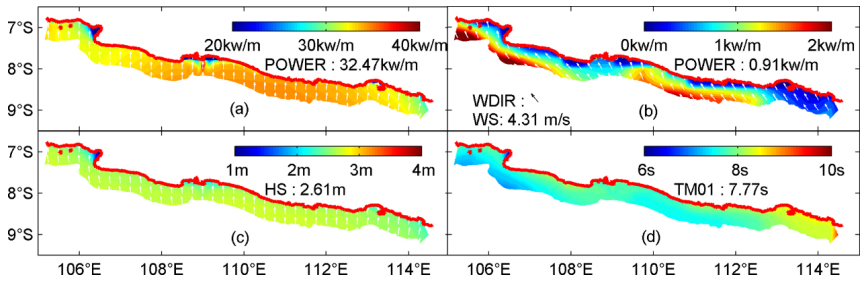


Figure 2.9: Monthly median wave conditions in Aug. 2014 within 30 nautical miles off the coast. (a) Wave power and energy transport direction due to swells; (b) Wave power and energy transport direction due to local winds; (c) Significant wave height and mean wave direction2014; (d) Mean wave period. POWER: average wave power over the area; WDIR: average wind direction over the area; WS: average wind speed over the area; HS: average significant wave height over the area; TM01: average mean wave direction over the area.

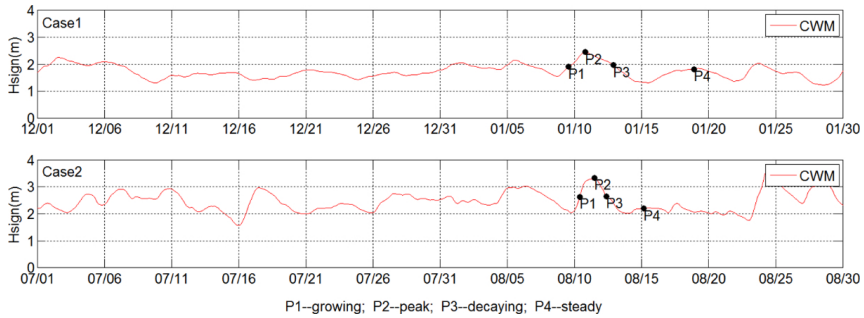


Figure 2.10: Wave case studies: (upper) rainy season; (lower) dry season.

where $P$ is the wave power, $c_g$ is the wave group speed and $E(\theta, f)$ is the power density as a function of the wave direction ($\theta$) and frequency ($f$). Monthly median significant wave height, mean wave period and wave power within 30 nautical miles

off the coast are estimated. Swells provide the majority of wave energy (Fig. 2.8), while mild local winds of speed about 3-5 m/s does not play an important role on wave conditions through the year. The average monthly median wave power for swells is estimated as 15 kW/m from November 2013 to April 2014, and 25 kW/m from May 2014 to October 2014. Meanwhile, the wave power for winds is less than 1 kW/m through the year and varies with the wind speed and direction. With the dominance of the swells, significant wave height in the dry season is higher than in the rainy season. The mean wave period in this area is around 6-8 s through the year. The stronger swells in dry season result in the larger mean wave period of around 8 s. The peak wave power appears in August 2014 during the period. The detailed information in that month is provided by Fig. 2.9. In August 2014, the monthly median wave power of more than 30 kw/m is mainly from the southerly swells. The local winds from southeast only provide the wave power of 0.9 kw/m.

### 2.3.3 Swell events

Wave conditions in rainy and dry seasons, each covering one swell event, are selected. Both cases can be broken into four stages: wave growing (P1), peak (P2), wave decaying (P3) and subsequently steady state according to the significant wave height (P4) at the location of the buoy (Fig. 2.10). Spatial variations of wave power within 30 nautical miles off the coast during each stage of swell events are shown in Fig. 2.11 (rainy season) and Fig. 2.12 (dry season). The swells selected in both seasons are from southwest with slightly different directionalities. The swell in the dry season approaches to the western part of the coast first, and the energy propagates from west to east. While in the wet season, the swell approaches directly to the middle part of the coastline (from 108°E to 112°E) and transfers the energy to both sides. The highest wave power, $P_{max}$, occurs during the steady stage in both seasons, when the energy flux mainly comes from the coast. That implies that even in steady stages when the primary swell has declined, the wave energy are mostly come from swells.

### 2.3.4 Site selection

The selection of locations for deployment of wave energy farms or converters is an issue involving wave conditions, technical feasibility, economic benefit and environmental impact. Three simple criteria for preliminary screening of locations suitable for wave energy farms are presented as follows: 1. Annual median power is larger than 20 kW/m 2. Water depth is less than 200 m and greater than 30 m 3.

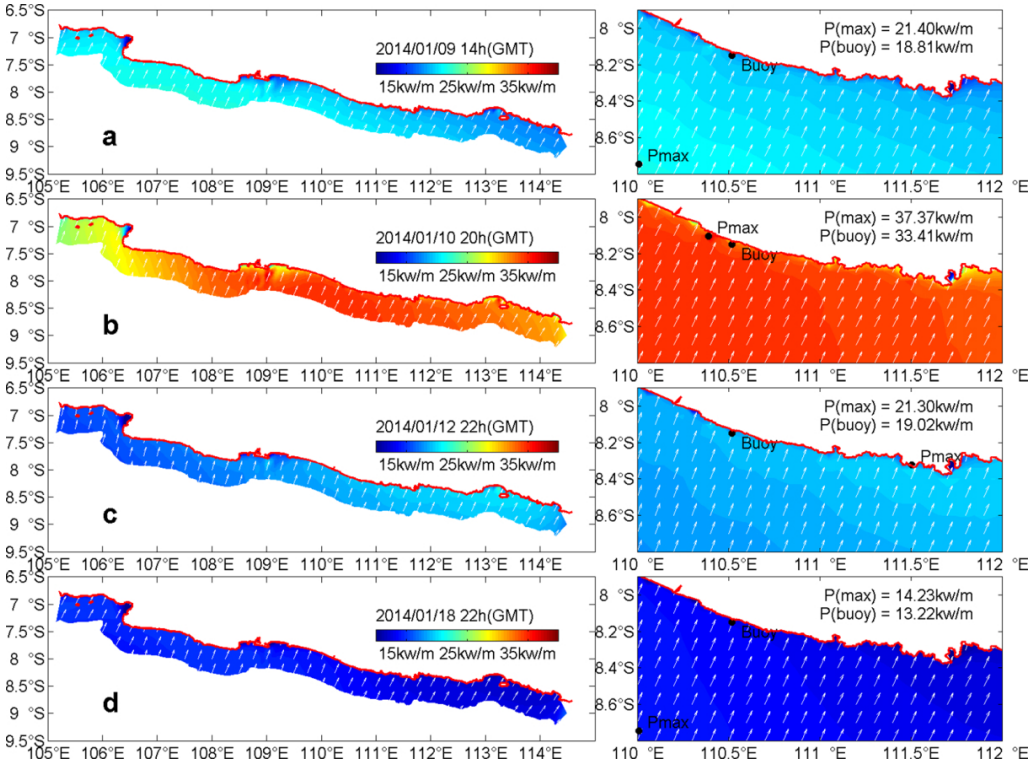


Figure 2.11: Wave power in wave case 1: (a) growing; (b) peak; (c) decaying; (d) steady.

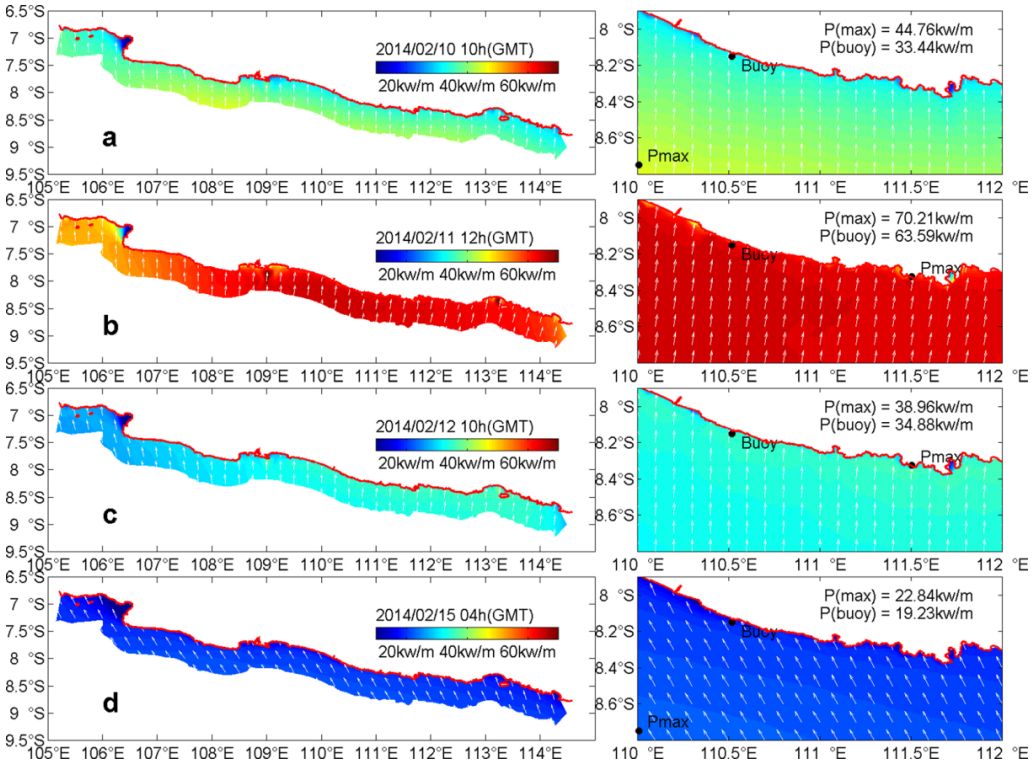


Figure 2.12: Wave power in wave case 2: (a) growing; (b) peak; (c) decaying; (d) steady.

Distance to the coast is less than 12 nautical miles Based on the described criteria

and one-year output from CWM, regions unfit for wave energy farms are filtered. Fig. 2.13 shows suitable locations, which appears mainly off the middle part of the coast, concentrating on two zones, marked by dash lines. Since the swells is more likely to approach the eastern and middle part of the Java Island at first, annual median power in most areas off the western part of the coast is lower than 20 kW/m, insufficient for wave energy farms. On the other hand, water depth off the eastern part of the coast is deep, more than 200 m in most areas. Mooring wave energy converters in that location is more difficult and more costly than in shallower water, although the annual median power is acceptable.

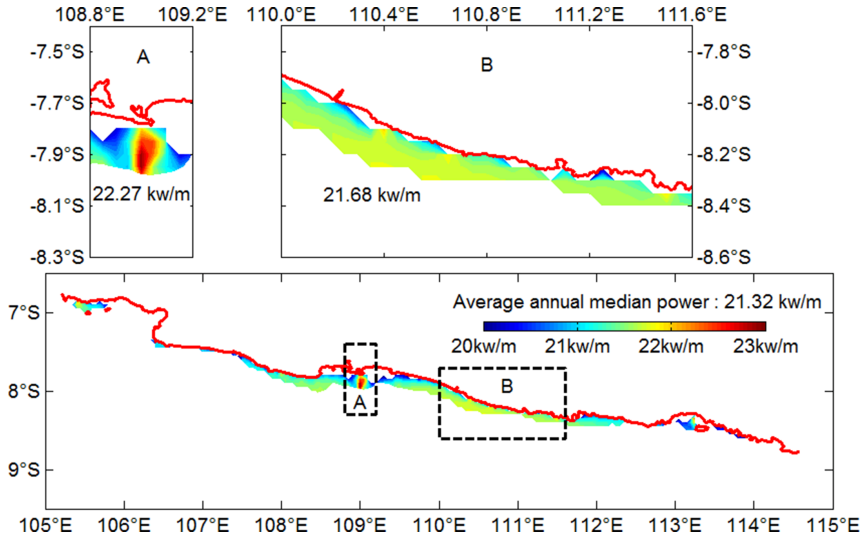


Figure 2.13: Distribution of Annual median wave power along the south coast of Java Island.

## 2.4 Summary

Long-term analysis of wave data from ERA-Interim over 10 years at the 18 points along the isobath of 2000 m suggests that there is considerable wave energy available off the south coast of Java Island. From the long-term wave data, the annual median significant wave height is around 2m and the mean wave period is around 11 s in this area. The mean annual median wave power of the 18 points reaches 22 kW/m. The mean median wave power in dry season (27 kW/m) is higher than in rainy season (17 kW/m). One advantage for setting up wave energy farms there is the smaller seasonal variation than the west coast of Australia.

More detailed wave conditions are revealed from the buoy data and the coastal wave model, CWM. Generally, the majority of wave energy in this area is provided by swells from southwest produced in mid-latitude region. Thus, the swells as well

as the wave power due to the swells in the study area strengthen or recede along with the seasonal variation of the westerlies. From 2013/11 to 2014/10, the highest monthly wave power of 31 kW/m appears in Aug., 2014. Additionally, from the 2D spectra of the buoy data and the wave case studies, another wave system due to southeasterly swells is found and dominates the wave field in average wave conditions in the dry season. Although the mild southwesterly trade wind of speed about 3-5m/s through the year only have limited local impact on waves, the waves will grow through the fetch and perform as relative weak southeasterly swells when approach the study coastal area. The wave energy distribution along the coast over two swell events are presented as well. After setting annual median wave power, water depth, and distance from the coast as criteria, two zones suitable for wave energy farms emerged. Zone A has the highest annual median power around 23 kW/m. Zone B has more suitable locations where some of them are close to the coast.

The model validation results of CWM are plausible (relative RMS of significant wave height is around 10%). However, CWM is not able to describe a two wave system when the both systems are due to swells. Fortunately, the southeasterly wave system due to the swell for the trade wind is much weaker than southwesterly one and its wave energy actually is overlapped to the primary swell system. Therefore, the difference of wave systems does not sway the assessment of wave energy potential. Even so, we still hope a model with larger domain can solve this problem in following research. Additionally, to further screen the suitable locations for deployment of wave energy farms, more detailed measurement and associated environmental and economical evaluation are required.

## Acknowledgements

We gratefully acknowledge financial support from China Scholarship Council.

## Bibliography

Antonio, F. d. O. (2010). Wave energy utilization: A review of the technologies. *Renewable and sustainable energy reviews*, 14(3):899–918.

Arinaga, R. A. and Cheung, K. F. (2012). Atlas of global wave energy from 10 years of reanalysis and hindcast data. *Renewable Energy*, 39(1):49–64.

Dee, D., Uppala, S., Simmons, A., Berrisford, P., Poli, P., Kobayashi, S., Andrae, U., Balmaseda, M., Balsamo, G., Bauer, P., et al. (2011). The era-interim reanalysis:

Configuration and performance of the data assimilation system. *Quarterly Journal of the royal meteorological society*, 137(656):553–597.

Hasselmann, S., Brüning, C., Hasselmann, K., and Heimbach, P. (1996). An improved algorithm for the retrieval of ocean wave spectra from synthetic aperture radar image spectra. *Journal of Geophysical Research: Oceans*, 101(C7):16615–16629.

Henfridsson, U., Neimane, V., Strand, K., Kapper, R., Bernhoff, H., Danielsson, O., Leijon, M., Sundberg, J., Thorburn, K., Ericsson, E., et al. (2007). Wave energy potential in the baltic sea and the danish part of the north sea, with reflections on the skagerrak. *Renewable Energy*, 32(12):2069–2084.

Iglesias, G. and Carballo, R. (2010). Wave energy resource in the estaca de bares area (spain). *Renewable Energy*, 35(7):1574–1584.

Iglesias, G., López, M., Carballo, R., Castro, A., Fraguela, J. A., and Frigaard, P. (2009). Wave energy potential in galicia (nw spain). *Renewable Energy*, 34(11):2323–2333.

Komen, G. J., Cavaleri, L., Donelan, M., Hasselmann, K., Hasselmann, S., and Janssen, P. (1994). *Dynamics and modelling of ocean waves*. Cambridge university press.

Nobre, A., Pacheco, M., Jorge, R., Lopes, M., and Gato, L. (2009). Geo-spatial multi-criteria analysis for wave energy conversion system deployment. *Renewable energy*, 34(1):97–111.

Pontes, M., Cavaleri, L., and Mollison, D. (2002). Ocean waves: energy resource assessment. *Marine Technology Society Journal*, 36(4):42–51.

Stopa, J. E. and Cheung, K. F. (2014). Intercomparison of wind and wave data from the ecmwf reanalysis interim and the ncep climate forecast system reanalysis. *Ocean Modelling*, 75:65–83.

Stopa, J. E., Cheung, K. F., and Chen, Y.-L. (2011). Assessment of wave energy resources in hawaii. *Renewable Energy*, 36(2):554–567.

Waters, R., Engström, J., Isberg, J., and Leijon, M. (2009). Wave climate off the swedish west coast. *Renewable Energy*, 34(6):1600–1606.

# Chapter 3

# Wave assimilation scheme

*A 4D variational assimilation scheme with partition method for nearshore wave models*. Song, Q. and R. Mayerle. Ocean Dynamics. 2017:1-14.

# A 4D variational assimilation scheme with partition method for nearshore wave models

**Qingyang Song and Roberto Mayerle**

**Abstract:** *This paper summarizes the development steps of a 4D variational assimilation scheme for nearshore wave models. A partition method is applied for adjusting both wave boundary conditions and wind fields. Nonstationary conditions are assimilated by providing defined correlations of model inputs in time. The scheme is implemented into the SWAN model. Twin experiments covering both stationary and nonstationary wave conditions are carried out to assess the adequacy of the proposed scheme. Stationary experiments are carried out considering separately windsea, swells and mixed sea. Cost functions decline to less than 5% and RMS spectrum errors are reduced to less than 10%. The nonstationary experiment covers one day simulation under mixed wave conditions with assimilation windows of 3 hours. RMS spectrum errors are reduced to less than 10% after 30 iterations in most assimilation windows. The results show that for spatially uniform model inputs, model accuracy is improved notably by the assimilation scheme throughout the computational domain. It is found that under wave conditions in which observed spectra can be well classified, the assimilation scheme is able to improve model results significantly.*

**Keywords:** 4D variational assimilation; Wave modeling; Adjoint; Partition

## 3.1 Introduction

Wave conditions are essential to many fields such as shipping, engineering and weather forecasts. Simulation of ocean waves provides improvement of understanding of coastal processes helping the design of coastal structures. However, accurate modelling of waves in coastal regions remains a major challenge as the quality of the predictions are very much dependent on model inputs. In particular, bathymetry,

open sea boundary conditions and winds play a major role in wave predictions. In this respect, data assimilation techniques integrating observations and simulations prove to be quite helpful.

Data assimilation has been applied to wave models from 1980s since remote sea surface observations as SAR and altimetry data became available. Early attempts by Esteva (1988), Lionello et al. (1992) and Bauer et al. (1992) used assimilation schemes with optimal interpolation techniques. This was followed by the adoption of variational assimilation scheme with adjoint method (De las Heras and Janssen, 1992; De Las Heras et al., 1994; Hersbach, 1998). Compared with early simple schemes as the optimal interpolations, variational schemes are more capable of reflecting correlations of model results in space and time by means of adjoint method (De Las Heras et al., 1994). Partitioned spectrum wave data has been used in assimilation schemes from the mid 1990s (Voorrips et al., 1997; Hasselmann et al., 1997). In this case, modeled spectrum information can be improved to some extent with optimal interpolations by partitioning the spectra into their various contributions. Partitioning methods are able to split the wave spectrum into windsea and swell components taking the topography of the spectrum into account. Hence, they are suitable to the identification of all the existing component wave trains (Waters et al., 2013). To date, although partition methods has been applied in several different assimilation schemes (eg. Portilla (2009); Emmanouil et al. (2010, 2012); Waters et al. (2013)), there are few researches addressing the application of partition methods in variational assimilation scheme with the full adjoint.

Several applications of assimilation schemes for waves in coastal regions have been reported recently (eg. Siddons et al. (2009); Veeramony et al. (2010); Waters et al. (2013); Wahle et al. (2015)). Most applications consider significant wave heights as observations. However, directional information is also important in coastal areas especially for studying sediment transport and wave-current coupling. Thus, Veeramony et al. (2010) developed a variational assimilation scheme in which the observed 2D spectra are directly included in the assimilation process by adjusting input wave spectra on open boundaries. In the derivation of the adjoint, all source terms are removed and only stationary simulations are considered. As the size of the area considered is of the order of a few kilometers, the effect due to local winds can usually be neglected.

As in larger areas, wind effect becomes relevant, both winds and boundary waves may need to be adjusted. Hence, a variational assimilation scheme should consider the source terms due to winds in the adjoint and the wave spectra should be split into its various components. In relatively small coastal areas where observations

react to boundary conditions quickly, boundary conditions in one time window can be reflected by the observations in the same time window. That implies that the model input at the start and end points during a time window can be improved effectively by combining the observations during the same time window provided their distributions in time are appropriate. Hence, for nonstationary wave conditions when model inputs during a time window can be represented explicitly by values at the start and end points of the window, a relatively simple assimilation scheme, different from the scheme by Orzech et al. (2013), is feasible. In this study, the derivation steps of a 4D variational assimilation scheme for nearshore wave model are described. The scheme considers errors from both winds and wave boundary conditions by means of a partition method. In this paper, results of the assessment of the scheme on the basis of several experiments considering both stationary and nonstationary conditions on the German Bight are presented.

## 3.2 Method

### 3.2.1 The wave model SWAN

SWAN (Simulating Waves Nearshore) is a third generation wave model widely suitable to coastal areas (Booij et al., 1999). The following action balanced is solved:

$$\frac{\partial N}{\partial t} + \vec{\nabla}(\vec{C}N) = \frac{S}{2\pi f} \tag{3.1}$$

where $N$ is the action density, $\vec{C} = (C_x, C_y, C_\theta, C_f)$ represents the propagation velocity of wave energy in space and spectrum domain and $S$ is the total source and sink terms of wave energy including wind input, dissipation and nonlinear wave-wave interaction. Details of the source terms used in the derivation of the adjoint is presented in Appendix A. As a phase-averaged wave model, Eq. (3.1) is solved with given model inputs such as wind fields and wave boundary conditions so as to obtain information of wave spectra throughout the computation domain. The version of the SWAN model applied in this study is 41.01.

### 3.2.2 Assimilation methodology

Variational assimilations are a class of algorithms to improve model results by minimizing a scalar function named cost function with respect to control variables (Lahoz et al., 2010). The 4D variational assimilation scheme adopted in this study is developed with reference to previous studies by De las Heras and Janssen (1992), De

Las Heras et al. (1994) and Veeramony et al. (2010). The cost function is minimized with the adjoint.

The cost function is made up of two parts: (1) deviation of analyzed model results from observations and (2) deviation from first guess model results. Normally, the deviations from first guess model results are related to the control variable selected for adjustment. Here, wind components and 2D wave spectra on open boundaries are set as control variables. Initial conditions are not regarded as control variables in this study. The assimilation effect for initial conditions depends on not only how well the assimilation scheme works but also on how accurately estimated background correlations are. Thus, to assess the assimilation scheme itself, the correlation problem and the assimilation for initial conditions are not be addressed in this study. Although other sets of the control variables can be considered, wind and wave boundary data are the most important inputs of a nearshore model. Regardless of realistic situations, they are considered suitable for testing purposes. The cost function reads as follows:

$$J = J_1 + J_2 + J_3 \tag{3.2}$$

where $J_1$, $J_2$, $J_3$ are related respectively to deviations from observations, first guess winds and first guess boundary conditions. Since the 2D spectra on open boundaries are control variables, the deviation from observations should be expressed by error variance of spectra. The $J_1$ reads as follows:

$$J_1(E) = \frac{1}{M_{obs}} \sum_{a=1}^{M_{obs}} \iint W_1 (E - \hat{E}_a)^2 \mathrm{d}\theta \mathrm{d}f \tag{3.3}$$

Where $E$ and $\hat{E}_a$ are the modeled and the observed spectrum power density respectively. $M_{obs}$ indicates the total number of the observations used for assimilation over space and time. $W_1$ is the corresponding weight and reflect the reliability of observations. In a real case, $W_1$ is a function of position, time, direction and frequency related to the covariance matrix of observations. $J_2$ is expressed by deviations from first guess wind components. $J_2$ is defined as follows:

$$J_2(u, v) = \iint W_2 [(u - u_{1st})^2 + (v - v_{1st})^2] \mathrm{d}x \mathrm{d}t \tag{3.4}$$

Where $(u, v)$ are the wind components and the subscript $1st$ indicates the first-guess values. $W_2$ is the weight. Although wind input is space and time dependent, it is always determined by linear interpolation between the wind at the end and start points of a given input interval in SWAN. The period over an input interval is named

here as input window. By setting control variables as wind components $u_0$, $v_0$ and $u_1$, $v_1$ respectively at a start and end points, the model wind during this wind input window can be explicitly expressed as:

$$\begin{aligned} u(x,t) &= (1 - w_1(t))u_0 + w_1(t)u_1 \\ v(x,t) &= (1 - w_1(t))v_0 + w_1(t)v_1 \end{aligned} \tag{3.5}$$

where $w_1(t)$ denotes the interpolation weighting function with respect to time. It should be pointed out that if time resolution of input wind fields is not capable of describing real winds properly, the interpolation algorithm is easily to be modified to a piecewise function by adding a new couple of wind components as control variables in the forward and the adjoint model. But in this study, for test purpose, the simplified form of $w_1(t)$ reads:

$$w_1(t) = \frac{t - t_{st}}{t_{ed} - t_{st}} \tag{3.6}$$

Where $t_{st}$ and $t_{ed}$ are the start and end time points of a input window respectively. Hence, by replacing time dependent $u$ and $v$ with $u_0$, $v_0$ and $u_1$, $v_1$ in an input window, $J_2$ becomes:

$$\begin{aligned} J_2(u_0, v_0, u_1, v_1) = \int W_2[(u_0 - u_{0_{1st}})^2 + (u_1 - u_{1_{1st}})^2 + \\ (v_0 - v_{0_{1st}})^2 + (v_1 - v_{1_{1st}})^2]\mathrm{d}x \end{aligned} \tag{3.7}$$

The form of $J_2$ implies the assumption that the winds at the start and end points are independent. Similarly, $J_3$ reads:

$$J_3(E_0, E_1) = \iiint W_3[(E_0 - E_{0_{1st}})^2 + (E_1 - E_{1_{1st}})^2]\,\mathrm{d}\theta\mathrm{d}f\mathrm{d}x \tag{3.8}$$

where $E_0$ and $E_1$ are respectively the input wave spectrum power density at the start and end point during the input window. $W_3$ is the weight.

$W_2$ and $W_3$ reflect the degrees of uncertainty of model input as pointed out by Bennett and McIntosh (1982). They are related to the covariance matrix of the first guess input. Since correlations of the input winds in time are actually determined by the above processes, $W_2$ and $W_3$ are no longer functions of time, but still functions of positions.

It is almost impossible to improve model results over the whole computational area with limited observations in space, particularly if correlations of the control variables are not known or the control variables are uncorrelated in space. In a relatively small nearshore area, strong correlations of the control variables are to

be expected. In this study, as stated above, for testing purposes, the correlation problem in space will not be addressed. Therefore, uniform winds and wave open boundary conditions in space are considered. As a result, Eq. (3.7) and Eq. (3.8) are reduced to:

$$\begin{aligned} J_2(u_0, v_0, u_1, v_1) = W_2[(u_0 - u_{0_{1st}})^2 + (u_1 - u_{1_{1st}})^2 + \\ (v_0 - v_{0_{1st}})^2 + (v_1 - v_{1_{1st}})^2] \end{aligned} \tag{3.9}$$

$$J_3(E_0, E_1) = W_3 \iint [(E_0 - E_{0_{1st}})^2 + (E_1 - E_{1_{1st}})^2] \, \mathrm{d}\theta \mathrm{d}f \tag{3.10}$$

In which $W_2$ and $W_3$ are set to be constants. Although the cost function is a quadratic function, it depends implicitly on the control variables. To minimize the function, the method of Lagrange multiplier is applied. Combining the action balance equation Eq. (3.1) with the cost function Eq. (3.2), the complete Lagrange function reads as:

$$L(u_0, v_0, u_1, v_1, E_0, E_1, E, \lambda) = J + \iiiint \lambda [\frac{\partial N}{\partial t} + \vec{\nabla}(\vec{C}N) - \frac{S}{2\pi f}] d\theta \mathrm{d}f \mathrm{d}x \mathrm{d}t \tag{3.11}$$

where $\lambda(x, t, \theta, f)$ is the Lagrange multipliers. The wave event taken for analysis is such that the wave systems due to swells and local winds can be classified and separated completely and the energy transfer from local winds to swells neglected. That means waves can be regarded as a linear superposition of different wave systems. Meanwhile, the observed and modeled 2D spectra can be separated by a partition method. Therefore, the Lagrange function is separated into two contributions as follows:

$$L(u_0, v_0, u_1, v_1, E_0, E_1, E, \lambda) = L_w(u_0, v_0, u_1, v_1, E, \lambda_w) + L_s(E_0, E_1, E, \lambda_s) \tag{3.12}$$

$L_w$ and $L_s$ represent the Lagrange function related to windsea and swell respectively. $L_w$ reads as follows:

$$\begin{aligned} L_w(u_0, v_0, u_1, v_1, E, \lambda_w) = \iiiint \lambda_w [\frac{\partial N}{\partial t} + \vec{\nabla}(\vec{C}N) - \frac{S_w}{2\pi f}] \mathrm{d}\theta \mathrm{d}f \mathrm{d}x \mathrm{d}t + \\ W_2 J_2 + \iiiint S_{ob1} \mathrm{d}\theta \mathrm{d}f \mathrm{d}x \mathrm{d}t \\ S_{ob1}(E) = W_1 J_w(E) \delta(x - x_a) \delta(t - t_a) \\ J_w(E) = \frac{1}{M_{obs}} \sum_{a=1}^{M_{obs}} (h(f, \theta) E - \hat{h}(f, \theta) \hat{E}_a)^2 \end{aligned} \tag{3.13}$$

In Eq. (3.13), $J_w$ is the windsea contribution of $J_1$, $S_w$ is the source term in the action balance equation due to winds, $h(f,\theta)$ and $\hat{h}(f,\theta)$ are Heaviside step functions denoting if a grid of the 2D spectrum belongs to windsea components. The source term $S_w$ includes wind growth, white capping and bottom friction. Nonlinear wave-wave interaction can only affect wave energy transfer over a frequency domain rather than the total wave energy. Gradients with respect to wind components are calculated by integrating a function of $\lambda_w$ over the whole spectrum domain which mainly reflect the total energy difference. Hence, the influence of the nonlinear interactions on the gradients of wind components is expected to be small. On the other hand, the derivation of the adjoint to the nonlinear interactions is very complex as pointed out by Hersbach (1998). After weighing advantages and disadvantages, nonlinear wave-wave interaction is not include in $S_w$. Similarly, $L_s$ reads as follows:

$$\begin{aligned} L_s(E_0,E_1,E,\lambda_s) &= \iiiint \lambda_s[\frac{\partial N}{\partial t}+\vec{\nabla}(\vec{C}N)-\frac{S_s}{2\pi f}]\mathrm{d}\theta\mathrm{d}f\mathrm{d}x\mathrm{d}t + W_3J_3 + \\ &\quad \iiiint S_{ob2}\mathrm{d}\theta\mathrm{d}f\mathrm{d}x\mathrm{d}t \\ S_{ob2}(E) &= W_1J_s(E)\delta(x-x_a)\delta(t-t_a) \\ J_s(E) &= \frac{1}{M_{obs}}\sum_{a=1}^{M_{obs}}((1-h)E-(1-\hat{h})\hat{E}_a)^2 \end{aligned} \tag{3.14}$$

where $S_s$ is the source term affecting swells. The assumption adopted by Veeramony et al. (2010) is taken in this study. Besides, only ' classic ' swell with narrow spectra as described in Hasselmann et al. (1973) is considered. In other words, only bottom friction is included in $S_s$. Different from the terms $S_s$ and $S_w$ used in the adjoint model, in the forward SWAN model, all the source terms are included. Based on Eq. (3.13) and Eq. (3.14), the resulting Euler equations by differentiating $L$ read as:

$$\text{for } \delta\lambda_w \text{ and } \delta\lambda_s\text{: } \frac{\partial N}{\partial t}+\vec{\nabla}(\vec{C}N)=\frac{S}{2\pi f} \tag{3.15}$$

$$\text{for } \delta N \text{ in } L_w\text{: } -\frac{\partial\lambda_w}{\partial t}-\vec{C}\vec{\nabla}\lambda_w=\lambda_w\frac{\partial S_w}{\partial E}-\frac{\partial S_{ob1}}{\partial N} \tag{3.16}$$

$$\text{for } \delta N \text{ in } L_s\text{: } -\frac{\partial\lambda_s}{\partial t}-\vec{C}\vec{\nabla}\lambda_w=\lambda_s\frac{\partial S_s}{\partial E}-\frac{\partial S_{ob2}}{\partial N} \tag{3.17}$$

for $\delta u_0, \delta u_1, \delta v_0$ and $\delta v_1$:

$$\begin{aligned}
\mathrm{grad}_{u_0} J &= \frac{\partial J_2}{\partial u_0} - \iiiint [\frac{\lambda_w (1 - w_1(t))}{2\pi f} \frac{\partial S_w}{\partial u}] \mathrm{d}\theta \mathrm{d}f \mathrm{d}x \mathrm{d}t \\
\mathrm{grad}_{u_1} J &= \frac{\partial J_2}{\partial u_1} - \iiiint [\frac{\lambda_w w_1(t)}{2\pi f} \frac{\partial S_w}{\partial u}] \mathrm{d}\theta \mathrm{d}f \mathrm{d}x \mathrm{d}t \\
\mathrm{grad}_{v_0} J &= \frac{\partial J_2}{\partial v_0} - \iiiint [\frac{\lambda_w (1 - w_1(t))}{2\pi f} \frac{\partial S_w}{\partial v}] \mathrm{d}\theta \mathrm{d}f \mathrm{d}x \mathrm{d}t \\
\mathrm{grad}_{v_1} J &= \frac{\partial J_2}{\partial v_1} - \iiiint [\frac{\lambda_w w_1(t)}{2\pi f} \frac{\partial S_w}{\partial v}] \mathrm{d}\theta \mathrm{d}f \mathrm{d}x \mathrm{d}t
\end{aligned} \tag{3.18}$$

for $\delta E_0$ and $\delta E_1$:

$$\begin{aligned}
\mathrm{grad}_{E_0} J &= \frac{\partial J_3}{\partial E_0} - \iint [\frac{1 - w_2(t)}{2\pi f} \lambda_s \vec{C} \vec{n_b}] \mathrm{d}x_b \mathrm{d}t \\
\mathrm{grad}_{E_1} J &= \frac{\partial J_3}{\partial E_1} - \iint [\frac{w_2(t)}{2\pi f} \lambda_s \vec{C} \vec{n_b}] \mathrm{d}x_b \mathrm{d}t
\end{aligned} \tag{3.19}$$

where $x_b$ is the grid location on the computational domain boundary and $\vec{n_b}$ is the direction normal to the wave boundary. Eq. (3.16) and Eq. (3.17) are the adjoints which can be solved backward in time to yield $\lambda_w$ and $\lambda_s$. For more detailed information of the adjoint model, the reader is referred to A and B. $\lambda_w$ and $\lambda_s$ represent the sensitivity of the cost function to changes in the control variables (De Las Heras et al., 1994). That means that errors due to different control variables can be separated by solving Eq. (3.16) and Eq. (3.17) independently. Hence, the gradients of the cost function with respect to the control variables can be calculated following Eq. (3.18) and Eq. (3.19) directly. The increments of the control variables are obtained in turn by means of the conjugate-gradient descent algorithm (Polak, 1971). After that, the forward model is solved with the updated control variables. As shown in Fig. 3.1, the procedure is repeated iteratively to find the control variables which minimize the cost function. The assimilation process for nonstationary simulations is illustrated in Fig. 3.2. Since correlations in time are determined, the assimilation and input windows can differ if the control variables at the points of each input windows are added to the cost function.

For classifying wave systems into windsea and swell parts, the partition algorithm after Hasselmann et al. (1997) is applied in this study. It is assumed that, in relatively small nearshore areas, wave systems due to local winds are unique and the first guess wind field is not accurate but reasonable. So if the first guess wind is strong enough, the wave system with the hightest frequency either from observations

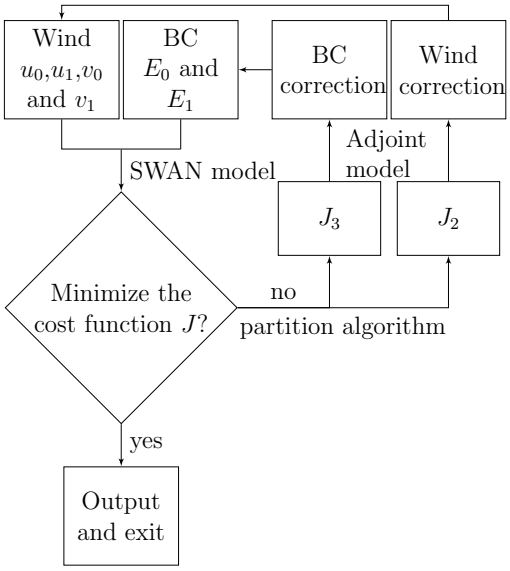


Figure 3.1: Adopted data assimilation scheme

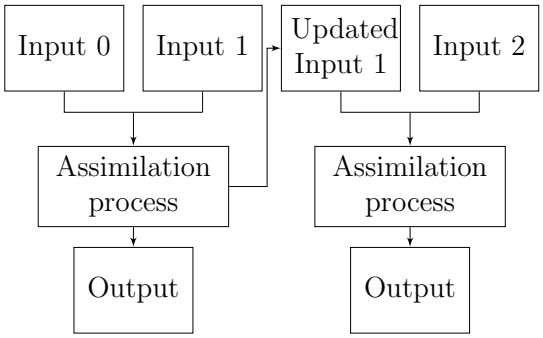


Figure 3.2: Nonstationary assimilation process

or model results is regarded as windsea part. The rest is regarded as swell. The applied partition steps are as follows:

1. Split the 2D spectra from both observations and model results with the watershed algorithm.

2. Discard the low energy portions with a given threshhold (energy below 1% of the total energy).

3. Based on the model input winds, identify if the partition with highest frequency of the modeled spectra belongs to windsea. If so, regard it as windsea partition and the rest as swell partitions. Otherwise, regard all partitions as swell partitions.

4. If there is a windsea partition of modeled spectra after step 3, regard the partition with highest frequency of the observed spectra as windsea partition and the other partitions as swell partitions. Otherwise, regard all partitions as swell partitions.

## 3.3 Validation of the adjoint

As stated above, the adjoint in this study is derived directly from differential equations. To ensure the consistency between the built adjoint model and the forward model, some validation tests are required. The validation of the adjoint aims at figuring out whether the adjoint model can describe the propergation of perturbations backwards properly so as to obtain correct gradients. There are several methods for the validation. In this study, a simple method suggested by De Las Heras et al. (1994) is applied.

For a change $\Delta c$ in a control variable $c$, the corresponding change of the cost function is:

$$\Delta J = J(c + \Delta c) - J(c) \tag{3.20}$$

If the norm of the difference, $|\Delta c|$, is small enough, the following equation holds:

$$\Delta J \approx \Delta c \cdot \mathrm{grad}_c J \tag{3.21}$$

$\Delta J$ can be directly calculated by Eq. (3.20) based on results from the forward model with the control variable $c$ and $c + \Delta c$. Meanwhile, $\mathrm{grad}_c J$ is obtained by running the adjoint model. Therefore, Eq. (3.21) can be checked through comparing $\Delta J$ and $\Delta c \cdot \mathrm{grad}_c J$. Defining that:

$$R = \left| \frac{\Delta J}{\Delta c \cdot \mathrm{grad}_c J} - 1 \right| \tag{3.22}$$

Where $R$ should converge to 0 for $|\Delta c|$ down to 0 if the adjoint is correct. In this study, the control variables $E_0$ and $u_0$ in stationary wave conditions are chosen for the validation tests. To be specific:

$$\begin{aligned} &\text{for } E_0\text{: } \Delta c \cdot \mathrm{grad}_c J = \iint \Delta E_0 \cdot \mathrm{grad}_{E_0} J \mathrm{d}\theta \mathrm{d}f \\ &\text{for } u_0\text{: } \Delta c \cdot \mathrm{grad}_c J = \Delta u_0 \cdot \mathrm{grad}_{u_0} J \end{aligned} \tag{3.23}$$

The validation tests are performed in a rectangular region of 50km $\times$ 50km with a uniform bathymetry of 20m. The 'observation' is set at the center of the region from the forward model driven by westerly swell with a wave height of 2m from the west boundaries and a westerly wind of 10m/s over the whole region. The first guess $E_0$ is a westerly swell with wave height of 2.5m and $u_0$ is 12.5m/s westerly. All the source terms not applied in the derivation of the adjoint are turned off in the forward model to keep the consistency. Then the first guess $E_0$ and $u_0$ are changed independently to calculate $R$. As shown in Fig. 3.3, $R$ is converged to a value down

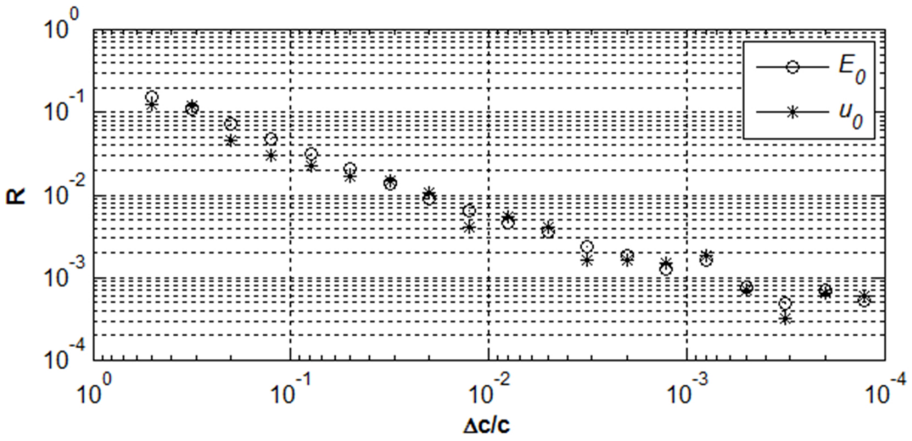


Figure 3.3: Validation of the adjoint. $E_0$:Changing the control variable $E_0$; $u_0$:Changing the control variable $u_0$

to a precision of $10^{-3}$ when the relative changes of $E_0$ and $u_0$ are approaching the magnitude of $10^{-3}$. The results suggest that the adjoint model is consistent with the forward model. The accuracy is in agreement with the tests by De Las Heras et al. (1994) in which the nonlinear wind growth term are not included. That is because the wind growth term applied in this study is linear as suggested by Snyder et al. (1981) and Komen et al. (1984).

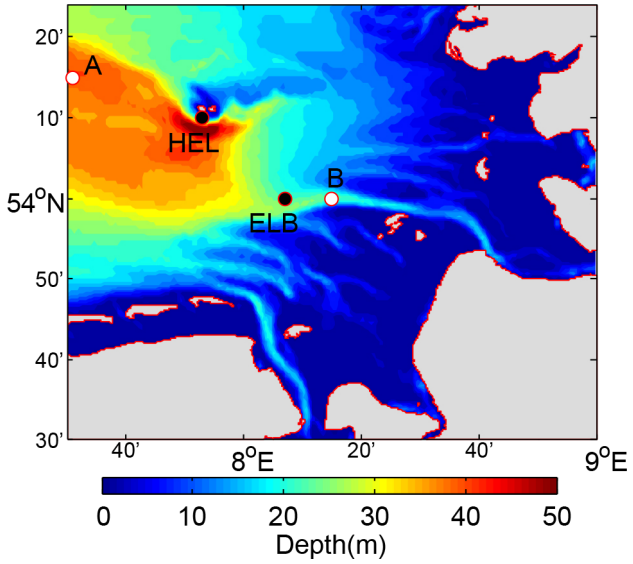


Figure 3.4: Computation domain for twin experiments

## 3.4 Twin experiments

Three stationary and one nonstationary experiments are carried out. The area chosen for testing the assimilation scheme is the German Bight on the North Sea.

Table 3.1: Assimilated input boundary conditions, Hs (significant wave height), Tm (mean wave period) and Dm (mean wave direction), and winds in pd (pseudo observation model), bf (model before the assimilatino) and af (model after the assimilation) in three stationary cases: W(Windsea), S(Swell) and M(Mixed sea).

| Case | | Boundary condition | | | Wind | |
|---|---|---|---|---|---|---|
| | | Hs(m) | Tm(s) | Dm(°) | u(m/s) | v(m/s) |
| W | pd | ----- | | | -9.78 | -2.84 |
| | bf | | | | -6.72 | -3.5 |
| | af | | | | -9.66 | -3.01 |
| S | pd | 1.26 | 7.46 | 162.4 | ----- | |
| | bf | 0.81 | 5.8 | 135.9 | | |
| | af | 1.22 | 7.52 | 156.7 | | |
| M | pd | 0.84 | 9.71 | 148.6 | -7.87 | -7.26 |
| | bf | 1.02 | 9.00 | 128.6 | -5.9 | -5.14 |
| | af | 0.83 | 9.75 | 145.8 | -7.94 | -7.54 |

The computational domain covers an area of around 100 km × 90 km (see Fig. 3.4). The spatial resolution of the model is 500 m. The time interval in the nonstationary simulation is 5 min. Pseudo observations are mainly obtained by two sets of input data. The wind data is obtained from the GME model (Majewski et al., 2002) whereas the wave boundary data is taken from the ERA-I dataset provided by ECMWF (European Centre for Medium-Range Weather Forecasts) (Dee et al., 2011). For generating pseudo observations, the wave data at location A (see Fig. 3.4) is set to be the wave boundary data for the whole open boundaries and the wind data at location B (see Fig. 3.4) is set to be the wind over the whole computational domain. The pseudo observations are produced by a model run with the prescribed 'correct' winds and boundary conditions. The directional resolution is 5 degree and the number of frequencies from 0.01 Hz to 0.64 Hz is 40. The input window is three hours. Although spectra data of ERA-I are available, only wave statistic parameters such as significant wave height, mean wave period and mean wave direction are used in this study. The wave data is interpolated into a 3-hour interval to match the input window. Those data are Swells from the open boundaries are assumed to be formed as a Gaussian swell spectrum. Thus, the input 2D spectra on the boundaries are able to be inversed by the wave parameters. The first guess inputs are generated by adding random errors on the 'real' model inputs. The errors are less than 30% of actual values of the corresponding inputs. The reason to set 30% as the limitation is to ensure that the classification for windsea or swell partitions is correct.

There are two wave buoys from BSH (Bundesamt Fuer Seeschifffahrt und Hydrographie) in the area. They are named Elbe (ELB) and Helgoland (HEL) as shown in Fig. 3.4. Although the observations from the stations are not used in this study,

their locations are chosen for the output of pseudo observations. Since the model inputs are uniform, only the output at the station ELB is used in the cost function for assimilation while the output at the station HEL is used for validation. The local bathymetry at the station HEL is complex in which case nonlinear wave interactions are expected. However, the adjoint applied in this study does not contain the nonlinear terms so that the errors at the station HEL may not be inversed correctly by the adjoint model. Therefore, using the observation at ELB for assimilation is a better option for assessing the scheme keeping nonlinear effects as weak as possible. The weights $W_1$, $W_2$, and $W_3$ are set as follows:

$$\begin{aligned} W_1 &= 1 \\ W_2 &= \frac{0.01\bar{E}^2}{\bar{w}^2} \\ W_3 &= 0.01 \end{aligned} \tag{3.24}$$

where $\bar{w}$ is the average value of the first guess wind and $\bar{E}$ is the average value of the wave energy of the first guess model results. The weights $W_1$ and $W_3$ are selected according to Walker (2006). The values 0.01 and 1 suggest that observations are much more credible than results from simulations. A smaller $W_3$ could be more reasonable if the observations are trusted as the true value. But in this study, 0.01 is small enough so as to correct the model results to the observations. The rate between$\bar{E}$ and $\bar{w}$ in $W_2$ is one kind of normalization to make the dimension of control variables uniform, provided that the orders of the variance are proportional to that of the corresponding variables. Different from the stationary simulations, initial conditions influence the model results in the nonstationy simulations especially for a short time window. As mentioned in Sect. 4.2.2, the assimilation for initial conditions requires spatially broad observations and credible correlations of model results in space which are not addressed in the study. So the initial conditions in the first assimilation window are kept correct here in nonstationary experiments. Thus, if a proper assimilation window is found, the control variables can be effectively corrected by combining the observations keeping the model results accurate enough for a hot-start of the next assimilation window. In this experiment, pseudo observations are provided with a time interval of 30 minute including the start and end points of the input window. Therefore, it is assumed that the analyzed results after the assimilation in every input window are accurate enough. So the input window is set as the assimilation window and the errors from the hot-start data and the model inputs of the start point in the next assimilation window are ignored. At the same time, since nonlinear effects and convergence speeds of every assimilation window

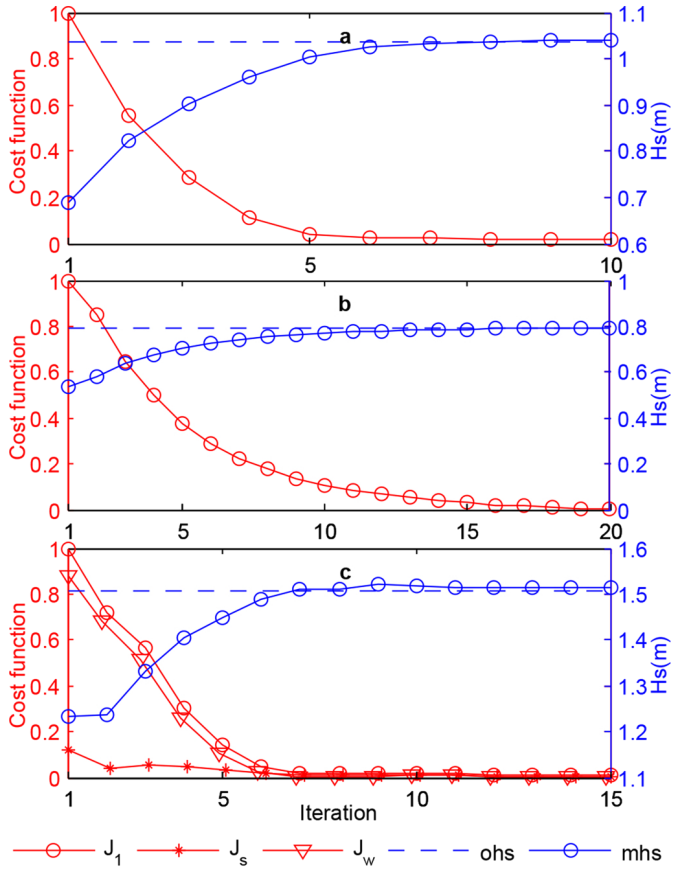


Figure 3.5: Cost function and differences between ohs ('observed' significant wave height) and mhs (modelled significant wave height) at station ELB with respect to iteration number. (a) Windsea; (b) Swells; (c) Mixed sea.

are unknown in advance, a constant number of iterations equal to 30 is set in the nonstationary experiment.

To assess the assimilation scheme, a normalized RMS spectrum difference is defined as follows:

$$E_{rms} = \sqrt{\frac{\langle (E_{obs} - E_{mod})^2 \rangle}{\langle E_{obs}^2 \rangle}} \tag{3.25}$$

Where $E_{mod}$ is the modelled spectrum density, $E_{obs}$ is the 'observed' spectrum density. The angular brackets denote averaging in space, time, and over the frequency domain. Similar metrics are used in Orzech et al. (2013) and Panteleev et al. (2015) to assess their assimilation schemes.

### 3.4.1 Stationary experiments

Three different wave cases are selected as stationary experiments:

1. Pure windsea at 12:00:00 on 2011/02/18 .

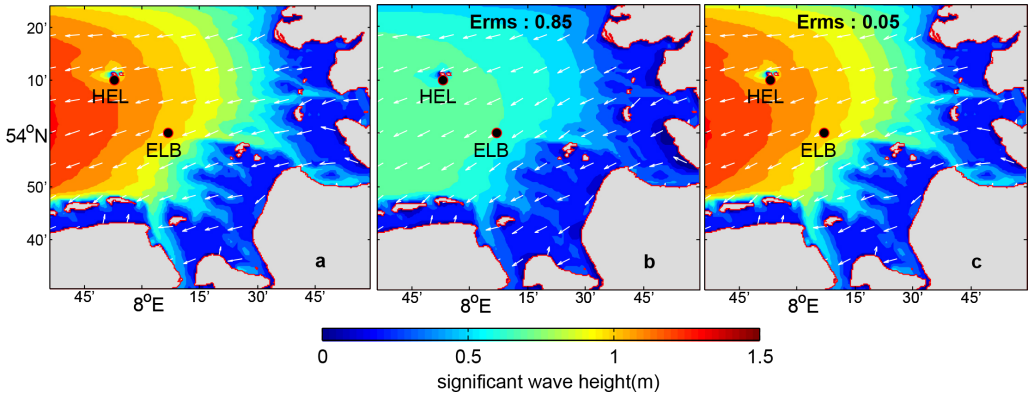


Figure 3.6: Significant wave height and mean wave direction throughout the computational domain in the windsea case. (a) Pseudo observations; (b) Before assimilation; (c) After assimilation.

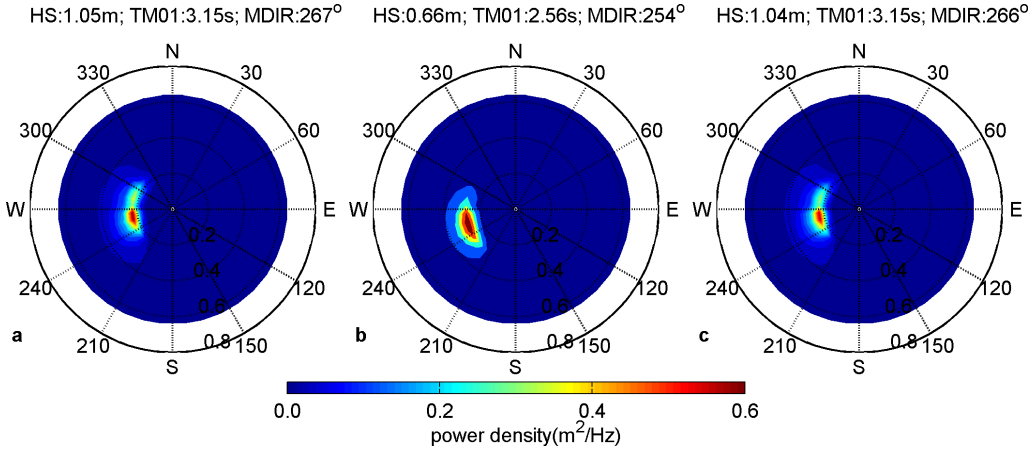


Figure 3.7: 2D spectrum at the station HEL in the windsea case. (a) Pseudo observations; (b) Before assimilation; (c) After assimilation.

2. Swells only at 00:00:00 on 2011/03/06 .
3. Mixed sea at 12:00:00 on 2011/03/14 .

Table 3.1 gives the 'real' and the corresponding first guess model inputs in the stationary experiments.

## Windsea

In this case, there are offshore winds throughout the domain and barely any swell energy input from open boundaries. Fig. 4.4 shows the variations of the cost function $J_1$ and significant wave height at ELB with respect to the iteration step. It can be seen that $J_1$ is reduced by around 50% from 1 to 0.5 in the first iteration. After ten iterations, the cost function almost converges to its minimum, corresponding to about 3% of the initial cost function value. The input $u$ and $v$ after the assimilation are not exactly the same as the 'real' wind components (Table 3.1). A small error

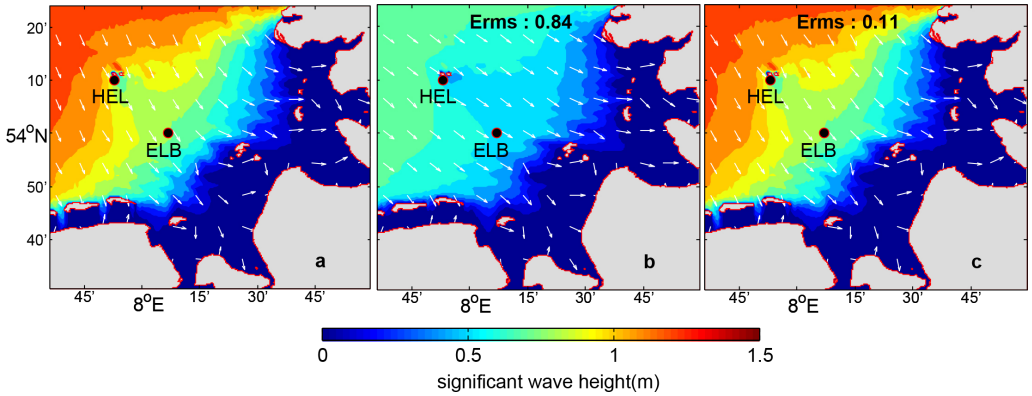


Figure 3.8: Significant wave height and mean wave direction throughout the computational domain in the swells case. (a) Pseudo observations; (b) Before assimilation; (c) After assimilation.

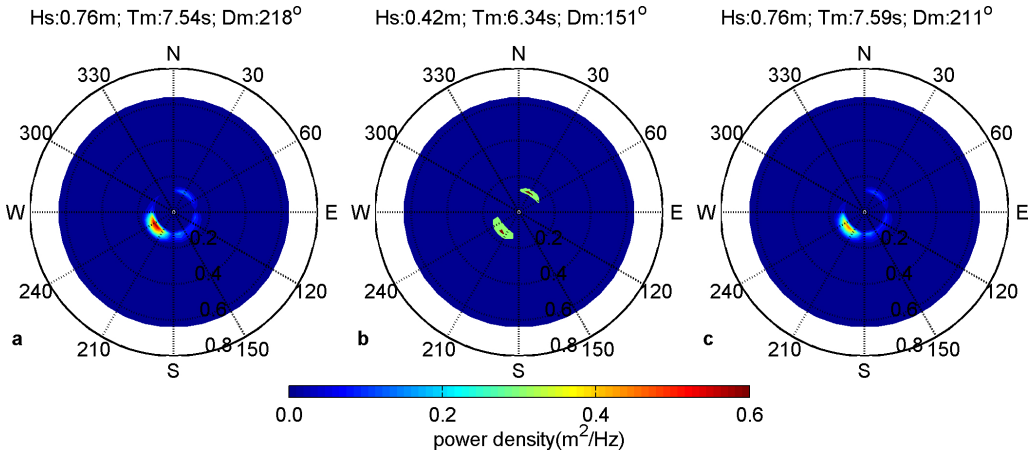


Figure 3.9: 2D spectrum at the station HEL in the swells case. (a) Pseudo observations; (b) Before assimilation; (c) After assimilation.

remains after the assimilation. As already mentioned, the absence of nonlinear terms in the adjoint leads to a slightly different distribution of $\lambda_w$ in the frequency domain. Although for calculating the gradient as Eq. (3.18), $\lambda_w$ is integrated, nonlinear interactions still have some influence on the total wave energy error. But based on Fig. 3.6, the assimilation is effective throughout the domain where the $E_{rms}$ declined from around 0.85 to 0.05, even under the conditions in which the obtained 'best' wind still contains some errors. Fig. 3.7 compares the 2D spectrum at the station HEL. The bathymetry surrounding the station HEL is much more irregular than at the station ELB. This leads to more complex spectrum at HEL. Before the assimilation, the modeled power density of the northern part is higher than the 'observation', and the high density domain is slightly wider. Notably, the 2D spectrum is corrected by the assimilation as well.

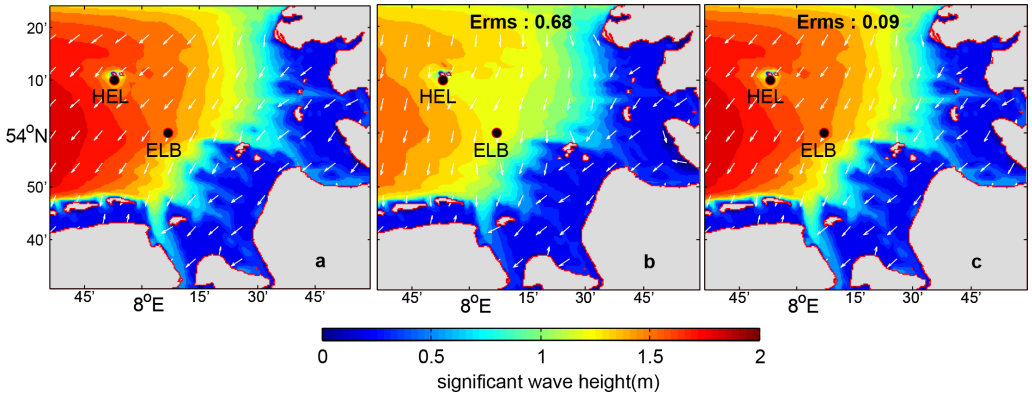


Figure 3.10: Significant wave height and mean wave direction throughout the computational domain in the mixed sea case. (a) Pseudo observations; (b) Before assimilation; (c) After assimilation.

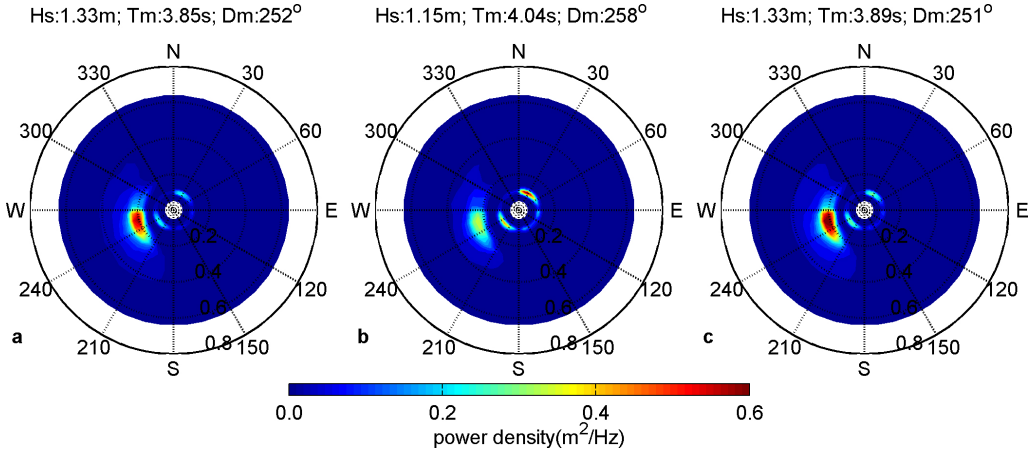


Figure 3.11: 2D spectrum at the station HEL in the mixed sea case. (a) Pseudo observations; (b) Before assimilation; (c) After assimilation.

## Swells

In this case, onshore swells originating from the northwest are considered and the wind speed of around 0.5m/s can be neglected. Different from the windsea case, the convergence of the cost function $J_1$ goes much slower with the iterations. However, the convergence speed is reasonable considering that the 2D wave spectrum on boundaries is a hundreds dimensional variable rather than a two-dimensional variable as the uniform wind in the windsea case. After 20 iterations, the cost function $J_1$ reduces to 0.01% and almost reaches its minimum. This is in agreement with the research made by Veeramony et al. (2010) in which the cost functions can be reduced to almost zero if the nonlinear effect is small. But the integral boundary conditions are not recovered to the 'real' values as seen in Table 3.1. That may be due to the fact that numerical noises and errors are inevitable in the calculation of the backward adjoint model and the gradient of the boundary condition with single

observation location. Although those computational errors adjusted in the boundary conditions do not affect the location of the observation due to dissipations, they have some influence on locations with relatively complicated bathymetry and closer to the open boundaries just as the station HEL. Therefore, $E_{rms}$ over the domain is 0.11 after the assimilation larger than that in the windsea case (see Fig. 3.8). And the 2D spectrum at HEL is not that well recovered as expected where the peak power density of analyzed spectrum is lower than the pseudo observation (see Fig. 3.9).

### Mixed sea

In this case, onshore swells and northeasterly offshore winds are included. The windsea and swell components of the 2D spectrum at the station ELB can be easily separated and classified. From Fig. 4.4, both the cost function components due to winds $J_w$ and swells $J_s$ reach convergence by the assimilation with the partition algorithm. $J_w$ captures more than 80% of the cost function $J_1$ and converges faster than $J_s$ in the experiment. As seen in Fig. 3.11, after 15 iterations, the remaining cost function is around 4% and the wind component is around 3%. The 2D spectrum at the station HEL presents both swell and windsea components. Although the power density of the windsea component becomes slightly higher than the 'observation', both windsea and swell components are almost recovered after the assimilation. The reduced $E_{rms}$ (from 0.68 to 0.09) and the integral wave parameters throughout the domain confirm the assimilation effect (see Fig. 3.10). The results suggest that the partition assimilation scheme is able to improve model results effectively for wave conditions under which the observed spectrum can be separated and classified into different components properly.

## 3.4.2 Nonstationary experiment

An experiment covering one day from 2011/03/14 to 2011/03/15 is carried out. It can be seen that, in general, the input winds in the experiment are from northeast to southwest. Wind speed increases from 5m/s to around 10m/s and the input swells rotates from southeast to south over the simulated period (see Fig. 3.12). Fig. 3.13a shows the assimilation results after 30 iterations. $E_{rms}$ throughout the region are reduced to less than 0.1 in most assimilation windows. The model inputs are almost entirely corrected (see Fig. 3.12). At the last assimilation window, the rest cost function is about 15% and the $E_{rms}$ is still 0.13 after the assimilation. This slightly larger value is related to the fact that at that window, the mean directions of the swells are closer to the wind direction. Additionally, the windsea part of

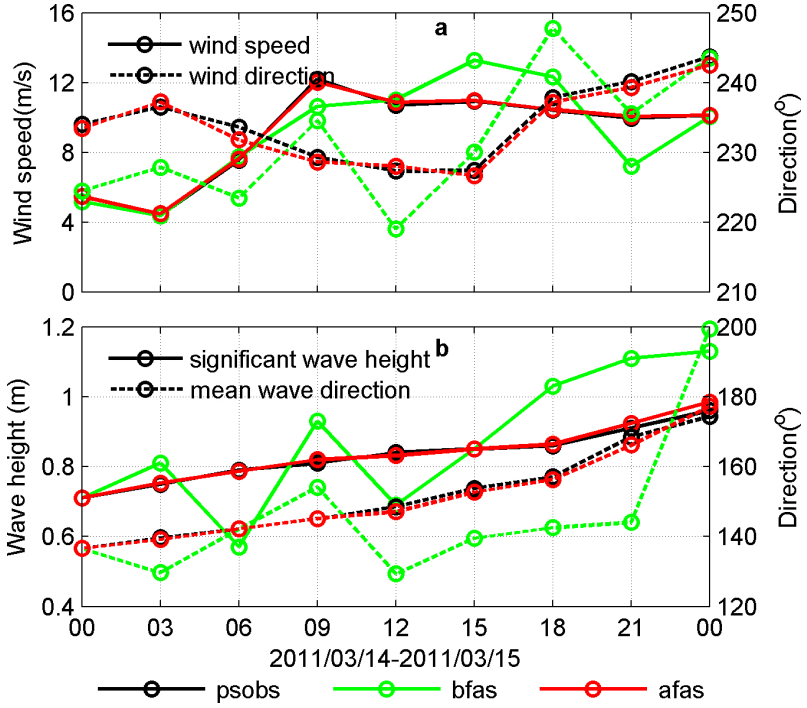


Figure 3.12: Differences of the model inputs among psobs (pseudo observations), bfas (model before the assimilation) and afas (model after the assimilation) in the nonstationary case. (a) Input winds; (b) Boundary conditions.

spectrum is in a lower frequency domain due to the larger wind speed (10m/s). Meanwhile, the mean wave period of the swells has declined to around 7s. Under such conditions, nonlinear wave-wave interactions and subsequent energy transport from windsea component to swells can be expected(Hasselmann, 1963). At the same time, the interaction between swell and windsea components also leads to some errors during the implementation of the partition algorithm. Even so, the integral wave parameters at HEL in the last window are well recovered. Based on the results of the experiments, the assimilation scheme is found to be feasible for nonstationary simulations.

## 3.5 Summary

In this study an assimilation scheme suitable to wave models in shallow waters is tailored to the SWAN wave model. The scheme based on the 4D variational method combined with adjoint technique is found to be effective to nearshore wave simulations. Winds and boundary conditions are assimilated by implementing the partition algorithm. Nonstationary conditions are solved by giving a determined correlation of the control variables in time. The twin experiments confirm that the assimilation scheme is capable of recovering the model results throughout the

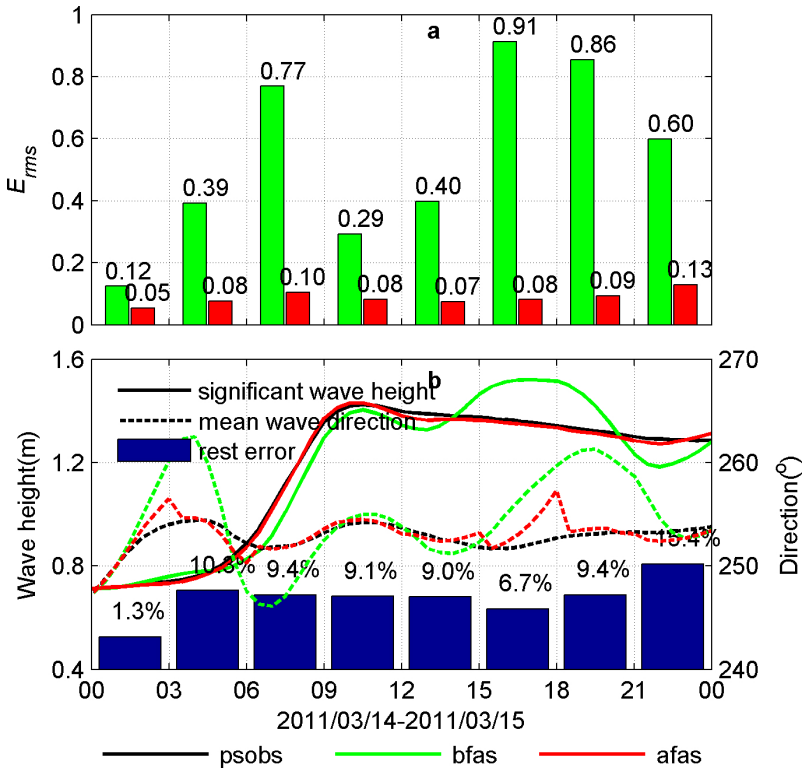


Figure 3.13: (a) $E_{rms}$ and (b) Cost function and wave parameters at the station HEL among psobs (pseudo observations), bfas (model before the assimilation) and afas (model after the assimilation) in the nonstationary case.

computational domain when model inputs are uniform. Both winds and boundary conditions are corrected even without including nonlinear wave-wave interactions in the adjoint. Nevertheless, to some extent, the nonlinear term still affects the reproduction of the wave energy due to wind. The deficiency of the assimilation scheme developed in this study is obvious. When the wave energy due to swells and local winds can not be properly separated, it is not possible to distinguish the error contributions from different model inputs. Hence, subsequent adjustments to the model inputs cannot be performed correctly. As pointed out by Veeramony et al. (2010), under such conditions, interactions between swells and windsea components will make the reproduction of the boundary conditions difficult with the adjoint excluding the nonlinear interaction term even if the boundary conditions are assimilated solely. On the other hand, uniform winds and boundary conditions actually give a perfect correlation of the control variables in space. Hence, it is expected that the assimilation scheme works in areas where the spatially varying model inputs are well correlated and the covariance matrix are well estimated even with limited observations. Therefore, even without spatially broad observations, practical applications are possible in the German Bight or other regions when credible correlations for

model inputs in space are obtained.

## Acknowledgements

We gratefully acknowledge financial support from China Scholarship Council. Also, we are grateful to SWAN group of Delft University of Technology, who kindly provides the open source of the SWAN model.

## Bibliography

Bauer, E., Hasselmann, S., Hasselmann, K., and Graber, H. C. (1992). Validation and Assimilation of Seasat Altimeter Wave Heights Using the Wam Wave Model. *Journal of Geophysical Research-Oceans*, 97(C8):12671–12682.

Bennett, A. and McIntosh, P. (1982). Open ocean modeling as an inverse problem: tidal theory. *Journal of Physical Oceanography*, 12(10):1004–1018.

Booij, N., Ris, R. C., and Holthuijsen, L. H. (1999). A third-generation wave model for coastal regions: 1. Model description and validation. *Journal of Geophysical Research*, 104(C4):7649.

De Las Heras, M. M., Burgers, G., and Janssen, P. a. E. M. (1994). Variational Wave Data Assimilation in a Third-Generation Wave Model. *Journal of Atmospheric and Oceanic Technology*, 11(5):1350–1369.

De las Heras, M. M. and Janssen, P. a. E. M. (1992). Data assimilation with a coupled wind-wave model. *J. Geophys. Res.*, 97(C12):20261–20270.

Dee, D., Uppala, S., Simmons, A., Berrisford, P., Poli, P., Kobayashi, S., Andrae, U., Balmaseda, M., Balsamo, G., Bauer, P., et al. (2011). The era-interim reanalysis: Configuration and performance of the data assimilation system. *Quarterly Journal of the royal meteorological society*, 137(656):553–597.

Emmanouil, G., Galanis, G., and Kallos, G. (2010). A new methodology for using buoy measurements in sea wave data assimilation. *Ocean dynamics*, 60(5):1205–1218.

Emmanouil, G., Galanis, G., and Kallos, G. (2012). Combination of statistical kalman filters and data assimilation for improving ocean waves analysis and forecasting. *Ocean Modelling*, 59:11–23.

Esteva, D. C. (1988). Evaluation of Preliminary Experiments Assimilating Seasat Significant Wave Heights Into a Spectral Wave Model. *J. Geophysical Res.*, 93(C11):14099–14105.

Hasselmann, K. (1963). On the non-linear energy transfer in a gravity-wave spectrum. Part 3. Evaluation of the energy flux and swell-sea interaction for a Neumann spectrum. *Journal of Fluid Mechanics*, 15(03):385.

Hasselmann, K., Barnett, T. P., Bouws, E., Carlson, H., Cartwright, D. E., Enke, K., Ewing, J. a., Gienapp, H., Hasselmann, D. E., Kruseman, P., Meerburg, a., Muller, P., Olbers, D. J., Richter, K., Sell, W., and Walden, H. (1973). Measurements of Wind-Wave Growth and Swell Decay during the Joint North Sea Wave Project (JONSWAP). *Ergnzungsheft zur Deutschen Hydrographischen Zeitschrift Reihe*, A(8)(8 0):p.95.

Hasselmann, S., Lionello, P., and Hasselmann, K. (1997). An optimal interpolation of spectral wave data. *Journal of Geophysical Research*, 102(C7):15,823–15,836.

Hersbach, H. (1998). Application of the adjoint of the WAM model to inverse wave modeling. *J. Geophys. Res.*, 103:10469–10487.

Komen, G., Hasselmann, K., and Hasselmann, K. (1984). On the existence of a fully developed wind-sea spectrum. *Journal of physical oceanography*, 14(8):1271–1285.

Lahoz, W., Khattatov, B., and Menard, R. (2010). *Data assimilation: making sense of observations*. Springer Science & Business Media.

Lionello, P., Günther, H., and Janssen, P. A. (1992). Assimilation of altimeter data in a global third-generation wave model. *Journal of Geophysical Research: Oceans*, 97(C9):14453–14474.

Majewski, D., Liermann, D., Prohl, P., Ritter, B., Buchhold, M., Hanisch, T., Paul, G., Wergen, W., and Baumgardner, J. (2002). The operational global icosahedral-hexagonal gridpoint model gme: Description and high-resolution tests. *Monthly Weather Review*, 130(2):319–338.

Orzech, M. D., Veeramony, J., and Ngodock, H. (2013). A variational assimilation system for nearshore wave modeling. *Journal of Atmospheric and Oceanic Technology*, 30(5):953–970.

Panteleev, G., Yaremchuk, M., and Rogers, W. E. (2015). Adjoint-free variational data assimilation into a regional wave model. *Journal of Atmospheric and Oceanic Technology*, 32(7):1386–1399.

Polak, E. (1971). Computational methods in optimization academic. *New York*.

Portilla, J. (2009). *Buoy data assimilation in nearshore wave modeling*. PhD thesis, Ph D dissertation, KU Leuven, Belgium.

Siddons, L. a., Wyatt, L. R., and Wolf, J. (2009). Assimilation of HF radar data into the SWAN wave model. *Journal of Marine Systems*, 77(3):312–324.

Snyder, R., Dobson, F., Elliott, J., and Long, R. (1981). Array measurements of atmospheric pressure fluctuations above surface gravity waves. *Journal of Fluid Mechanics*, 102:1–59.

Veeramony, J., Walker, D., and Hsu, L. (2010). A variational data assimilation system for nearshore applications of SWAN. *Ocean Modelling*, 35(3):206–214.

Voorrips, a. C., Makin, V. K., and Hasselmann, S. (1997). Assimilation of wave spectra from pitch-and-roll buoys in a North Sea wave model. *Journal of Geophysical Research*, 102(C3):5829.

Wahle, K., Staneva, J., and Guenther, H. (2015). Data assimilation of ocean wind waves using Neural Networks: A case study for the German Bight. *Ocean Modelling*, 96:117–125.

Walker, D. T. (2006). Assimilation of sar imagery in a nearshore spectral wave model. Technical report.

Waters, J., Wyatt, L. R., Wolf, J., and Hines, A. (2013). Data assimilation of partitioned HF radar wave data into Wavewatch III. *Ocean Modelling*, 72:17–31.

# Chapter 4

# Applications of assimilation schemes

*An application study on 4D variational wave assimilation scheme in German Bight with low spatial observation coverage.* Song, Q. and R. Mayerle.

# An application study on 4D variational wave assimilation scheme in German Bight with low spatial observation coverage

**Qingyang Song and Roberto Mayerle**

**Abstract:** *A 4D variational assimilation scheme with partition method is modified for practical application of wave simulation in German Bight. Sensitivity analysis reveals that limited observing locations cannot be sensitive to errors of boundary conditions over the whole wave boundaries under varying wave conditions. Therefore, a scheme designed for low spatial observation coverage by assuming couple of 'basic' inputs containing all errors is proposed. Twin experiments with pseudo observations are carried out to assess the feasibility of the scheme with basic inputs. The proposed scheme using a single observing location shows comparable assimilation effect with the original scheme without the basic inputs assumption using 25 observing locations, reducing spectrum RMS errors by around 50% throughout the whole computation domain. The practical experiment is performed over one day, considering both wave boundary conditions and wind fields as control variables. The spectrum RMS errors at the validation buoy decline by more than 60% by means of the proposed assimilation scheme with observations from a single in-situ buoy. Overall, although the basic input assumption will somehow overestimate the spatial correlation of the input errors and consequently adjust the model inputs improperly in some areas, the scheme is still a good option for nearshore wave simulation where sea states are strong correlated when observations are spatially limited.*

**Keywords:** 4D variational assimilation; Wave modeling; sensitivity; observation coverage

## 4.1 Introduction

Ocean wave conditions are crucial for human activities in coastal areas. The need of the accurate information about waves is keeping increasing since marine exploitation, commercial transportation and coastal construction are becoming more and more frequent. Numerical simulation is a convenient and economical option to hindcast or forecast ocean waves. However, in practice, modeling ocean waves is always challenging, especially in coastal areas. Nowadays, assimilation techniques are widely applied to improve the accuracy of numerical ocean models with various assimilation approaches eg. 4D variation, optimal interpolation, and Kalman filters. But regardless of the approaches applied, observations are always essential for assimilation effects. In-situ wave observations in coastal area are occasionally restricted to irregular bathymetry or extreme wave conditions and in most case, relatively expensive. It is almost impossible to provide spatially broad distributed wave data. On the other hand, using of remote sensing data is handicapped by its long measuring cycles and difficulties in information retrieval. Therefore, effective assimilation schemes requiring only limited observations are useful in nearshore wave simulations.

Recently, several assimilation schemes have been applied in regional wave models concentrating on coastal process (Portilla, 2009; Siddons et al., 2009; Veeramony et al., 2010; Waters et al., 2013; Wahle et al., 2015; Song and Mayerle, 2017). Compared with large scale models, sea state conditions in coastal domains with the size in the order of a few kilometers are usually strong correlated in space, which makes it possible to provide spatially uniform model inputs over the study area such as wind fields, boundary conditions or drag coefficients (Veeramony et al., 2010). But obviously, the simplication is inappropriate for larger area. Siddons et al. (2009) employed HF radar wave data so as to improve the assimilation scheme incorporating spatially correlated errors. Portilla (2009) designed a specific gain matrix in their optimal interpolation scheme according to the topography off the Belgian continental shelf. The gain matrix allows for a more realistic correlations of wave conditions surrounding the location of a single buoy and consequently improves the assimilation effect. Besides, Panteleev et al. (2015) developed a regional wave assimilation scheme based on adjoint-free methods to correct initial wave conditions and Wahle et al. (2015) applied neural networks to improve input wind fields. Those two studies both utilized pseudo observations to assess their assimilation schemes and the results revealed the importance of spatial observation coverage in the research domains to some extent. At the same time, some attempts were made to extend the beneficial influence of the assimilation combining limited observations in time

and space (Emmanouil et al., 2010, 2012). They kept the observation information longer in the simulation procedure by applying a bias correction within the forecasting horizon in their second-order KF and optimal interpolation schemes to improve the model performance in the North Atlantic. Additionally, Orzech et al. (2014) applied adjoint-based sensitivity map for waves to identify alternate locations whose spectral energy levels are most correlated with the concerned area. The technique can also be utilized to identify sensitivity of observations to control variables in an adjoint-based assimilation scheme.

In the present study, the 4D variational assimilation scheme with partition methods for nearshore wave model developed by Song and Mayerle (2017) is modified and applied in the German Bight using buoy in-situ observations provided by BSH (Bundesamt Fuer Seeschi fahrt und Hydrographie). To improve the assimilation effect with limited observations from a single buoy, it is assumed that there is a set of basic model inputs containing all the errors. Therefore, spatially varying model inputs such as wind fields and wave conditions can be explicitly represented by the basic inputs combined with some perturbations. Hence, under the basic input assumption, observations at a selected buoy location become sensitive to the model inputs throughout the whole computation area, which makes the scheme capable of correcting the spatially varying model inputs with low spatial observation coverage. Experiments with pseudo observations are performed to examine the feasibility of the proposed scheme after sensitivity analysis. The assimilation effect by adjusting wave boundary conditions of the modified scheme using a single observational location is compared with that of the original scheme without basic inputs assumption using varying numbers of observational locations in the experiments. After that, a practical experiment under nonstationary conditions considering both wind fields and wave boundary conditions as control variables is carried out to further assess the proposed scheme.

## 4.2 Method

### 4.2.1 SWAN wave model

SWAN (Simulating Waves Nearshore) is a third generation wave model widely used in coastal areas, lakes, and estuaries (Booij et al., 1999). As a phase-averaged stochastic wave model, SWAN solves the following action balanced equation:

$$\frac{\partial N}{\partial t} + \vec{\nabla}(\vec{C}N) = \frac{S}{\sigma} \tag{4.1}$$

The first term in the left is the local variation of the action density $N(x, y, \theta, \sigma)$. The second term describes the propagation of $N$, where $\vec{C} = (C_x, C_y, C_\theta, C_\sigma)$ is the propagation velocity of wave energy in space and spectrum domain. The term in the right is the source and sink term of $N$, where $\sigma$ is the circular frequency and $S$ includes wind growth, dissipations and nonlinear wave-wave interactions. By provided correct bathymetry, wave boundary conditions, wind fields and other model inputs, SWAN is able to solve Eq. (4.1) with limited difference method obtaining 2D wave spectra throughout whole computational domains.

### 4.2.2 Assimilation scheme

The assimilation scheme applied in this study is a 4D variational assimilation scheme with partition methods tailored for SWAN wave model. The scheme applies a full adjoint model derived directly from differential equations apart from the nonlinear terms to minimize the cost function. Partition methods are implemented in the scheme to correct swell and windsea contributions of wave spectra separately. By providing defined correlations of model inputs in time, the scheme can be applied under nonstationary wave conditions. For assessing the scheme, a set of uniform model inputs, wave boundary conditions and wind components, is selected as control variables by Song and Mayerle (2017). Nevertheless, the uniform model inputs in space are obviously inappropriate in this study. Therefore, spatially varying model inputs are employed in the modified schemes. However, initial sea state is still not set as the control vector in this study. Actually, accurate initial sea state can be obtained by adjusting other model inputs such as winds and wave boundary conditions under stationary simulations in which case the initial sea state will not affect the eventual simulation results through several iterations. On the other hand, occasionally, sea state over the whole computation domain is difficult to be effectively assimilated with limited observations by means of the scheme proposed in this study. Hence, the cost function reads:

$$J = J_1 + J_2 + J_3 \tag{4.2}$$

where $J_1$, $J_2$ and $J_3$ are observation deviation, wind deviation and boundary spectrum deviation terms respectively. The deviation from observations is expressed by error variance of spectra. The $J_1$ reads:

$$J_1(E) = \frac{1}{M_{obs}} \frac{1}{T} \iiint (\boldsymbol{E} - \boldsymbol{E_a})^T \boldsymbol{W_1} (\boldsymbol{E} - \boldsymbol{E_a}) \mathrm{d}\theta \mathrm{d}f \mathrm{d}t \tag{4.3}$$

Where $\boldsymbol{E}$ is a compact form in space of the wave spectrum density and the subscript $a$ denotes the observations. $\boldsymbol{W_1}$ reflects the uncertainty of observations. In this case, $\boldsymbol{W_1}$ is the inverse spatial error covariance matrix of observed wave energy assuming that the observed spectrum density has the same spatial correlations in all the frequencies and directions. $M_{obs}$ indicates the total number of the observations used for assimilation over space and time. $J_2$ is the wind deviation, it reads:

$$J_2(u,v) = \frac{1}{A_D}\iint [(\boldsymbol{u}-\boldsymbol{u_{1st}})^T \boldsymbol{W_{2u}} (\boldsymbol{u}-\boldsymbol{u_{1st}}) + (\boldsymbol{v}-\boldsymbol{v_{1st}})^T \boldsymbol{W_{2v}} (\boldsymbol{v}-\boldsymbol{v_{1st}})] \mathrm{d}x\mathrm{d}t \tag{4.4}$$

Where $\boldsymbol{u}$ and $\boldsymbol{v}$ are the space vectors of wind components and the subscript $1st$ indicates the first guess value. $\boldsymbol{W_{2u}}$ and $\boldsymbol{W_{2v}}$ are the inverse error covariance matrix of $\boldsymbol{u}$ and $\boldsymbol{v}$ respectively. $A_D$ is the area of computation domain. Similarly, $J_3$ reads:

$$J_3(E_b) = \tfrac{1}{L_b}\iiiint (\boldsymbol{E_b}-\boldsymbol{E_{b_{1st}}})^T \boldsymbol{W_3} (\boldsymbol{E_b}-\boldsymbol{E_{b_{1st}}})\, \mathrm{d}\theta \mathrm{d}f \mathrm{d}x_b \mathrm{d}t \tag{4.5}$$

Where the subscript $b$ denotes the input wave spectra on open boundaries and $L_b$ is the length of the boundaries. Analogously, $\boldsymbol{W_3}$ is the inverse spatial covariance matrix of the first guess input wave energy on open boundaries.

Time dependent model inputs such as wind fields or wave boundaries in a forward model are normally obtained by interpolating the inputs at the start and end points of an input interval to match the computation time step. Therefore, a time dependent control variable $c$ can be expressed by a linear combination of multiple time independent control variables:

$$c(t) = \textstyle\sum_{n=1}^{N} w_n(t) c_n \tag{4.6}$$

where $w_n(t)$ denotes the interpolation weighting function with respect to time and $c_n$ is the control variable at the start or end time point of an input interval. Normally, $w_n(t)$ is a linear function of time. Thus, the time dependent control variables $E_b$ and $u$, $v$ in Eq. (4.4) and Eq. (4.5) can be replaced by time independent control variables $E_{bn}$ and $u_n$, $v_n$. The expressions of $J_2$ and $J_3$ are changed to:

$$J_2(u_n,v_n) = \frac{1}{A_D}\sum_{n=1}^{N}\int [(\boldsymbol{u_n}-\boldsymbol{u_{n_{1st}}})^T \boldsymbol{W_{2nu}} (\boldsymbol{u_n}-\boldsymbol{u_{n_{1st}}}) + (\boldsymbol{v_n}-\boldsymbol{v_{n_{1st}}})^T \boldsymbol{W_{2nv}} (\boldsymbol{v_n}-\boldsymbol{v_{n_{1st}}})] \mathrm{d}x \tag{4.7}$$

$$J_3(E_{bn}) = \tfrac{1}{L_b}\textstyle\sum_{n=1}^{N}\iiint (\boldsymbol{E_{bn}}-\boldsymbol{E_{bn_{1st}}})^T \boldsymbol{W_{3n}} (\boldsymbol{E_{bn}}-\boldsymbol{E_{bn_{1st}}})\, \mathrm{d}\theta \mathrm{d}f \mathrm{d}x_b \tag{4.8}$$

According to Song and Mayerle (2017), it is assumed that waves can be regarded as linear superpositions of swell and windsea contributions. Hence, following Lagrange multiplier method, the resulting adjoints read:

for windsea:

$$-\frac{\partial \lambda_w}{\partial t} - \vec{C}\vec{\nabla}\lambda_w = \lambda_w \frac{\partial S_w}{\partial E} - \frac{\partial J_{1w}}{\partial N}\delta(x - x_a)\delta(t - t_a) \tag{4.9}$$

for swell:

$$-\frac{\partial \lambda_s}{\partial t} - \vec{C}\vec{\nabla}\lambda_s = \lambda_s \frac{\partial S_s}{\partial E} - \frac{\partial J_{1s}}{\partial N}\delta(x - x_a)\delta(t - t_a) \tag{4.10}$$

$J_{1w}$ and $J_{1s}$ are the windsea and swell contributions of $J_1$ respectively. The windsea and swell contributions are separated and classified by the partition method (Hasselmann et al., 1997). $S_w$ and $S_s$ are the source/sink terms related to local winds and swells respectively. After obtaining the Lagrange multipliers $\lambda_w$ and $\lambda_s$, through solving Eq. (4.9) and Eq. (4.10), gradients of the cost function with respect to the control variables can be calculated using the formulas as follows:

for wind fields:

$$\begin{aligned} \mathrm{grad}_{u_n} J &= \frac{\partial J_2}{\partial u_n} - \iiint [\frac{\lambda_w w_n(t)}{2\pi f}\frac{\partial S_w}{\partial u}]\mathrm{d}\theta \mathrm{d}f\mathrm{d}t \\ \mathrm{grad}_{v_n} J &= \frac{\partial J_2}{\partial v_n} - \iiint [\frac{\lambda_w w_n(t)}{2\pi f}\frac{\partial S_w}{\partial v}]\mathrm{d}\theta \mathrm{d}f\mathrm{d}t \end{aligned} \tag{4.11}$$

for wave boundaries:

$$\mathrm{grad}_{E_{bn}} J = \frac{\partial J_3}{\partial E_{bn}} - \int [\frac{w_n(t)}{2\pi f}\lambda_s \vec{C}\vec{n_b}]\mathrm{d}t \tag{4.12}$$

where $(u_n, v_n)$ are the input wind components, $E_{bn}$ is the input wave spectra on open boundaries and $\vec{n_b}$ is the direction vector normal to the boundary. Since the gradients are accessible, increments of the control variables can be obtained by means of optimization algorithms such as the conjugate-gradient descent algorithm (Polak, 1971) to update the forward wave model. From Eq. (4.2) to Eq. (4.12), the assimilation scheme, hereafter referred to as OAS (the original assimilation scheme), requires accurately estimated spatial error covariance matrix of observations and the chosen model inputs. Meanwhile, the assimilation effect with spatially limited observations is doubtful, since the sensitivity of the observations to the control variables is unknown.

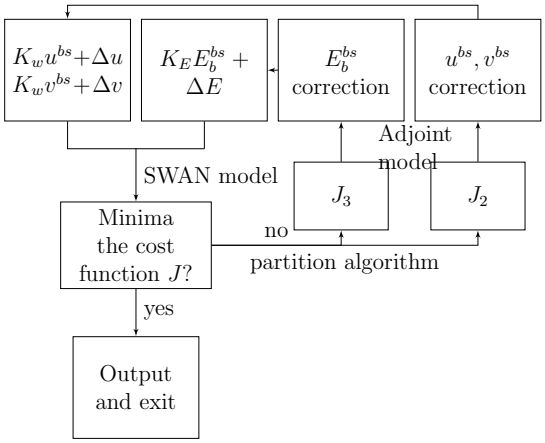


Figure 4.1: Adopted data assimilation scheme

### 4.2.3 Basic model inputs

It is expected that, in the coastal sea area where the sea states are strong correlated, dimensionality reduction of the control variable vectors is a good option for applications when only limited observations are available.

It is assumed that there are a spatially uniform basic wave boundary condition and a couple of basic wind components in the study area. The spatially varying local inputs such as wave boundary conditions and winds can be regarded as the 'bases' combined with perturbations in which way the model inputs are spatially correlated. Another assumption is that the errors of the input waves and wind fields only exist in the 'bases'. In other words, it is assumed that errors in the chosen model inputs throughout certain coastal area are related to a same error source. Hence, in this study, $E_b^{bs}$ and $(u^{bs}, v^{bs})$ are set as the basic model inputs and as well the control variables. In the view of energy, the basic model inputs are regarded as the energy source thereby dissipating or growing to the magnitude of the local inputs. So spatially varying wave boundary conditions and wind components are represented as follows:

$$\begin{aligned} E_b(x) &= K_E(x)E_b^{bs} + \Delta E(x) \\ u(x) &= K_w(x)u^{bs} + \Delta u(x) \\ v(x) &= K_w(x)v^{bs} + \Delta v(x) \end{aligned} \tag{4.13}$$

where $K_E$ and $K_w$ are the coefficients to adjust the magnitude of the basic inputs to that of the local inputs. Hence, they are related to the ratio of the wave energy

and wind speed between basic and local inputs as follows:

$$K_E(x) = (\frac{H_s(x)}{H_s^{bs}})^2; K_w(x) = \frac{w(x)}{w^{bs}} \tag{4.14}$$

where $H_s$ is the significant wave height and $w$ is the wind speed. Since the control variables are changed, the cost function $J_2$ and $J_3$ should be modified to:

$$\begin{aligned} J_2(u_n^{bs}, v_n^{bs}) &= \sum_{n=1}^{N}[W_{2nu}(u_n^{bs} - u_{n_{1st}}^{bs})^2 + W_{2nv}(v_n^{bs} - v_{n_{1st}}^{bs})^2] \\ J_3(E_{bn}^{bs}) &= \sum_{n=1}^{N}\iint [W_{3n}(E_{bn}^{bs} - E_{bn_{1st}}^{bs})^2]\,\mathrm{d}\theta\mathrm{d}f \end{aligned} \tag{4.15}$$

Therefore, the gradient Eq. (4.11) and Eq. (4.12) are subsequently changed as:

for wind fields:

$$\begin{aligned} \mathrm{grad}_{u_n^{bs}} J &= \frac{\partial J_2}{\partial u_n^{bs}} - \iiiint [\frac{\lambda_w w_n(t)}{2\pi f}\frac{\partial S_w}{\partial u}\frac{\partial u}{\partial u^{bs}}]\mathrm{d}\theta\mathrm{d}f\mathrm{d}x\mathrm{d}t \\ \mathrm{grad}_{v_n^{bs}} J &= \frac{\partial J_2}{\partial v_n^{bs}} - \iiiint [\frac{\lambda_w w_n(t)}{2\pi f}\frac{\partial S_w}{\partial v}\frac{\partial v}{\partial v^{bs}}]\mathrm{d}\theta\mathrm{d}f\mathrm{d}x\mathrm{d}t \end{aligned} \tag{4.16}$$

for wave boundaries:

$$\mathrm{grad}_{E_{bn}^{bs}} J = \frac{\partial J_3}{\partial E_{bn}^{bs}} - \iint [\frac{\lambda_s w_n(t)}{2\pi f}\vec{C}\vec{n_b}\frac{\partial E_b}{\partial E_{bn}^{bs}}]\mathrm{d}x_b\mathrm{d}t \tag{4.17}$$

In this study, the first guess $E_{1st}^{bs}$ and $(u_{1st}^{bs}, v_{1st}^{bs})$ in Eq. (4.13) are obtained through averaging the first guess input wave boundary conditions and wind fields. After that, $K_E$ and $K_w$ can be calculated through Eq. (4.14). Then, $\Delta E(x)$ and $(\Delta u(x), \Delta v(x))$, are obtained by Eq. (4.13). The calculation is completed before wave simulations and assimilations. In the assimilation process (see Fig. 4.1), keeping $K_E$, $K_w$, $\Delta E(x)$ and $(\Delta u(x), \Delta v(x))$ constant, $E_{bs}$ and $(u_{bs}, v_{bs})$ are updated by using the gradient calculated through Eq. (4.16) and Eq. (4.17). It is expected that the assimilation scheme, hereafter referred to as BAS (the 'base' assimilation scheme), would work well when errors are only contained in $E_{bs}$ and $(u_{bs}, v_{bs})$. But what should be pointed out is that the method proposed in this section is essentially an interpolation method to provide a assumed spatial correlations of the wave boundary conditions or the wind fields. In that sense, it is analogous to what is applied in time domain. This scheme is consistent with the scheme provided by Song and Mayerle (2017). Actually, when $K_E$ and $K_w$ equal one and $\Delta E(x)$ and $(\Delta u(x), \Delta v(x))$ equal zero, the

assimilation scheme will return to the case with uniform wave boundary conditions and wind fields. What should be pointed out is that the intension of the proposed scheme is not to reduce the dimension of control vectors. The reduction can be done through some schemes such as 4D-PSAS by transferring the control variables from model space to observation space (Courtier, 1997). But those schemes are designed to save computation resources rather than making contributions to improving assimilation results with limit observations. Differently, the proposed scheme BAS is an expedient and convenient method for sea areas with well-correlated sea stats when lack of broadly distributed observations.

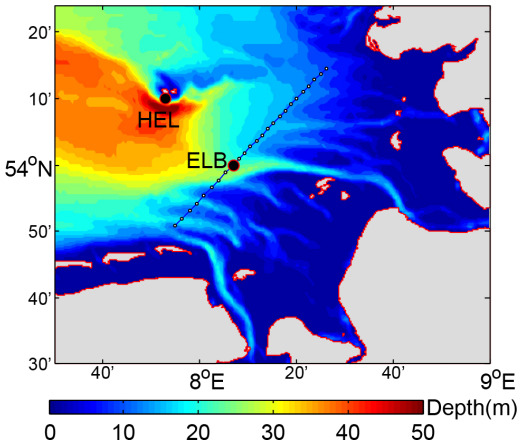


Figure 4.2: Computation domain in German Bight

## 4.3 Twin experiments

Twin experiments are performed to verify the feasibility of the proposed 'base' scheme. The two different schemes, OAS and BAS, are applied in the German Bight with pseudo observations. The experiments are designed to reveal the impact of observation distributions on the assimilation effect of OAS and to compare the assimilation effects of the two schemes in the study area.

### 4.3.1 Experiment setup

The computational domain in the German Bight on the North Sea covers an area of around 100km × 90km (see Fig. 4.2). The spatial resolution of the model is 500 m. The bathymetry data is provided by GEBCO (The General Bathymetric Chart of the Oceans) dataset (Becker et al., 2009). The wind data is obtained from the GME model (Majewski et al., 2002) whereas the wave boundary data is taken from the ERA-I dataset provided by ECMWF (European Centre for Medium-Range Weather

Forecasts) (Dee et al., 2011). A scenario (at 00:00:00 on 2011/03/06) in which swells are dominant in the study area is selected for the experiments. Therefore only wave boundary conditions are considered as the control variables.

There are three groups of input wave boundary conditions used in the experiments: the 'real' wave boundaries, the wave boundaries providing pseudo observations and the first guess boundaries. The original wave boundary conditions from ERA-I are regarded as the 'real' wave boundaries. Since only the wave statistic parameters are used in this study providing the boundary conditions, the total wave energy on the boundaries is changed by altering the significant wave height to produce the other two groups of the wave boundaries. The experiments are only performed at 00:00:00 on 2011/03/06 under the stationary wave condition but the calculation of covariance requires a relative large sample number so as to prevent producing a singular covariance matrix with low rank by accidents. Although the singular matrix will not handicap the calculation if using a pseudo inverse, it is not normally consistent with the real case for boundary conditions. Therefore, the alteration of the significant wave height is processed as follows:

$$\begin{aligned} H_S^p(x_b,t) &= H_S^r(x_b,t) + N_{0.1}(t),\ N_{0.1} \sim N(0, 0.1H_S^r(x_b,t_0)) \\ H_S^f(x_b,t) &= H_S^r(x_b,t) + N_{0.3}(t),\ N_{0.3} \sim N(0, 0.3H_S^r(x_b,t_0)) \end{aligned} \tag{4.18}$$

where $N_{0.1}$ and $N_{0.3}$ are random functions with normal distributions, the superscripts $r$, $p$ and $f$ denotes the 'real' case, the pseudo case and the first guess case, $t_0$ denotes the time chosen for the stationary experiments. The three groups of the wave boundaries are applied in the SWAN model covering the period from 2011/02/17 to 2011/03/17 to calculate the variance of the wave energy of the pseudo observations and the first guess wave boundary conditions. Additionally, spatially homogeneous and isotropic error correlation structure is assumed in the study area as a exponential decay curves with distance (Voorrips et al., 1997; Portilla, 2009):

$$\rho_{ij} = \exp[-(\frac{|x_i - x_j|}{L})^a] \tag{4.19}$$

where $|x_i - x_j|$ gives the distance between two grids, $L$ is a correlation length and $a$ is a estimated power. $L$ is set to be 200 km and $a$ is set to be 1.5 following the research form Voorrips et al. (1997); Portilla (2009). Thus, the error covariance matrix of wave energy can be obtained through multiplying the correlation structure with the calculated variance and subsequently obtaining $W_1$ and $W_3$. The motivation not to calculate the covariance directly is that the identical boundary conditions at some grids on boundaries due to the relatively lower spatial resolution of ERA-I data are

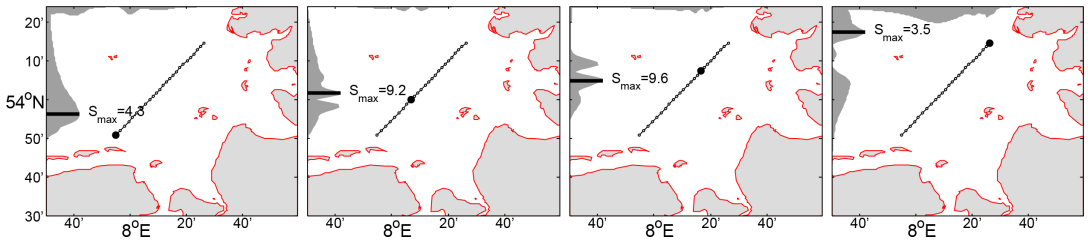


Figure 4.3: sensitivity map of boundary conditions to single observing location on the selected curve

easier to result in a singular covariance matrix.

Another issue required to be addressed in the experiments is the locations of pseudo observations used for assimilations. There are two wave buoys from BSH (Bundesamt Fuer Seeschifffahrt und Hydrographie) named Elbe (ELB) and Helgoland (HEL) in this area. Since the derived adjoint does not include non-linear wave-wave interactions, keeping the non-linear effect as weak as possible around the observing location for assimilations will be important to guarantee assimilation effects of the schemes. Therefore, the locations with complex local bathymetry as the station HEL where bottom refractions are expected or at the very shallow water where steep waves will lead to strong non-linear interactions (Beji and Battjes, 1993) are not proper options for assimilated observing locations. Hence, a curve crossing the station ELB (Fig. 4.2) and almost covering all the wave traveling paths from the open boundaries is selected for the pseudo observing locations. 25 locations are determined with constant distance from the station ELB spreading towards two sides along the curve. The station ELB will be the single observation selected for the scheme BAS. In the scheme OAS, the number of observing locations increases in turn as 1, 2, 4, 7, 13, 25 to reveal the effect of spatial observation coverage.

A normalized RMS spectrum difference is defined as follows to assess the two schemes (Song and Mayerle, 2017):

$$E_{rms} = \sqrt{\frac{\langle (E_{real} - E_{mod})^2 \rangle}{\langle E_{real}^2 \rangle}} \tag{4.20}$$

Where $E_{mod}$ is the modeled spectrum density, $E_{real}$ is the 'real' spectrum density. The angular brackets denote averaging in space, time, and over the frequency domain (Panteleev et al., 2015).

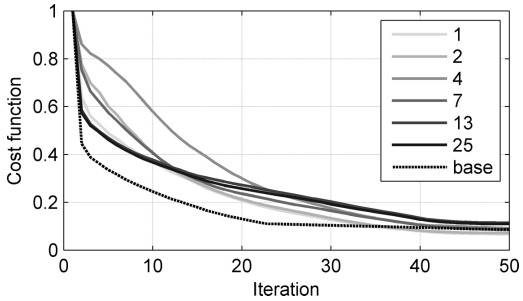


Figure 4.4: Relative cost function with respect to iteration number of BAS and OAS with different numbers of observing locations and in twin experiments.

### 4.3.2 Sensitivity map

system indicator by computing the differential of that indicator at all domain locations in response to a unit impulse applied to a specific system parameter at a chosen location (Orzech et al., 2014). A sensitive map over open boundaries in response to impulses at observing locations is helpful to understand the importance of the observation coverage in the study area under certain wave conditions. A sensitivity metrics based on adjoint-estimated gradient of the cost function with respect to the control variables is defined as follows:

$$G(x_b) = (\frac{\lambda_s}{2\pi f}\vec{C}\vec{n_b}\frac{\partial E_b}{\partial E_b})|_{x_b}\mathrm{d}x_b \tag{4.21}$$

$$\boldsymbol{S(G)} = \sqrt{\iint (\boldsymbol{G})^2 \mathrm{d}\theta \mathrm{d}f} \tag{4.22}$$

Where $\boldsymbol{G}$ is analogous to the gain matrix in the Kalman Filter method reflecting the sensitivity of the analytic system with respect to the observations (Cardinali, 2014), the sensitivity metrics $\boldsymbol{S}$ is defined as sensitive energy integrated over the spectral sensitivity. The sensitivity metrics is calculated through the adjoint model along the whole open boundaries setting the spectral deviation of the first guess results from the pseudo observations at each observing location on the curve as an impulse.

Four different sensitivity maps are shown in Fig. 4.3 with different source locations of the impulse on the curve. The sensitivity metrics $\boldsymbol{S}$ has a peak segment on each the west and north boundary. The directionally distributed wave energy at source locations of impulses comes from different segments in each boundaries. Thus, the peak segments are roughly located on each boundaries where providing most wave energy to selected source locations. The mean wave direction of the input swells is around 300 degree in nautical coordinates alongside with the south-north isobath

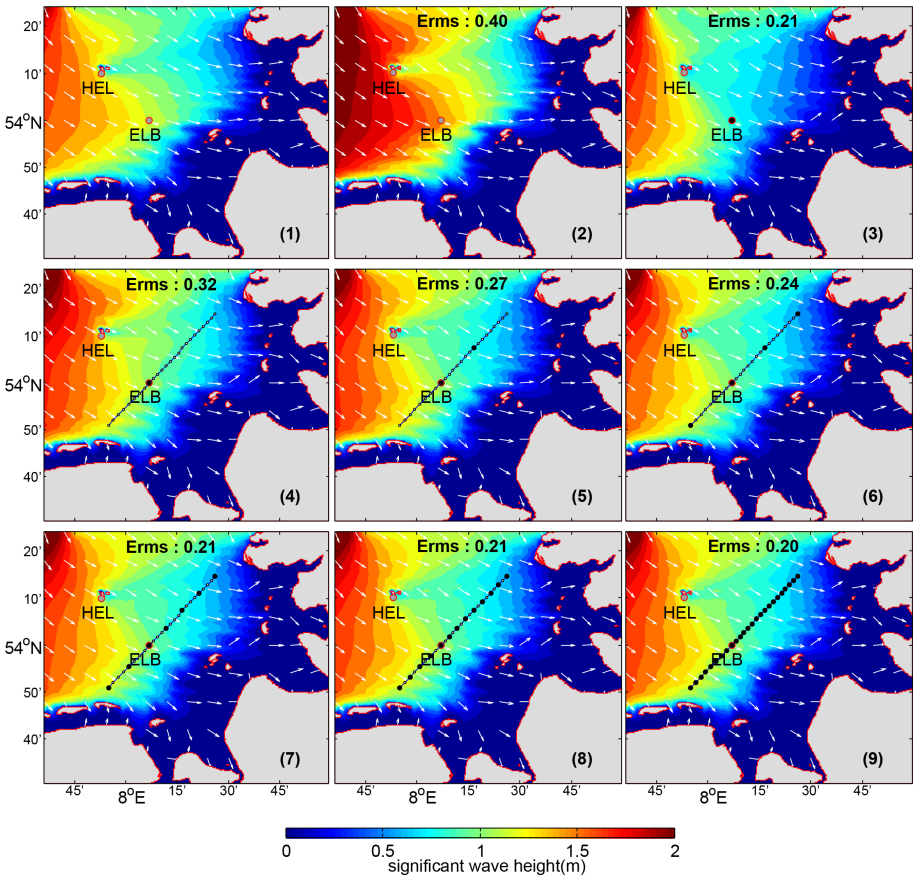


Figure 4.5: Significant wave height and mean wave direction throughout the computational domain. (1) Real; (2) First guess results; (3) BAS; (4)-(9) OAS with 1,2,4,7,13,25 observational locations respectively. Black solid circles denote the involved observing locations in the assimilations

direction causing more wave energy from the west boundary and consequently high sensitivities on it. A double-peak structure appears on both boundaries when the source locations are moved to the center region of the study area where are further away from the boundaries. The fact indicates the spectral differences on the source locations further from the boundaries mainly come from two different segments on one boundary due to directional spreading of the input wave spectra and diffusions when wave propagates. oppositely, if the source locations are closer to the boundaries or the island Heligoland is in wave travel paths blocking incoming waves by reflection and refraction, the double-peaked structure disappears. Generally, the sensitivity distribution on the wave open boundaries depends on wave travel paths affected by topography, wave diffusion, wave reflection and directional spreading of wave spectra as expected. In other words, sensitivity maps varies with wave conditions even impulses come from the same location, which implies that it is difficult to guarantee spatial observation coverage sufficient when applying OAS if wave conditions are

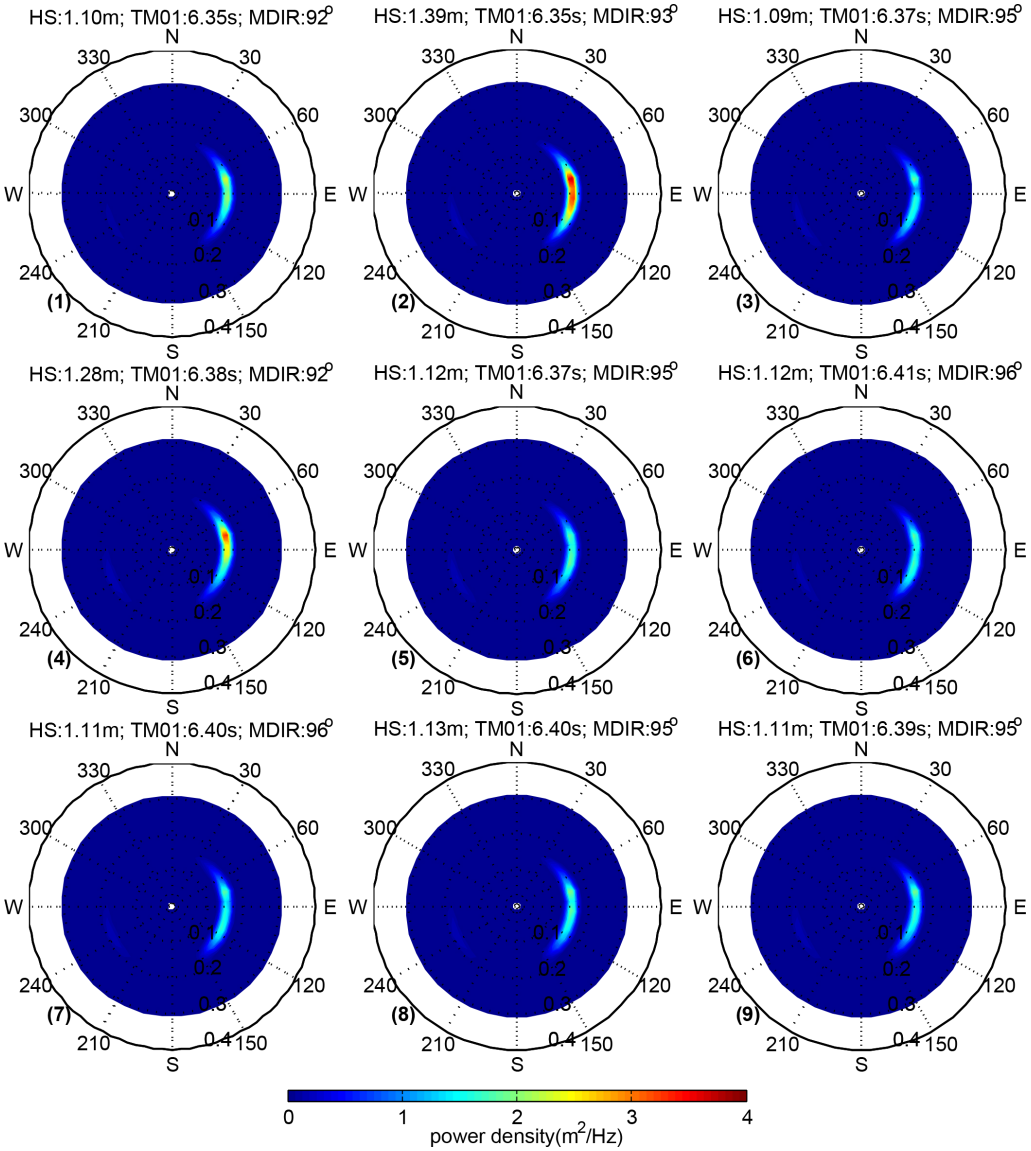


Figure 4.6: 2D spectrum at the station HEL. (1) Real; (2) First guess results; (3) BAS; (4)-(9) OAS with 1,2,4,7,13,25 observational locations respectively.

arbitrary.

### 4.3.3 Experiment results

The assimilation results after 50 iterations are presented in this section. In the experiments, the scheme BAS is proved to have a higher convergence rate due to a lower dimension of the control vectors. The cost function $J$ of BAS converges to around 10% after 20 iterations, while OAS converges after 40 iterations (see Fig. 4.4). The coverage of observations does not have a notable influence on eventual iteration steps of convergence but it does affect the early convergence rate which may be resulted from the varying sensitivity of the observing locations to the boundary

conditions (Fig. 4.4).

Fig. 4.5 reveals that, for the assimilation scheme OAS, broadening the observation coverage makes contributes to improve the assimilation effect by which through the whole computation domain, the remaining $E_{rms}$ after assimilations declines from 0.32 to 0.20. Actually, the reduction of $E_{rms}$ slows down when the two endpoints of the curve have been occupied as the observing locations(Fig. 4.5(6) to Fig. 4.5(9)). In the view of the sensitivity, the four observations in Fig. 4.5(6) are the most efficient strategy to correct boundary conditions for the scheme OAS in the experiments. Nevertheless, the remaining $E_{rms}$ is still 0.2 even with 25 observations on the selected curve which is larger than the results of Song and Mayerle (2017) with uniform inputs. It is noticed that the assimilation scheme dose not function properly in the segment on the boundaries around the upwave side of the Heligoland island. The island blocks the wave propagation in which case observations on the curve contain few wave energy from that segment. Therefore, errors of the input waves from the segment can not be inversed and corrected by the adjoint properly, unless provided a strong spatial correlations such as assuming a uniform boundary condition. The scheme BAS actually gives a relative strong correlations with the basic boundary conditions consequently being more influential in that area (Fig. 4.5(3)). The scheme BAS shows better performance with the remaining $E_{rms}$ of 0.21 than OAS when using the same single observation at the station ELB. Also, the adjustment for the north open boundary in BAS is more prominent than the OAS due to the basic boundary conditions. But at the same time, the scheme BAS overly adjust the boundary conditions in some segments compared with the results from OAS with multiple observations. For example, at the station HEL, the spectrum density after BAS becomes lower than the 'real' one in some directions (Fig. 4.6). Even so, the experiments confirm that the scheme BAS is feasible in the study area as an expedient with limited observations.

## 4.4 Practical experiment

A practical experiment in the German Bight is presented here to further assess the proposed assimilation scheme BAS, as the feasibility has been proved in the twin experiments. The experiment is carried out with nonstationary wave conditions over one day (From 2011/03/12 to 2011/03/13). The first guess wind fields and wave boundary conditions are from the same database as applied in the twin experiments. According to the first guess input data on 2011/03/12, in the study area, the average wind speed fluctuate from 5m/s to 10m/s and there are swells entering from the west

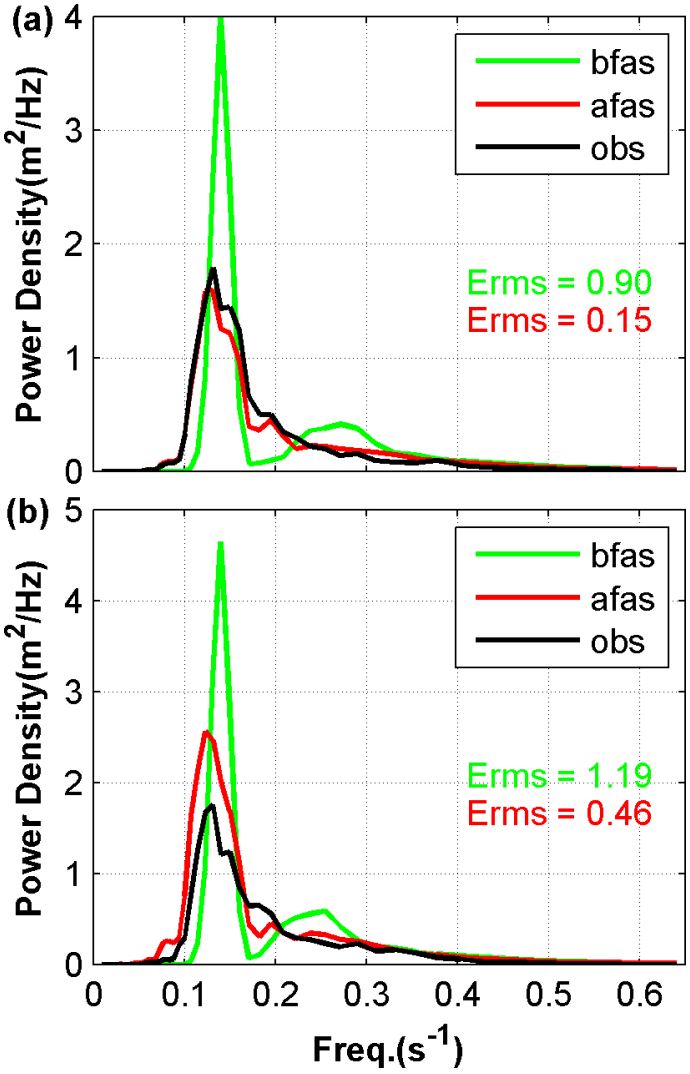


Figure 4.7: Initial 1D frequencial spectrum at the buoy locations from obs (observation), bfas (first guess results before assimilation) and afas (analyzed results after assimilation) at 23:49:00 on 2011/03/11. (a) ELB station; (b) HEL station.

and north boundaries. Hence, wind fields and wave boundary conditions are both considered as the control variables. The involved in-situ data is 1D wave spectra with peak direction and directional spread in each frequencies at the station HEL and ELB provided by BSH. The data at ELB is used for assimilation, while the data at HEL is for validation. The 2D spectra assimilated are reconstructed from the in-situ 1D spectra through the method given by Kuik et al. (1988). Different from the twin experiments, the buoy observations are trusted to be credible assumed as the 'real' sea state. Thus, in the practical experiment, using the scheme BAS,

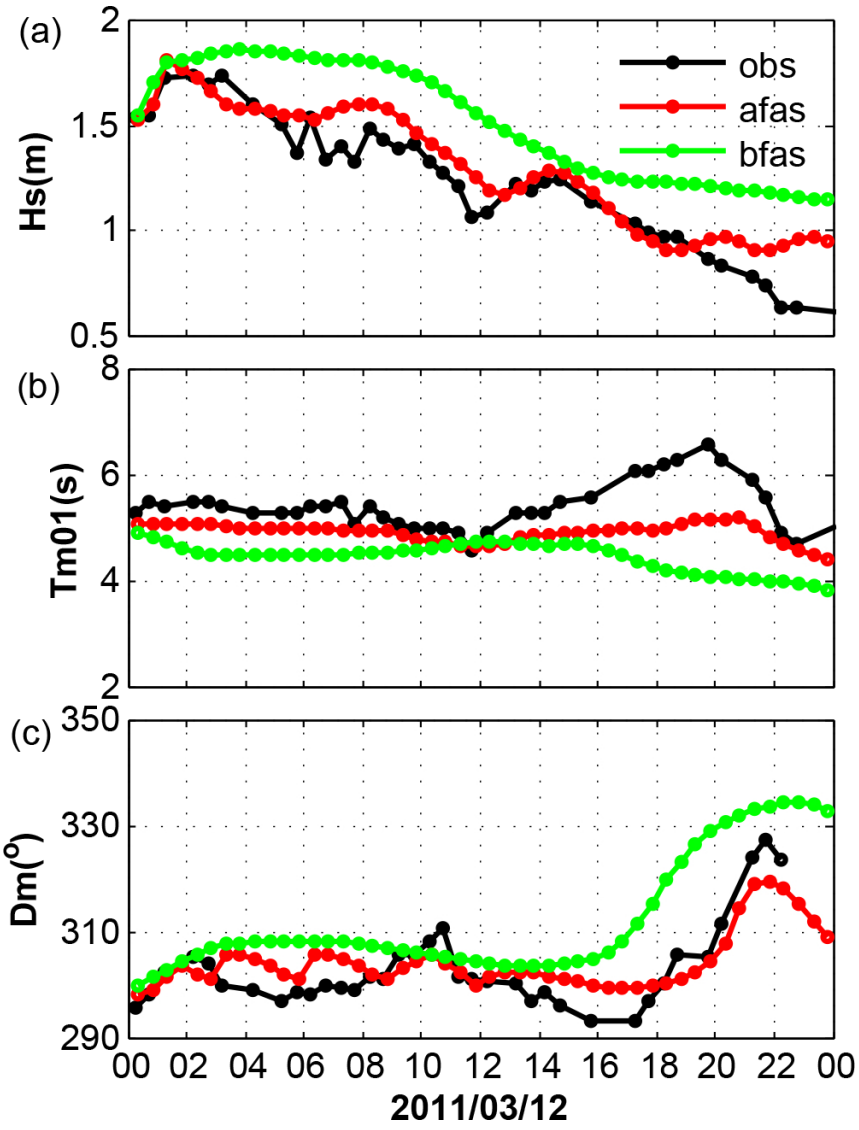


Figure 4.8: Time series from obs (observation), bfas (first guess results before assimilation) and afas (analyzed results after assimilation) at the station HEL in the practical experiment of (a) Significant wave height; (b) Mean wave period; (c)Mean wave direction.

the weights are dimensionally reduced to scalars as follows:

$$\begin{aligned} W_1 &= 1 \\ W_{2u} &= \frac{0.01\bar{E}^2}{\bar{u}^2} \\ W_{2v} &= \frac{0.01\bar{E}^2}{\bar{v}^2} \\ W_3 &= 0.01 \end{aligned} \tag{4.23}$$

where $(\bar{u}, \bar{v})$ is the average value of the first guess wind components and $\bar{E}$ is the average value of the first guess wave energy. The weights $W_1$ and $W_3$ are selected

according to Walker (2006). The values 0.01 and 1 suggest that observations are much more credible than results from simulations. The rate between wave energy and wind speed in $W_2$ is to make the dimension of control variables uniform, provided that the orders of the variance are proportional to that of the corresponding variables.

Initial sea states are obtained by assimilating the in-situ data under stationary conditions at 23:49:00 on 2011/03/11 so as to assume the initial conditions correct in the practical experiment (see Fig. 4.7). It should be pointed out that the 1D in-situ spectrum at HEL is obtained by interpolation due to the absence of measurements at that time.

On 2011/03/12, the $E_{rms}$ at the validation station HEL declined from around 1.9 to 0.7 after assimilation through 30 iterations (Fig. 4.8 and Fig. 4.9). The assimilation scheme is proved to be most effective on the total wave energy represented by significant wave height (Fig. 4.8). On the contrary, mean wave period at HEL is not well corrected, especially when wave energy from swells recedes after 18:00. The fact suggests the wave energy distribution in frequencies is inaccurate, as the mean wave period Tm01 is obtained by calculating the first moment of the power-density-weighted wave period. Different from normally irregular-shaped observation spectra, the 1D spectra from simulation results driven by first guess model inputs reveal relative notable dividing frequencies between swell and wind-sea contributions and regular shapes in both contributions (see Fig. 4.9). Some spectrum shape of swell contributions can be corrected closely to the irregular-shaped in-situ spectra by adjusting the input wave spectra directly on open boundaries in the assimilations. Nevertheless, wind-sea contributions can only be corrected through adjusting the wind components by which total wave energy, peak directions and peak frequencies rather subtle spectrum shapes will be modified. Therefore, the assimilation scheme becomes even more difficult to take effect on redistribution of wave energy in frequencies when wind-sea contributions become more dominant such as on late 03/12. Additionally, some fluctuates of the wave conditions are not emerged in the results after assimilations. That is because a three-hour input window with linear time weights $w_n(t)$ between control variables is almost impossible to recur all the fluctuates of half-hour observations. Even so, the scheme BAS generally covers more than 60% of the errors at the station HEL after assimilations proved to be feasible in practical applications.

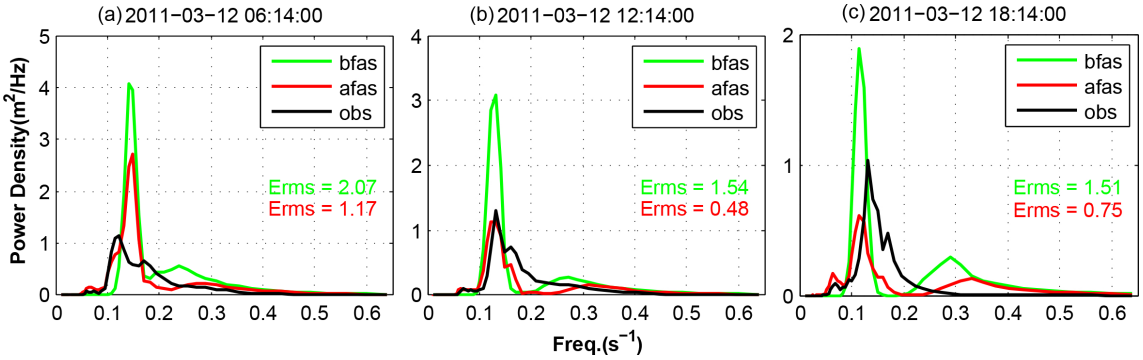


Figure 4.9: 1D frequencial spectrum at the validation station HEL from obs (observation), bfas (first guess results before assimilation) and afas (analyzed results after assimilation). (a) At 06:14:00; (b) At 12:14:00; (c) At 18:14:00 on 2011/03/12.

## 4.5 Summary

In this study, to apply the 4D variational assimilation scheme provided by Song and Mayerle (2017) in the German Bight with a single observation station, basic model inputs are proposed assuming that they contain all the errors. Hence, the spatially varying model inputs such as wave boundary conditions and wind fields can be corrected through adjusting the basic inputs. Before the practical experiment, sensitivity analysis of boundary conditions in response to impulses at observing locations are carried out suggesting that a single observing location is not possible to be sensitive to the input waves over the whole open boundary under varying wave conditions. Since at locations without observations, innovations will be regarded as zero meaning no errors there, the boundary conditions sensitive to the locations will not be adjusted correctly. Further, the twin experiments with pseudo observations confirm the impact of the spatial observation coverage on the assimilation effect through comparing the assimilation results with different coverage of observations. The twin experiments also reveal the feasibility of the basic input assumption, although the scheme BAS with a single observation does not show remarkable advantages compared with OAS using 25 observations on the selected curve. In the one-day practical experiment, the $E_{rms}$ is reduced by more than 60% with the scheme BAS. The assimilation results suggest that basic input assumption is appropriate not only for boundary conditions but also for wind fields in this area if regardless of the deficiency of the original assimilation scheme itself such as incapacity of correcting the spectrum shape of wind-sea contributions and absence of the non-linear terms in the adjoint model for the present. According to the experiments results, it is believed that for the nearshore areas where sea states are strong correlated, the proposed scheme with basic input assumption is a feasible expedient

when the observation coverage is low in space occasionally. Besides, although the proposed scheme are designed for wave hindcast systems, the obtained sea states through assimilations under stationary conditions are adequate as initial conditions contributing to wave forecast.

## Acknowledgements

We gratefully acknowledge financial support from China Scholarship Council. Also, we are grateful to BSH (Bundesamt Fuer Seeschifffahrt und Hydrographie), who kindly provides the in-situ spectra data from buoys in the study area.

## Bibliography

Becker, J., Sandwell, D., Smith, W., Braud, J., Binder, B., Depner, J., Fabre, D., Factor, J., Ingalls, S., Kim, S., et al. (2009). Global bathymetry and elevation data at 30 arc seconds resolution: Srtm30_plus. *Marine Geodesy*, 32(4):355–371.

Beji, S. and Battjes, J. (1993). Experimental investigation of wave propagation over a bar. *Coastal Engineering*, 19(1-2):151–162.

Booij, N., Ris, R. C., and Holthuijsen, L. H. (1999). A third-generation wave model for coastal regions: 1. Model description and validation. *Journal of Geophysical Research*, 104(C4):7649.

Cardinali, C. (2014). Observation impact on the short-range forecast. *Advanced Data Assimilation for Geosciences: Lecture Notes of the Les Houches School of Physics: Special Issue, June 2012*, page 165.

Courtier, P. (1997). Dual formulation of four-dimensional variational assimilation. *Quarterly Journal of the Royal Meteorological Society*, 123(544):2449–2461.

Dee, D., Uppala, S., Simmons, A., Berrisford, P., Poli, P., Kobayashi, S., Andrae, U., Balmaseda, M., Balsamo, G., Bauer, P., et al. (2011). The era-interim reanalysis: Configuration and performance of the data assimilation system. *Quarterly Journal of the royal meteorological society*, 137(656):553–597.

Emmanouil, G., Galanis, G., and Kallos, G. (2010). A new methodology for using buoy measurements in sea wave data assimilation. *Ocean dynamics*, 60(5):1205–1218.

Emmanouil, G., Galanis, G., and Kallos, G. (2012). Combination of statistical kalman filters and data assimilation for improving ocean waves analysis and forecasting. *Ocean Modelling*, 59:11–23.

Hasselmann, S., Lionello, P., and Hasselmann, K. (1997). An optimal interpolation of spectral wave data. *Journal of Geophysical Research*, 102(C7):15,823–15,836.

Kuik, A., Van Vledder, G. P., and Holthuijsen, L. (1988). A method for the routine analysis of pitch-and-roll buoy wave data. *Journal of Physical Oceanography*, 18(7):1020–1034.

Majewski, D., Liermann, D., Prohl, P., Ritter, B., Buchhold, M., Hanisch, T., Paul, G., Wergen, W., and Baumgardner, J. (2002). The operational global icosahedral-hexagonal gridpoint model gme: Description and high-resolution tests. *Monthly Weather Review*, 130(2):319–338.

Orzech, M., Veeramony, J., and Flampouris, S. (2014). Optimizing spectral wave estimates with adjoint-based sensitivity maps. *Ocean Dynamics*, 64(4):487–505.

Panteleev, G., Yaremchuk, M., and Rogers, W. E. (2015). Adjoint-free variational data assimilation into a regional wave model. *Journal of Atmospheric and Oceanic Technology*, 32(7):1386–1399.

Polak, E. (1971). Computational methods in optimization academic. *New York*.

Portilla, J. (2009). *Buoy data assimilation in nearshore wave modeling*. PhD thesis, Ph D dissertation, KU Leuven, Belgium.

Siddons, L. a., Wyatt, L. R., and Wolf, J. (2009). Assimilation of HF radar data into the SWAN wave model. *Journal of Marine Systems*, 77(3):312–324.

Song, Q. and Mayerle, R. (2017). A 4d variational assimilation scheme with partition method for nearshore wave models. *Ocean Dynamics*, pages 1–14.

Veeramony, J., Walker, D., and Hsu, L. (2010). A variational data assimilation system for nearshore applications of SWAN. *Ocean Modelling*, 35(3):206–214.

Voorrips, a. C., Makin, V. K., and Hasselmann, S. (1997). Assimilation of wave spectra from pitch-and-roll buoys in a North Sea wave model. *Journal of Geophysical Research*, 102(C3):5829.

Wahle, K., Staneva, J., and Guenther, H. (2015). Data assimilation of ocean wind waves using Neural Networks: A case study for the German Bight. *Ocean Modelling*, 96:117–125.

Walker, D. T. (2006). Assimilation of sar imagery in a nearshore spectral wave model. Technical report.

Waters, J., Wyatt, L. R., Wolf, J., and Hines, A. (2013). Data assimilation of partitioned HF radar wave data into Wavewatch III. *Ocean Modelling*, 72:17–31.

# Chapter 5

# Summary

This study concerns on simulations of wave conditions in coastal areas. Simulated wave conditions are applied in the assessment of wave energy potential in coastal area of the Java Island. In addition, a new 4D variational scheme is developed to improve the accuracy of the nearshore wave models. The scheme is tailored to SWAN wave model. Application experiments are performed in the German Bight. In this section, the main findings of each part are briefly summarized. Deficiencies and strengths of the applied methods and techniques are also discussed providing a guideline for future works.

## 5.1 Conclusions

### 5.1.1 Wave energy assessment

The study on wave energy potential along the south coast of the Java Island in Ch. 2 describes an approach according to wave conditions and other geographical conditions for selecting suitable deployment locations of wave farms in nearshore areas. The assessments of wave energy in the study mainly rely on the wave information from numerical models. Long-term analysis based on the data from a global wave model over 10 years along the isobath of 2000 m provides a rough estimation and general knowledge of wave climate in the study area. From the long-term wave data, the wave energy along the south coast of Java Island with slight annual variation is proved to be adequate for wave energy farms (the annual median significant wave height is around 2 m and the mean annual median wave power reaches 22 kW/m). Additionally, although the mean median wave power in dry seasons (27 kW/m) is higher than in rainy seasons (17 kW/m), there is a smaller seasonal vari-

ation than at the west coast of Australia which makes it more suitable for wave energy extraction. Later, wave conditions have been simulated for a period over one year by the coastal wave model (CWM) demonstrate the wave energy contributions in this area. Generally, the majority of wave energy in this area is due to swells from two different sources rather than waves due to local winds. The primary swell is from southwest initiated in mid-latitude region caused by the westerlies. Thus, the wave power due to the swell strengthen and weaken with the seasonal variation of the westerlies in which case the highest monthly wave power appears in summer (wet seasons in Indonesia) and the lowest appears in winter (dry seasons in Indonesia). The other founded southeasterly swell is caused by the trade winds. It dominates the wave field in average wave conditions in dry seasons. Although the trade winds are only about 3-5 m/s through the year having limited local impact on waves, the induced waves will grow through the fetch and perform as relative weak southeasterly swells when approaching the study area. In the coastal areas, the annual wave power from Nov. 2013 to Oct. 2014 is around 21 kW/m and the highest monthly median wave power appears in Aug. reaching about 33 kW/m. Wave conditions along with water depth, and distance from the coast are set as criteria for the selection of wave farms. The general criteria lead to a visible map which raises suitable wave farm regions providing useful reference for further feasibility investigations. Generally, the process is appropriate in most cases for wave energy assessment as long as the wave information is credible.

### 5.1.2 4D wave assimilation scheme

A 4D variational assimilation scheme with partition method is developed for SWAN wave model in Ch. 3. The scheme is modified by providing a set of basic inputs thereby being more effective in scenarios with spatially limited observations in Ch. 4. The German Bight is selected as the computational domain for the twin experiments and practical experiments in both studies. Spatially uniform wind fields and wave boundary conditions are assumed in Ch. 3 to assess the original scheme. Although the derived adjoints abandon the nonlinear wave-wave interaction terms, the twin experiment results still demonstrate remarkable effects of the assimilation scheme (the RMS errors of spectra decrease by around 80%) under the wave conditions when the swell and windsea contributions are able to be classified and separated completely. Nevertheless, uniform model inputs actually provide an assumption of spatially perfect correlations reducing the rank of the error covariance matrix. In other words, under the uniform assumption, observations can be always sensitive to model inputs regardless of where the specific observing site is. But in real cases,

model inputs are not perfectly correlated even in a relative small area. Accordingly, as presented specifically in the sensitive analysis in Ch. 4, the location of observing sites will not be sensitive to wave conditions over the whole boundaries. Therefore, twin experiments are carried out in Ch. 4 to assess the original assimilation scheme (OAS) with spatially varying model inputs using various number of observing sites for assimilations. At the same time, the scheme with basic model input assumption (BAS) is proposed and compared with the original one. The results of twin experiments confirm that the assimilation effect is improved with the extension of the spatial observation coverage. Also, the scheme BAS with a single observation site shows comparable assimilation results with OAS using 25 observation sites on the selected curve (both of the schemes reduce $E_{rms}$ by around 50% throughout the whole computational domain). Additionally, in the one-day practical experiment in the German Bight, the BAS reduces the $E_{rms}$ at the validation station by more than 60%, despite the fact that the windsea contributions is not well corrected as expected during some periods. Hence, according to the experiments, when the nonlinear interactions are not prominent, the developed 4D assimilation scheme is believed to be suitable for nearshore wave simulations even with spatially limited observations. Besides, as presented in the practical experiment, the obtained analysis sea states through assimilations under stationary conditions are adequate as initial conditions contributing to wave forecast.

## 5.2 Discussions

### 5.2.1 Wave energy assessment

In the assessment of wave energy potential, the total extractable wave energy over the study areas is always attractive for researchers. But in Ch. 2, the wave power per unit length named wave power density rather than the exploitable wave energy is defined to evaluate the wave energy potential. The motivation not to involve exploitable wave energy directly is that the computation of exploitable wave energy crucially depends on the type of deployed instruments. For instance, Gunn and Stock-Williams (2012) considered Pelamis P2 as the wave converter to estimate wave energy resources. The basic conception for wave energy calculation is to multiply wave power density obtained from wave data with the 'effective length' of coasts (the projection length of coasts in the direction normal to incoming waves). Hence, they gave a roughly estimation of the wave source globally (mean wave power of 2.11 TW). However, for a specific instrument, the extraction efficiency must be considered when calculating the exploitable wave energy. In fact, the quantity of

deployed instruments can not be unlimited over the whole coast, since the extraction of wave energy leads to the drop of wave fluctuation over the area surrounding the instrument (Bernhoff et al., 2006). Hence, a space between two adjacent converters is required. Specifically, for Pelamis P2 the space is 400 m. Thus Gunn and Stock-Williams (2012) gave a global wave power of 96.6 GW that can be extracted by the selected converter. In our case, the same approach can be applied to roughly estimate the exploitable wave energy. The total wave power is around 506 MW and the consequently exploitable wave power by Pelamis P2 is around 20 MW along the coast. So the exploitable wave energy is convenient to be obtained from the wave information provided by numerical wave models if the instruments which will be deployed are decided. Another inevitable problem is the accuracy of global wave data used in long-term analysis and as open boundary conditions in the coastal wave model. Stopa and Cheung (2014) compared global wave and wind database from ECMWF and NCEP (National Centers for Environmental Predictions). But there are few buoys in south Indian Ocean involved in their study. Thus, wave conditions from both database are applied and compared as wave boundary conditions in the coastal wave model along the Java coast in the preliminary test stage. It is found that the wave data from ERA-I have a better agreement with the observations than that from CFSR-W (NCEP Climate Forecast System Reanalysis) which occasionally overestimates the wave heights in this area. Therefore, finding a credible method to correct model inputs is necessary in case global wave and wind data are inaccurate when applying the assessment method to other sea areas.

### 5.2.2 4D wave assimilation scheme

The main problem in the developed assimilation scheme is the exclusion of the nonlinear wave-wave interaction terms in the adjoints. In this study, the nonlinear terms are neglected with consideration of the separation for windsea and swell contributions. But there is no doubt that the nonlinear impact on the waves in nearshore area is crucial in some situations. For wave conditions that are dominated by a single wave system or contain errors from an unique and identified source, the introduction of nonlinear terms in the derivation of the adjoints is expected to make the adjoints more consistent with the governing equations. The nonlinear wave-wave interactions theory given by Phillips (1960) and Hasselmann (1962, 1963) describe the energy exchange between different wave components, thereby redistributing the energy over the spectrum. Since the full computation of wave-wave interactions is extremely time consuming and not convenient in an operational wave model (Team et al., 2009), the calculations of nonlinear terms in SWAN model are carried out

with the DIA (Discrete Interaction Approximation) for quadruplet wave-wave interactions and LTA (Lumped Triad Approximation) for triad wave-wave interactions (Hasselmann et al., 1985; Eldeberky and Battjes, 1996). It is much easier to obtain the adjoints from discretized equations through an adjoint compiler when nonlinear terms are considered (Hersbach, 1998). Some studies have developed the adjoints from the discretized form of DIA (De Las Heras et al., 1994), although the results in their studies did not demonstrate the advantage of the nonlinear terms. Other easier approach to employ the nonlinear terms is to parameterize the wave-wave interactions. Bauer et al. (1996) replaced the derivative of source terms with a linear combination of source terms themselves. Similar processes can be applied in the derivative of the nonlinear source terms with respect to action density or wind speed, to obtain linear explicit expressions so that the derivation of the adjoints becomes easier. Nevertheless, the parameterization always requires plenty of experiments to obtain an optimal approximation in advance. Even then, the universality of the parameterized forms under various wave conditions is still doubtful. Besides, theoretically, although there are no approximation in the derivation from Tangent Linear Model (TLM) to the adjoint, TLM is linearlized from forward equations and holds when perturbations are small enough if high order nonlinear terms exist. Normally, perturbations will increase with the evolution of the forward model. Therefore, when nonlinear interaction terms are considered, the range of validity of the TLM is expected to become shorter and requires to be reexamined (Tanguay et al., 1995). Apart from the nonlinear terms, there are still some problems in the reproduction for the spectrum of windsea contributions emerging in Ch. 4. Despite the fact that SWAN does not predefine spectrum shapes, the properties of the spectrum shape due to winds is still affected by some coefficients. Generally, the spectrum shape is formed by the balance between wind input terms and dissipation terms. However, among the source terms, only the exponential wind growth coefficient by Komen et al. (1984) and Janssen (1991) explicitly relates to wind components. Therefore, corrections of wind components which are selected as the control variables in the proposed schemes, are incapable of adjusting the spectrum shape subtly. The facts imply that other coefficients in dissipation terms should be added as control variables if accurate spectrum shapes are required. For example, in the white capping dissipation terms, the coefficient $F_w$ in Eq. (A.4) by Janssen (1991); Günther et al. (1992) is a polynomial consisted of mean frequency, mean wave number, steepness and frequencies thereby affecting the widths and positions of spectrum peaks in frequency domain. So if $p$ and $\delta$ are set as parts of control variables, the spectrum shape is expected to be corrected more effectively. But certainly, the selection of

control variables should be according to sensitivity analysis with consideration of physical processes and realities.

## 5.3 Future work

On account of the problems discussed in the above sections, future works mainly concentrate on several different aspects as follows:

- Applications of the approach of wave energy potential assessment. The developed assimilation scheme is able to be applied in coastal wave models to improve the results in other attractive areas where the accuracy of global wave and wind data used to drive the coastal models is doubtful. On the other hand, different types of wave converters can be considered to provide more detailed information for the selection of deployment locations by setting specific criteria according to the properties of the converters.

- Impact assessment of nonlinear wave-wave interaction terms. The influence of the nonlinear terms on the assimilation effect of the proposed scheme is unknown. The nonlinear terms need to be added in the adjoint model and experiments should be designed to reveal the effect of the nonlinear terms under different wave conditions. Hence, adjoint compliers will be considered as a option to develop a new adjoint model.

- Improvement of the correction for the spectrum shape of windsea contributions. As mentioned in proceeding sections, merely choosing wind components as control variables is not sufficient to reform accurate spectrum shapes. Experiments should be performed to find suitable sets of coefficients in the dissipation terms which can be used to efficiently correct spectrum shapes along with the wind components.

- Applications in wave predictions. Although the 4D variational scheme originally is designed for hindcast systems requiring continuous observations through a time window, the applications in wave forecasting systems are possible if accurate initial wave conditions and other model inputs are obtained by the scheme. In that case, studies on benefit period and the optimal assimilation window of the assimilation scheme are required. Additionally, different sources of the assimilated observations such as remote sensing data from SAR images should be attempted.

- Coupling with flow models. Although the action balance equation is conserved with currents, interactions of currents and ocean waves actually transfer energy between each other. Accurate wave fields will make contributions to flow simulations and vise versa. Since previous works presented encouraging results in flow assimilations by Zheng et al. (2016), an assimilation system includes flows and waves in coastal areas is expected. Experiments through full coupled ocean models Delft3D (externally coupled with the SWAN model) (Hydraulics, 1999) with assimilation technique implemented both in waves and flows will be carried out to assess the potential of the assimilation system.

# Bibliography

Bauer, E., Hasselmann, K., Young, I., and Hasselmann, S. (1996). Assimilation of wave data into the wave model wam using an impulse response function method. *Journal of Geophysical Research: Oceans*, 101(C2):3801–3816.

Bernhoff, H., Sjöstedt, E., and Leijon, M. (2006). Wave energy resources in sheltered sea areas: A case study of the baltic sea. *Renewable Energy*, 31(13):2164–2170.

De Las Heras, M. M., Burgers, G., and Janssen, P. a. E. M. (1994). Variational Wave Data Assimilation in a Third-Generation Wave Model. *Journal of Atmospheric and Oceanic Technology*, 11(5):1350–1369.

Eldeberky, Y. and Battjes, J. A. (1996). Spectral modeling of wave breaking: application to boussinesq equations. *Journal of Geophysical Research: Oceans*, 101(C1):1253–1264.

Gunn, K. and Stock-Williams, C. (2012). Quantifying the global wave power resource. *Renewable Energy*, 44:296–304.

Günther, H., Hasselmann, S., and Janssen, P. A. (1992). The WAM model cycle 4.

Hasselmann, K. (1962). On the non-linear energy transfer in a gravity-wave spectrum part 1. general theory. *Journal of Fluid Mechanics*, 12(4):481–500.

Hasselmann, K. (1963). On the non-linear energy transfer in a gravity-wave spectrum. Part 3. Evaluation of the energy flux and swell-sea interaction for a Neumann spectrum. *Journal of Fluid Mechanics*, 15(03):385.

Hasselmann, S., Hasselmann, K., Allender, J., and Barnett, T. (1985). Computations and parameterizations of the nonlinear energy transfer in a gravity-wave

specturm. part ii: Parameterizations of the nonlinear energy transfer for application in wave models. *Journal of Physical Oceanography*, 15(11):1378–1391.

Hersbach, H. (1998). Application of the adjoint of the WAM model to inverse wave modeling. *J. Geophys. Res.*, 103:10469–10487.

Hydraulics, D. (1999). User manual delft3d-flow. *WLjDelft Hydraulics, The Netherlands*.

Janssen, P. A. (1991). Quasi-linear theory of wind-wave generation applied to wave forecasting. *Journal of Physical Oceanography*, 21(11):1631–1642.

Komen, G., Hasselmann, K., and Hasselmann, K. (1984). On the existence of a fully developed wind-sea spectrum. *Journal of physical oceanography*, 14(8):1271–1285.

Phillips, O. (1960). On the dynamics of unsteady gravity waves of finite amplitude part 1. the elementary interactions. *Journal of Fluid Mechanics*, 9(2):193–217.

Stopa, J. E. and Cheung, K. F. (2014). Intercomparison of wind and wave data from the ecmwf reanalysis interim and the ncep climate forecast system reanalysis. *Ocean Modelling*, 75:65–83.

Tanguay, M., Bartello, P., and Gauthier, P. (1995). Four-dimensional data assimilation with a wide range of scales. *Tellus A*, 47(5):974–997.

Team, S. et al. (2009). Swan, scientific and technical documentation, swan cycle iii version 40.72 abc. *Delft University of Technology*.

Zheng, X., Mayerle, R., Xing, Q., and Jaramillo, J. M. F. (2016). Adjoint free four-dimensional variational data assimilation for a storm surge model of the german north sea. *Ocean Dynamics*, 66(8):1037–1050.

# Appendix A

# Source terms in the adjoint and the gradient

$S_w$ including three terms: wind growth, whitecapping dissipation and bottom friction dissipation. It reads:

$$S_w = S_{wg} + S_{dw} + S_{df} \tag{A.1}$$

where $S_{wg}$ is the wind growth, $S_{dw}$ is the whitecapping dissipation and $S_{df}$ is the bottom friction dissipation. The wind growth term $S_{wg}$ applied in this study is based on Snyder et al. (1981) and Komen et al. (1984). It reads:

$$S_{wg} = 0.25\rho_{aw}(\frac{28U_*\cos(\theta - \theta_w)}{2\pi f/k} - 1)2\pi f E(f,\theta) \tag{A.2}$$

where $\rho_{aw}$ is a ratio between the density of air and the density of water, $\theta_w$ is the direction of wind vector, k is the wave number and $U_*$ is a friction velocity. $U_*$ reads:

$$\begin{aligned} U_*^2 &= C_D U_{10}^2 \\ C_D &= \begin{cases} 1.2875 \times 10^{-3} & U_{10} < 7.5\text{m/s} \\ (0.8 + 0.065U_{10})10^{-3} & U_{10} \geq 7.5\text{m/s} \end{cases} \end{aligned} \tag{A.3}$$

where $U_{10}$ is the wind speed at 10 meters elevation and $C_D$ is the drag coefficient from Wu (1982). The expression of white capping dissipation is (Janssen, 1991;

Günther et al., 1992):

$$\begin{aligned} S_{dw} &= F_w(\bar{f}, \bar{k}, E_t)E(f,\theta) \\ F_w &= -\frac{C_{ds}}{\bar{s}_{pm}^p} 2\pi \bar{f} \bar{k}^p E_t^{p/2}((1-\delta)\frac{k}{\bar{k}} + \delta(\frac{k}{\bar{k}})^2) \end{aligned} \tag{A.4}$$

where $\bar{f}$ is a mean frequency, $\bar{k}$ is a mean wave number, $E_t$ is the total wave energy and $\bar{s}_{pm}$ is the wave steepness in Pierson-Moskowitz spectrum (Pierson and Moskowitz, 1964). $C_{ds}$, $\delta$ and $p$ are tunable coefficients. Following Komen et al. (1984), the default number of $C_{ds}$ in the SWAN model equals to $2.36 \times 10^{-}5$, $p$ equals to 2 and $\delta$ equals to 1. The bottom friction dissipation term $S_{df}$ reads:

$$S_{df} = -C_b \frac{(2\pi f)^2}{g^2 \sinh^2(kd)} E(f,\theta) \tag{A.5}$$

where $C_b$ is the bottom friction coefficient set to be $0.067\mathrm{m}^2/\mathrm{s}^3$. Based on Eq. (A.1) to (A.5), derivatives of $S_w$ with respect to $E$ in Eq. (3.16) are:

$$\frac{\partial S_{wg}}{\partial E} = 0.25\rho_{aw}(\frac{28U_* \cos(\theta - \theta_w)}{2\pi f/k} - 1)2\pi f \tag{A.6}$$

$$\frac{\partial S_{df}}{\partial E} = -C_b \frac{(2\pi f)^2}{g^2 \sinh^2(kd)} \tag{A.7}$$

$$\begin{aligned} \frac{\partial S_{dw}}{\partial E} &= \frac{\partial F_w}{\partial E} E + F_w \\ \frac{\partial F_w}{\partial E} &= \frac{\partial F_w}{\partial E_t}\frac{\partial E_t}{\partial E} + \frac{\partial F_w}{\partial \bar{f}}\frac{\partial \bar{f}}{\partial E} + \frac{\partial F_w}{\partial \bar{k}}\frac{\partial \bar{k}}{\partial E} \end{aligned} \tag{A.8}$$

$\frac{\partial E_t}{\partial E}$, $\frac{\partial \bar{f}}{\partial E}$ and $\frac{\partial \bar{k}}{\partial E}$ in Eq. (A.8) can be calculated as (De Las Heras et al., 1994):

$$\begin{aligned} \frac{\partial E_t}{\partial E} &= 1 \\ \frac{\partial \bar{f}}{\partial E} &= \frac{\bar{f}}{E_t}(1 - \frac{\bar{f}}{f}) \\ \frac{\partial \bar{k}}{\partial E} &= \frac{2\bar{k}}{E_t}[1 - (\frac{\bar{k}}{k})] \end{aligned} \tag{A.9}$$

Hence, the source terms $\frac{\partial S_w}{\partial E}$ in Eq. (3.16) can be calculated explicitly with Eq. (A.1) to (A.9). The source term $\frac{\partial S_s}{\partial E}$ in Eq. (3.17) can also be obtained by Eq. (A.7)

since the friction bottom dissipation is the only term in $S_s$.

The wind components $u$ and $v$ only explicitly relate to $S_{wg}$. Therefore, $\frac{\partial S_w}{\partial u}$ and $\frac{\partial S_w}{\partial u}$ in Eq. (3.18) can be obtained as

$$\begin{aligned}\frac{\partial S_w}{\partial u} &= \frac{\partial S_{wg}}{\partial u} = \frac{\partial S_{wg}}{\partial U_*}\frac{\partial U_*}{\partial u} + \frac{\partial S_{wg}}{\partial \theta_w}\frac{\partial \theta_w}{\partial u} \\ \frac{\partial S_w}{\partial v} &= \frac{\partial S_{wg}}{\partial v} = \frac{\partial S_{wg}}{\partial U_*}\frac{\partial U_*}{\partial v} + \frac{\partial S_{wg}}{\partial \theta_w}\frac{\partial \theta_w}{\partial v}\end{aligned} \tag{A.10}$$

where $\frac{\partial S_{wg}}{\partial U_*}$ and $\frac{\partial S_{wg}}{\partial \theta_w}$ can be expressed as

$$\begin{aligned}\frac{\partial S_{wg}}{\partial U_*} &= 0.25\rho_{aw}(28k\cos(\theta-\theta_w))E(f,\theta) \\ \frac{\partial S_{wg}}{\partial \theta_w} &= 0.25\rho_{aw}(28kU_*\sin(\theta-\theta_w))E(f,\theta)\end{aligned} \tag{A.11}$$

From Eq. (A.3), obviously, $U_*$ is related to the wind speed. So we have

$$\begin{aligned}\frac{\partial U_*}{\partial u} &= \frac{\partial U_*}{\partial U_{10}}\frac{\partial U_{10}}{\partial u} \\ \frac{\partial U_*}{\partial v} &= \frac{\partial U_*}{\partial U_{10}}\frac{\partial U_{10}}{\partial v}\end{aligned} \tag{A.12}$$

That means the only required information for Eq. (A.10) is the conversion from the wind speed $U_{10}$ and the wind direction $\theta_w$ to the wind components $u$ and $v$ which can be easily obtained as:

$$\begin{aligned}&\frac{\partial U_{10}}{\partial u} = \frac{u}{U_{10}}, \frac{\partial U_{10}}{\partial v} = \frac{v}{U_{10}} \\ &\frac{\partial \theta_w}{\partial u} = \begin{cases}\frac{u^2-U_{10}^2}{U_{10}^3\sin(\theta_w)} & \sin(\theta_w)\neq 0 \\ \frac{-uv}{U_{10}^3\cos(\theta_w)} & \sin(\theta_w)=0\end{cases} \\ &\frac{\partial \theta_w}{\partial v} = \begin{cases}\frac{U_{10}^2-v^2}{U_{10}^3\cos(\theta_w)} & \cos(\theta_w)\neq 0 \\ \frac{uv}{U_{10}^3\sin(\theta_w)} & \cos(\theta_w)=0\end{cases}\end{aligned} \tag{A.13}$$

Hence, based on Eq. (A.10) to (A.13), the gradient calculation for the wind components in Eq. (3.18) can be processed.

The wind growth expression used in the Cycle 4 of the WAM model is also optional (Komen et al., 1994). In that case, the calculation of the deviation is much more complicated. The details can be found in De Las Heras et al. (1994) .

# Appendix B

# Discrete forms of the adjoints

Generally, the discrete schemes applied in the adjoints of Eq. (3.16) and Eq. (3.17) are based on the SWAN forward model which is a implicit scheme but being solved explicitly (Team et al., 2010). The discrete forms of Eq. (3.16) and Eq. (3.17) are:

$$\frac{1}{\Delta t}((\lambda_w)^{n-1}_{i,j,l,m} - (\lambda_w)^{n}_{i,j,l,m}) + \frac{1}{\Delta x}C_x((\lambda_w)^{n-1}_{i-1/2,j,l,m} - (\lambda_w)^{n-1}_{i+1/2,j,l,m}) + C_y((\lambda_w)^{n-1}_{i,j-1/2,l,m} - (\lambda_w)^{n-1}_{i,j+1/2,l,m}) + \frac{1}{2\pi\Delta f}C_f((\lambda_w)^{n-1}_{i,j,l-1/2,m} - (\lambda_w)^{n-1}_{i,j,l+1/2,m}) + \frac{1}{\Delta\theta}C_\theta((\lambda_w)^{n-1}_{i,j,l,m-1/2} - (\lambda_w)^{n-1}_{i,j+1/2,l,m+1/2}) = (\lambda_w)^{n}_{i,j,l,m}(S^E_{wg})^n_{i,j,l,m} + (\lambda_w)^{n}_{i,j,l,m}(S^E_{dw})^n_{i,j,l,m} + (\lambda_w)^{n}_{i,j,l,m}(S^E_{df})^n_{i,j,l,m} - (S^N_{ob1})^n_{i,j,l,m} \tag{B.1}$$

$$\frac{1}{\Delta t}((\lambda_s)^{n-1}_{i,j,l,m} - (\lambda_s)^{n}_{i,j,l,m}) + \frac{1}{\Delta x}C_x((\lambda_s)^{n-1}_{i-1/2,j,l,m} - (\lambda_s)^{n-1}_{i+1/2,j,l,m}) + C_y((\lambda_s)^{n-1}_{i,j-1/2,l,m} - (\lambda_s)^{n-1}_{i,j+1/2,l,m}) + \frac{1}{2\pi\Delta f}C_f((\lambda_s)^{n-1}_{i,j,l-1/2,m} - (\lambda_s)^{n-1}_{i,j,l+1/2,m}) + \frac{1}{\Delta\theta}C_\theta((\lambda_s)^{n-1}_{i,j,l,m-1/2} - (\lambda_s)^{n-1}_{i,j+1/2,l,m+1/2}) = (\lambda_s)^{n}_{i,j,l,m}(S^E_{df})^n_{i,j,l,m} - (S^N_{ob2})^n_{i,j,l,m} \tag{B.2}$$

Where $S^E_{wg}$, $S^E_{dw}$, $S^E_{df}$, $S^N_{ob1}$ and $S^N_{ob2}$ represent the discrete forms of $\frac{\partial S_{wg}}{\partial E}$, $\frac{\partial S_{dw}}{\partial E}$, $\frac{\partial S_{df}}{\partial E}$, $\frac{\partial S_{ob1}}{\partial N}$ and $\frac{\partial S_{ob1}}{\partial N}$ respectively. Their expressions read:

$$
\begin{aligned}
(S^E_{wg})^n_{i,j,l,m} =& (\frac{\partial S_{wg}}{\partial E})^n_{i,j,l,m} \\
(S^E_{dw})^n_{i,j,l,m} =& (\frac{\partial S_{dw}}{\partial E})^n_{i,j,l,m} \\
(S^E_{df})^n_{i,j,l,m} =& (\frac{\partial S_{df}}{\partial E})^n_{i,j,l,m} \\
(S^N_{ob1})^n_{i,j,l,m} =& \frac{4\pi f W_1}{M_{obs}} \sum_{a=1}^{M_{obs}} (hE - \hat{h}\hat{E}_a) \\
& \delta_i^{i_a} \delta_j^{j_a} \delta_l^{l_a} \delta_m^{m_a} \delta_n^{n_a} |^n_{i,j,k,m} \\
(S^N_{ob2})^n_{i,j,l,m} =& \frac{4\pi f W_1}{M_{obs}} \sum_{a=1}^{M_{obs}} ((1-h)E - (1-\hat{h})\hat{E}_a) \\
& \delta_i^{i_a} \delta_j^{j_a} \delta_l^{l_a} \delta_m^{m_a} \delta_n^{n_a} |^n_{i,j,k,m}
\end{aligned}
\tag{B.3}
$$

First order upwind schemes are employed for the discretization in both geographical and spectral space for the forward model (Team et al., 2010). But the adjoint model is calculated backward in time so that the upwind scheme must turn to the 'downwind' scheme. Therefore, the schemes become:

$$
\begin{aligned}
&\text{If } (C_f)_{i,j,l,m} > 0 \text{ then} \\
&\lambda_{i,j,l+1/2,m} = (1 - 0.5\mu)\lambda_{i,j,l+1,m} + 0.5\mu\lambda_{i,j,l,m} \\
&\lambda_{i,j,l-1/2,m} = (1 - 0.5\mu)\lambda_{i,j,l,m} + 0.5\mu\lambda_{i,j,l-1,m} \\
&\text{If } (C_f)_{i,j,l,m} < 0 \text{ then} \\
&\lambda_{i,j,l+1/2,m} = (1 - 0.5\mu)\lambda_{i,j,l,m} + 0.5\mu\lambda_{i,j,l+1,m} \\
&\lambda_{i,j,l-1/2,m} = (1 - 0.5\mu)\lambda_{i,j,l-1,m} + 0.5\mu\lambda_{i,j,l,m} \\
&\text{If } (C_\theta)_{i,j,l,m} > 0 \text{ then} \\
&\lambda_{i,j,l,m+1/2} = (1 - 0.5\nu)\lambda_{i,j,l,m+1} + 0.5\nu\lambda_{i,j,l,m} \\
&\lambda_{i,j,l,m-1/2} = (1 - 0.5\nu)\lambda_{i,j,l,m} + 0.5\nu\lambda_{i,j,l,m-1} \\
&\text{If } (C_\theta)_{i,j,l,m} < 0 \text{ then} \\
&\lambda_{i,j,l,m+1/2} = (1 - 0.5\nu)\lambda_{i,j,l,m} + 0.5\nu\lambda_{i,j,l,m+1} \\
&\lambda_{i,j,l,m-1/2} = (1 - 0.5\nu)\lambda_{i,j,l,m-1} + 0.5\nu\lambda_{i,j,l,m}
\end{aligned}
\tag{B.4}
$$

$$
\begin{aligned}
\text{If } (C_x)_{i,j,l,m} > 0 \text{ then } \lambda_{i+1/2,j,l,m} &= \lambda_{i+1,j,l,m} \\
\lambda_{i-1/2,j,l,m} &= \lambda_{i,j,l,m} \\
\text{If } (C_x)_{i,j,l,m} < 0 \text{ then } \lambda_{i+1/2,j,l,m} &= \lambda_{i,j,l,m} \\
\lambda_{i-1/2,j,l,m} &= \lambda_{i-1,j,l,m} \\
\text{If } (C_y)_{i,j,l,m} > 0 \text{ then } \lambda_{i,j+1/2,l,m} &= \lambda_{i,j+1,l,m} \\
\lambda_{i,j-1/2,l,m} &= \lambda_{i,j,l,m} \\
\text{If } (C_y)_{i,j,l,m} < 0 \text{ then } \lambda_{i,j+1/2,l,m} &= \lambda_{i,j,l,m} \\
\lambda_{i,j-1/2,l,m} &= \lambda_{i,j-1,l,m}
\end{aligned}
\tag{B.5}
$$

where $\mu = 0$ and $\nu = 0$ are set for the downwind scheme.

# Bibliography

De Las Heras, M. M., Burgers, G., and Janssen, P. a. E. M. (1994). Variational Wave Data Assimilation in a Third-Generation Wave Model. *Journal of Atmospheric and Oceanic Technology*, 11(5):1350–1369.

Günther, H., Hasselmann, S., and Janssen, P. A. (1992). The WAM model cycle 4.

Janssen, P. A. (1991). Quasi-linear theory of wind-wave generation applied to wave forecasting. *Journal of Physical Oceanography*, 21(11):1631–1642.

Komen, G., Hasselmann, K., and Hasselmann, K. (1984). On the existence of a fully developed wind-sea spectrum. *Journal of physical oceanography*, 14(8):1271–1285.

Komen, G. J., Cavaleri, L., Donelan, M., Hasselmann, K., Hasselmann, S., and Janssen, P. (1994). *Dynamics and modelling of ocean waves*. Cambridge university press.

Pierson, W. J. and Moskowitz, L. (1964). A proposed spectral form for fully developed wind seas based on the similarity theory of sa kitaigorodskii. *Journal of geophysical research*, 69(24):5181–5190.

Snyder, R., Dobson, F., Elliott, J., and Long, R. (1981). Array measurements of atmospheric pressure fluctuations above surface gravity waves. *Journal of Fluid Mechanics*, 102:1–59.

Team, S. et al. (2010). Swan scientific and technical documentation, swan cycle iii version 40.81. *Delft University of Technology*.

Wu, J. (1982). Wind-stress coefficients over sea surface from breeze to hurricane. *Journal of Geophysical Research: Oceans*, 87(C12):9704–9706.